PHYSICAL PROPERTIES OF INTERLOCKING CORE STRUCTURES OF FLAX FIBRE-REINFORCED POLYLACTIC ACID COMPOSITE

By

SALEH NAJI MUSAED AL SUBARI

Thesis Submitted to the School of Graduate Studies, Universiti Putra Malaysia, in Fulfilment of the Requirements for the Degree of Doctor of Philosophy

April 2023

FK 2023 41

Abstract of thesis presented to the Senate of Universiti Putra Malaysia in fulfilment of the requirements for the degree of Doctor of Philosophy

PHYSICAL PROPERTIES OF INTERLOCKING CORE STRUCTURES OF FLAX FIBRE-REINFORCED POLYLACTIC ACID COMPOSITE

By

SALEH NAJI MUSAED AL SUBARI

April 2023

Chair : Mohd Zuhri bin Mohamed Yusoff, PhD
Faculty : Engineering

In the composite industry, natural fibre flax has great potential to replace synthetic fibres like carbon and glass due to their versatile characteristics like biodegradability, lightweightness, low cost, and environmentally friendly materials. Therefore, this thesis presents the findings of investigating the compression and fire properties of a range of sandwich structures made from flax fibre reinforced polylactic acid (flax/PLA) composite. Initial testing was focused on the effect of variation in manufacturing processes on the tensile properties of flax/PLA composites. Then, a novel double cell wall interlocking square core with three different cell sizes and honeycomb cores with three different lengths were fabricated and tested under quasi-static compression loading to determine their strength and specific energy absorption (SEA) capabilities. Following this, the interlocking square and honeycomb cores were filled with two different high-density foams and their strength and SEA values were determined. Furthermore, the fire properties of empty interlocking square and honeycomb core sandwich structure composites were investigated by cone calorimeter measurements at three different heat fluxes. The findings on tensile testing revealed that flax/PLA composites manufactured at a temperature of 180 ℃ and pressed for 10 mins gave the highest value of tensile strength, whereas a temperature of 190 ℃, pressed for 15 mins, was the lowest. Furthermore, testing on empty and foam-filled double cell wall interlocking square core sandwich structures showed that empty double cell wall significantly increased the compressive strength and SEA values for foam-filled interlocking square core increased up to 126 % and 64 %, respectively, as compared to the empty core structure. It was also demonstrated that the higher the foam density filled in a smaller cell size core structure, the greater the effect on its strength and SEA. In addition, the variation of the cell core sizes was more pronounced in the case of the empty core structure compared to their foam-filled core counterparts. It was also observed that the average SEAs of foam-filled and empty honeycomb cores showed no significant difference, lying around 8.7 kJ/kg and 8.2 kJ/kg, respectively. In contrast, its compressive strength was clearly pronounced, in which the foam-filled core outperformed the empty counterparts by around 33 %. Clearly, the addition of foam inside both core structures improved the literal support to the core cell wall, resulting in a considerable delay in cell wall buckling and a significant

improvement in strength and SEA values relative to the empty core structures. The mechanical strength and SEA values of these structures compare very favourably with data from tests on a wide range of cores with and without foam reported in the literature. Finally, the cone colorimeter and the results showed that, in terms of time-to-ignition and heat release rate (HRR), the honeycomb core structure performed better than the square core structure in almost all three heat fluxes. However, this advantage was only really noticeable in the case of 35kW/m^2, where the time–to–ignite was higher by 17 seconds. It is critical to note that the skin of sandwich structures played a significant role in increasing HRR; as a result, improving the skin of the sandwich structures by applying fire retardant is necessary for these structures to be used in engineering applications.

Abstrak tesis yang dikemukakan kepada Senat Universiti Putra Malaysia sebagai memenuhi keperluan untuk ijazah Doktor Falsafah

SIFAT FIZIKAL STRUKTUR TERAS BERSEGI KOMPOSIT POLILAKTIK ASID BERTETULANG SERAT FLAX

Oleh

SALEH NAJI MUSAED AL SUBARI

April 2023

Pengerusi : Mohd Zuhri bin Mohamed Yusoff, PhD
Fakulti : Kejuruteraan

Tesis ini membentangkan hasil dapatan kajian penyelidikan pemampatan dan sifat kebakaran berbagai struktur komposit pelbagai lapisan diperbuat daripada komposit gentian rami dikukuhkan oleh asid polilaktik (Flax/PLA). Ujikaji permulaan tertumpu kepada kesan variasi proses pembuatan terhadap sifat tegangan komposit rami/PLA. Seterusnya, dinding dua sel baharu menghubungkan teras segi empat sama dengan tiga sel yang berbeza saiz dan teras sarang lebah yang mempunyai tiga kepanjangan yang berbeza telah disediakan dan diuji dengan beban mampatan statik kuasi untuk menentukan kekuatan dan keupayaan penyerapan tenaga spesifik (SEA). Berikutan ini, teras segi empat sama yang berhubung dan sarang lebah telah diisi dengan dua busa berketumpatan tinggi yang berbeza, dan kekuatannya serta nilai SEA ditentukan. Kesan penggunaan dinding dua sel, saiz, dan panjang sel yang berbeza serta struktur teras berisi busa turut dikaji. Teras segi empat sama berhubung disediakan melalui teknik "slotting", manakala teras sarang lebah dibuat menggunakan acuan beralun yang pada mulanya digunakan untuk mencipta profil teras beralun, yang kemudiannya dipotong kepada sarang beralun dan dipasang untuk membentuk teras sarang lebah. Tambahan pula, sifat kebakaran teras segi empat sama berhubung yang kosong dan struktur teras komposit pelbagai lapisan telah disiasat dengan pengukuran kon kalorimeter pada tiga fluks haba yang berbeza. Hasil dapatan ujian tegangan mendedahkan bahawa komposit rami/PLA yang dihasilkan pada suhu 180 °C dan dimampatkan selama 10 minit menunjukkan nilai kekuatan tertinggi manakala suhu 190 °C, dimampatkan selama 15 minit adalah yang terendah. Tambahan pula, ujian ke atas teras segi empat sama berstruktur pelbagai lapisan yang kosong dan berisi busa menunjukkan bahawa dinding dua sel berstruktur pelbagai lapisan yang kosong menunjukkan kekuatan dan keupayaan penyerapan tenaga yang lebih baik. Di samping itu, kekuatan mampatan dan nilai SEA bagi teras segi empat sama berhubung berisi busa masing-masing meningkat sehingga 126 % dan 64 % jika dibandingkan dengan teras berstruktur kosong. Ia juga menunjukkan bahawa semakin tinggi ketumpatan busa yang diisi di dalam struktur teras saiz sel yang lebih kecil, semakin besar kesannya terhadap kekuatan dan SEA. Di samping itu, variasi saiz sel teras lebih ketara dalam kes teras berstruktur kosong berbanding pasangannya teras berisi busa. Ia juga dapat dilihat bahawa purata SEA bagi teras sarang lebah berisi busa dan

kosong tidak menunjukkan perbezaan yang signifikan, masing-masing pada anggaran 8.7 kJ/kg dan 8.2 kJ/kg. Sebaliknya, kekuatannya lebih ketara, pada teras berisi busa mengatasi pasanganya yang kosong sekitar 33 %. Jelas sekali, pengisian busa di dalam kedua-dua struktur teras telah memperkukuhkan sokongan literal ke atas dinding sel teras, menyebabkan kelewatan yang besar dalam lengkungan dinding sel dan peningkatan yang ketara dalam kekuatan dan nilai SEA berkait dengan struktur teras kosong. Perbandingan kekuatan mekanikal dan nilai SEA struktur-struktur ini adalah baik daripada data ujikaji pelbagai teras berisi dan tidak berisi busa seperti dilaporkan di dalam kajian lepas. Akhir sekali, kon kalorimeter dan ujian asap menunjukkan kedua-dua struktur teras mempunyai gerakan yang sama dengan sifat kebakaran, kecuali apabila fluks haba meningkat kepada 70 kW/m^2 di mana sarang lebah bertindak balas secara berbeza daripada teras berhubung.

ACKNOWLEDGEMENTS

Bismillahirrahmanirrahim. In the Name of Allah, the Most Beneficent, the Most Merciful. First and foremost, my highest gratitude to Allah, the Most Merciful, for his blessings for giving me health, patience, and strength to complete my studies. The writing of this thesis has been one of the most significant academic challenges I have ever experienced in my life. Without the support, patience, and guidance from special people around me, the journey of this study would not have been completed. This thesis is a special gift to the soul of my brother Maeen. May Allah bless his soul, as he was my supporter and advisor. This thesis is also dedicated to my friends and relatives for their prayers, encouragement, and understanding in order to see me another step ahead in academic achievement. My special appreciation and heartfelt thanks also go to my supervisor, Dr. **Mohd Zuhri Mohamed Yusoff**, for his effort, time, patience, and guidance throughout my studies. This study would not have been completed without his enormous help and worthy experience. I would also like to express my deep gratitude to my supervisory committee members; Prof. Ir. Dr. **Mohd Sapuan Salit** and Assoc. Prof. Dr. **Mohamad Ridzwan Ishak** for their fruitful advice and guidance. Not to forget my appreciation to the Ministry of Higher Education of Malaysia for awarding me a Malaysian International Scholarship (MIS) that has supported me throughout my studies at the Universiti Putra Malaysia. Last but not least, to all those people who were directly or indirectly involved in the completion of this thesis, my sincere thanks to each and every one of you. May Allah bless you for all the kindness and help you have showered on me.

This thesis was submitted to the Senate of Universiti Putra Malaysia and has been accepted as fulfilment of the requirement for the Degree of Doctor of Philosophy. The members of the Supervisory Committee were as follows:

Mohd Zuhri bin Mohamed Yusoff, PhD
Senior Lecturer
Faculty of Engineering
Universiti Putra Malaysia
(Chairman)

Mohd Sapuan bin Salit @ Sinon, PhD
Professor, Ir.
Faculty of Engineering
Universiti Putra Malaysia
(Member)

Mohamad Ridzwan bin Ishak, PhD
Associate Professor
Faculty of Engineering
Universiti Putra Malaysia
(Member)

____
ZALILAH MOHD SHARIFF, PhD
Professor and Dean
School of Graduate Studies
Universiti Putra Malaysia

Date: 11 January 2024

TABLE OF CONTENTS

			Page
ABSTRACT			i
ABSTRAK			iii
ACKNOWLEDGEMENTS			v
APPROVAL			vi
DECLARATION			viii
LIST OF TABLES			xii
LIST OF FIGURES			xiii
LIST OF NOMENCLATURES			xvi
LIST OF ABBREVIATIONS			xvii

CHAPTER

1	**INTRODUCTION**		1
	1.1	Overview	1
	1.2	Sandwich structure	1
	1.3	Potential Application of Natural Fibre Reinforced Polymer Composite	3
	1.4	Problem Statement	6
	1.5	Objectives	6
	1.6	Scope and Limitation of the Study	7
	1.7	Thesis Layout	7
2	**LITERATURE REVIEW**		9
	2.1	Introduction	9
	2.2	Natural Fibre Composites: Background, Properties, and Applications	9
	2.3	Sandwich Core Structure	12
		2.3.1 Cellular Foams	13
		2.3.2 Corrugated Core	15
		2.3.3 Honeycomb	16
	2.4	Fabrication Process of Core Structure	18
	2.5	NFC material characterization	20
	2.6	Methodology standards	21
	2.7	Mechanical Properties of NFC Core Sandwich Structures	22
	2.8	Cone calorimeter properties of sandwich structure	24
	2.9	Summary	25
3	**METHODOLOGY**		29
	3.1	Introduction	29
	3.2	Materials	31
	3.3	Fabrication of composite panel	31
	3.4	Fabrication of Sandwich Structures	33
		3.4.1 Square interlocking core structure	33
		3.4.2 Honeycomb core structure	36
	3.5	Fire Test Methodology	39
		3.5.1 Fabrication of composite structure	39

3.5.2 Fabrication of square core structure 39
3.5.3 Fabrication of honeycomb core structure 40
3.6 Mechanical characterization 42
3.6.1 Tensile testing 42
3.6.2 Quasi-static compression testing 43
3.6.3 Cone calorimeter testing 44

4 **RESULTS AND DISCUSSION** 45
4.1 Mechanical properties of flax/PLA composites 45
4.1.1 Influence of processing temperature 45
4.2 Compression properties of square interlocking core structure 47
4.2.1 Core without foam filling 47
4.2.2 Effect of foam filling 48
4.2.3 Effect of varying cell size 51
4.2.4 Energy absorption capability 52
4.3 Quasi-static compression properties of honeycomb core structure 56
4.3.1 Core without foam filling 56
4.3.2 Foam filling core 57
4.3.3 Effect of foam-filled core 58
4.3.4 Effect of varying core lengths and width 59
4.3.5 Energy absorption capability with and without foam 61
4.4 Comparison between square core and honeycomb core structures 62
4.5 Cone calorimeter properties of square and honeycomb cores structure 64

5 **CONCLUSION AND RECOMMENDATIONS** 72
5.1 Conclusion 72
5.2 Recommendations 73

REFERENCES 74
APPENDICES 89
BIODATA OF STUDENT 102
LIST OF PUBLICATIONS 103

LIST OF TABLES

Table		Page
1.1	Summary and conclusion of some of the related works	4
1.2	The application of NFPC in automotive industry.	5
2.1	Benefits and drawbacks of natural fibre composites (NFCs)	10
2.2	Classification of cellular materials as sandwich structures cores.	13
2.3	Core fabrication techniques.	19
2.4	Specific mechanical properties of sisal-polypropylene core	19
2.5	Summary of selected papers on the natural fibres-based core developments.	27
3.1	Summary of the total samples square interlocking flax/PLA core structures	35
3.2	Dimensions of the square interlocking flax/PLA core structures and their relative densities	35
4.1	The tensile properties of flax/PLA composites with different manufacturing temperatures	47
4.2	Comparison of properties between current flax/PLA composite structures with published works	54
4.3	Cone calorimeter data measured for flax/PLA square interlocking and honeycomb core structures subjected to an applied heat flux of 35, 50, and 70 kW/m^2	67

LIST OF FIGURES

Figure		Page
1.1	(a) Seat panelling element and (b) 'green' biocomposite material option for carriage door leaves at a comparable cost to aluminium bonded door leaves, with a 35 % weight saving.	3
2.1	Effect of water absorption of natural fibre on mechanical properties of composite laminate .	11
2.2	Energy absorption of sandwich panels under different impact energies: (a) sandwich panels with different face sheets and (b) sandwich panels with homogeneous and various graded foam cores.	15
2.3	Average properties of sandwich specimens: (a) compression stiffness, (b) specific compression stiffness, (c) peak load, and (d) energy absorption .	17
2.4	A comparison between the energy absorption capacities per unit mass of competing metallic and composite grids sandwich panels,	18
2.5	The compression strength and energy absorption of (a, b) flax/PP and (c, d) flax/PLA interlocking structures.	23
3.1	Detailed Research Framework	30
3.2	Manufacturing process cycle of flax/PLA composite	32
3.3	Tensile specimen based on ASTM D3039 standards	33
3.4	The details design of the double cell wall square interlocking cores	34
3.5	Illustration of (a) empty and (b) filled-foam of square core structure	34
3.6	Detailed design of corrugated mould	36
3.7	Fabrication process of corrugated core profile	37
3.8	Illustration of the assembly of honeycomb core structure	38
3.9	Schematic top view and photograph of honeycomb cores of different lengths	38
3.10	Photos of filled-foam honeycomb sandwich structure	39
3.11	Process of fabricating square interlocking core structure	40

3.12	Photos of the complete process of fabrication of honeycomb core sandwich structure	41
3.13	Tensile test setup	42
3.14	Photograph of Instron machine used for the compression test	43
3.15	(a) Cone calorimeter tester; (b) combustion process after spark	44
4.1	Tensile stress-strain curves at 5 minutes pressing time	45
4.2	Tensile stress-strain curves at 10 minutes pressing time	46
4.3	Tensile stress-strain curves at 15 minutes pressing time	46
4.4	Compressive strain-compressive stress curves of empty square core structure with three different cell sizes	48
4.5	Stress-strain curve of 20 mm cell size core, empty, and foam-filled (HP80 and F150 foam)	49
4.6	Stress-strain curve of 30 mm cell size core, empty and foam-filled (HP80 and F150 foam)	50
4.7	Stress-strain curve of 40 mm cell size core, empty, and foam-filled (HP80 and F150 foam)	50
4.8	Progress failure modes in the core flax/PLA composites structure with (a) foam-filled core structure and (b) empty core structure	51
4.9	Stress-strain curves of (a) SC20HP80, SC30HP80 and SC40HP80 (b) SC20F150, SC30F150, and SC40F150, and (c) SC20EM, SC30EM, and SC40EM	52
4.10	Comparison of specific energy absorption with different core parameters	53
4.11	Stress-strain curve of empty honeycomb core	56
4.12	Progress failure modes in the core flax/PLA composites structure with empty core structure	57
4.13	Progress failure modes in the core flax/PLA composites structure with foam-filled cores (a) HP80 core structure and (b) F150 core structure	58
4.14	Typical stress-strain graphs (a) HC1 with and with foam-filled, (b) HC2 with and with foam-filled, and (c) HC3 with and with foam-filled	59

4.15	Stress-Strain curves of empty honeycomb core structure with different core sizes	60
4.16	Stress–strain curves of HC2 and HC2 filled with HP80 foam	60
4.17	Stress–strain curves of HC2 and HC3 filled with F150 foam	61
4.18	Comparison of specific energy absorption of honeycomb cores	62
4.19	A compressive strength of both empty square interlocking and empty honeycomb core structure	62
4.20	A strength of both square interlocking and honeycomb cores structure filled with HP80 foam	63
4.21	A strength of both square interlocking and honeycomb cores structure filed with F150 foam	63
4.22	A strength of both square interlocking and honeycomb cores structure	64
4.23	The heat release rate vs time at 35 kW/m^2	65
4.24	The heat release rate vs time at 50 kW/m^2	66
4.25	The heat release rate vs time at 70 kW/m^2	66
4.26	Photos after the test of both core sandwich structures (a) honeycomb and (b) square	68
4.27	Mass loss % under three different heat fluxes	69
4.28	Total heat rate under three different heat fluxes	70
4.29	Total smoke production ratse under three different heat fluxes	71

LIST OF NOMENCLATURES

%	Percentages
^{o}c	Degree Celsius
ρ	Density
$\bar{\rho}$	Specific Density
ε	Strain
σ	Stress
E	Young's Modulus

LIST OF ABBREVIATIONS

ASTM	American Society for Testing and materials
Ds	Smoke Density
FIGRA	Fire Growth Rate
HRR	Heat Release Rate
NFCs	Natural Fibre Composites
PLA	Polylactic Acid
SEA	Specific Energy Absorptions
THR	Total Heat Release
TSP	Total Smoke Production
TSR	Total Smoke Rate

CHAPTER 1

INTRODUCTION

This chapter contains a brief introduction to the research project and an overview of composite materials, along with their applications. The rationale behind the need for an efficient and lightweight energy-absorbing structure will be presented. Additionally, the motivation, objectives of the research, and significance of the study are discussed. The chapter closes with an overview of the thesis.

1.1 Overview

In recent years, there has been a growing interest in the research of sandwich structures, particularly in enhancing the energy-absorbing ability and environmentally-friendly lightweight structures. This leads to the introduction of natural fibres into many engineering applications due to their explicit advantages as compared to synthetic, conventional fibres. Here, the potential advantages, such as low cost, lower tool wear, low density per unit volume, and acceptable specific strength, are some of the important properties of natural fibres, along with their sustainable, renewable, and degradable characteristics, which lead to the emergence of new inventions of composite materials. This work presents contributions towards the development of lightweight sandwich structures by employing natural fibre composite material. The sandwich structure is completely made of flax fibre reinforced PLA and later embedded with different types of foams with a view to enhancing the energy absorption capabilities of the structure. The process of discovering the developed sandwich structure with and without a foam-filled core was achieved through extensive experimental testing and knowledge gathered from previous investigations. This study assesses the specific energy absorption (SEA) and the corresponding failure modes by executing a range of tests based on several parameters.

1.2 Sandwich structure

The sandwich structure is known as a core attached to the two identifiable skins. Stiff and strong skins are utilised by sandwich composite structures, and the core distributes the load from one skin to another. While the skins contribute to the bending and turgidity, the adhesive that conveys the shear and axial loads to the core material is used as a bonding agent. The skin (sometimes called a face sheet), which in rare cases weighs some millimetres, is commonly composed of light alloys. These light alloys range from aluminium, a single metallic layer, and laminated or fibre reinforced composite. In sandwich structures, core designs such as honeycomb, lattice, truss designs or web-reinforced options, and cellular are commonly used. Opting for particular sandwich materials is largely dependent on a number of factors, which include the structure's use, lifetime loading, and the value and price of the materials. For aerospace applications, carbon epoxy and graphite epoxy with multi-layered facings are used. However, for the facings of civil and marine structures, glass epoxy or glass vinyl ester is utilised.

According to Gay and Hoa [1], aerospace structures use a core made of aluminium or Nomex honeycomb. Also, Birman [2] suggested that civil engineering requires the use of closed-cell or open-cell foam, while ship sandwich structures require the use of balsa. Therefore, this combination of materials resulted from a competitive structure in various application areas such as aerospace, transport, marine, and civil structures where high strength, low weight material, and fuel economy are essential factors.

The science and technology of sandwich structures and materials have advanced significantly over the past several years, and an increasing number of products, from sports equipment to satellites, are using these structures and materials [3]. The use of composite sandwich structures in aeronautical, automotive, aerospace, marine, and civil engineering applications is becoming extensive as these structures have excellent stiffness-to-weight ratios that lead to weight reduction and fuel consumption. They are characterised by high structural crashworthiness since they are capable of absorbing large amounts of energy in a sudden collision. In aerospace applications, various honeycomb core sandwich structures have been used for space shuttle constructions as well for both military and aircraft.

More recently, due to their affordability and superior thermal efficiency, sandwich structures are increasingly being employed in civil engineering projects like building walls, roofs, and bridge decks. Additionally, sandwich structures are used in railcars for rapid transit trains, buses, yachts, racing boats, racing vehicles, snow skis, water skis, and canoes, according to Petras reports [4].

Because of the demands on safety criteria as well as the need to reduce the environmental effect of the aviation manufacturing sectors, the creation of aircraft parts and components has become a significant responsibility for engineers and scientists in the connected field throughout the years. These parts and components must exceed severe safety criteria imposed by the Federal Aviation Administration's Federal Aviation Regulations (FAR) without sacrificing important aspects such as lightweight, cost, and durability. Because weight plays a vital role in the aviation industry, lowering overall weight has a big advantage for both the producer and the operator because it lowers overall production and operating costs. This is because a lightweight aircraft has a lower carbon footprint because it uses less fuel when in operation [5]. Consequently, weight-related issues with aircraft were largely solved with the development of polymeric-based composites, which have been used in interior components like flooring, bulkheads, cabin dividers, restrooms, walls, ceiling panels, stowage bins, and galleys as well as aircraft parts, including the wing and body (Figure 1.1). Therefore, in order to resolve the traditional core materials' problems with the environment, weight, cost, and availability, a novel core design made up of natural fibre is developed.

Figure 1.1 : (a) Seat panelling element and (b) 'green' biocomposite material option for carriage door leaves at a comparable cost to aluminium bonded door leaves, with a 35 % weight saving [6].

1.3 Potential Application of Natural Fibre Reinforced Polymer Composite

There are many industries that are exploring the use of natural fibre composites and sandwich structures. Today, many efforts to develop environmentally friendly composite and sandwich structures, with the aim of cost reduction, weight reduction, and even pollution abatement, have been undertaken. Here, the applications of natural fibre composites and sandwich structures in engineering applications are discussed.

Environmentally-friendly aircraft interiors made of natural fibres have received attention in the aviation industry. For example, Boegler et al. [7] studied the potential use of ramie fibre composites for aircraft wing boxes, providing a weight reduction over aluminium alloy. In addition, Kling et al. [8] addressed the possibility of using renewable raw materials for wing designs in the future. As of right now, a partnership consisting of 214 biomasses, biopolymer-based materials, and Bioenergy Aimplas (Spain), Boeing Research and Technology Europe (Spain), INvent GmbH (Germany), and Lineo (France) has been established under the European project [9]. The goal is to commercialise environmentally friendly aircraft interiors made of natural fibres and reinforce them with biodegradable polymer matrix composites for the aviation industry. The purpose of these sandwiched composites made from natural fibres is to be used as cabin partitions, in addition to preserving environmental sustainability by reducing the influence of climate change. In a similar study, John et al. [10] focused on using woven flax fabric and polymeric matrices to produce commercial interior cabin panels. They also worked more on finding solutions to the problems of strength, moisture absorption, and adhesion between the fibre and matrix in order to meet airworthiness regulations. Similarly, Haris et al. [11] examined the characteristics of five different natural fibres—bamboo, oil palm, banana, kenaf, and pineapple leaf—as a reinforcement for biocomposites for use in aircraft radomes. Subash [12] highlighted the use of natural fibres as reinforcement for aircraft interior structures, including hemp, kenaf, flax, and others. Furthermore, a report by Red [13] indicated that by 2022, the market for aircraft interiors will see demand that is two times greater than that for aircraft airframe structures. Additionally, it is suggested that one of the possible uses for polymer composites is the construction of aircraft seats, enabling the adoption of thinner seat designs for greater space. Eloy et al. [14] also investigated the use of cotton fibre with polyurethane (PU) matrix as a promising natural fibre composite for aeronautical interior components. The authors claimed that the use of PU resin obtained from castor bean oil would allow a complete composite to be fully manufactured utilising natural resources. In another report, [15] developed a novel honeycomb from unidirectional kenaf-reinforced epoxy composites. This honeycomb design allows it to support higher loads, making it suitable for usage in aircraft constructions. The summary and conclusion of some of the related works are shown in Table 1.1.

Table 1.1: Summary and conclusion of some of the related works [16]

Drown conclusion	Reference
Ramie fibre-based composite is excellent for aircraft wing boxes since it is lightweight and still maintains its structural integrity.	[7, 16]
Due to its mechanical properties and resistance to rain erosion, hybrid kenaf/glass fibre-reinforced polymer composites can be used for aircraft radome applications.	[11]
Better mechanical properties at low density will result from using honeycomb cores in composite structures, and they are also resistant to buckling and bending.	
For aircraft cabin interior panels, composites with honeycomb cores and woven flax fibres between them are acceptable, although they must adhere to FAR regulations (fire performance). Therefore, during the fabrication of the composite structure, it is important to spray a fire retardant material on the surface of the natural fibre.	[10]
Green composites using bast fibres can be utilised for non-load-bearing components like seat cushions, cabin linings, package shelves, etc.	
In order to reuse and recycle the aircraft structure, commercial aircraft manufacturers like Airbus and Boeing started their research utilising natural fibre.	
When selecting natural fibre, it is crucial to carefully verify its microbial resistance, fire resistance, and moisture absorption.	[16]
Natural fibre can be utilised in the cabin of the aircraft but not in situations where it requires exceptional fire resistance.	
The proper selection of natural fibre for a particular aircraft component must be made throughout the product's design process.	

Natural fibres are already being used in the automotive industry by German automakers Mercedes, BMW, Audi, and Volkswagen for interior and exterior applications such as inner door panels and door trim panels, [17] as shown in Table 1.2.

Table 1.2: The application of NFPC in automotive industry [18].

Manufacturer	Model	Application
Peugeot	406	Front and rear door panels, seat backs, and parcel shelves.
Citroen	C3 Picasso, C5	Parcel shelves, boot linings, door panels, interior door panellings, and mudguards.
Opel	Vectra, Astra, Zafira	Door panels, pillar cover panels, head-liner panels, and instrumental panels.
Volkswagen	Passat Variant, Golf, A4, Bora	Seat backs, door panels, boot-lid finish panels, and boot-liners.
Audi	A2,A3, A4,A4Avant,A6, A8, Roadstar, Coupe	Boot-liners, spare tire-linings, side and back door panels, seat backs, and hat racks.
Daimler Chrysler	A, C, E, and S class, EvoBus (exterior)	Pillar cover panels, door panels, car windshields/car dashboards, and business tables.
BMW	3, 5, and 7 series and other Pilot	Seat backs, headliner panels, boot-linings, door panels, noise insulation panels, and moulded footwell linings.
Mercedes Benz	C, S, E, and A classes	Door panels (flax/sisal/wood fibres with epoxy resin/UP matrix), glove boxes (cotton fibres/wood moulded, flax/sisal), instrument panel supports, insulations (cotton fibre), moulding rod/apertures, seat backrest panels, (cotton fibre), trunk panels (cotton with PP/PET fibres), and seat surfaces/backrests (coconut fibre/natural rubber).
Fiat	Punto, Brava, Marea, Alfa Romeo 146, 156, 159	Door panels.
Toyota	ES3	Pillar garnishes and other interior parts.
Mitsubishi	Fiat SpA	Floor mats, indoor claddings, seat back linings, cargo area floors, door panels, instrumental panels, and floor panels.
Rover	2000 and others	Rear storage shelves/panels and insulations.
Lotus	Eco Elise (July 2008)	Body panels, spoilers, seats, and interior carpets.
Vauxhall	Corsa, Astra, Vectra, Zafira	Headliner panels, interior door panels, pillar cover panels, and instrument panels.
General Motors	Cadillac De Ville, Chevrolet Trail Blazer	Seat backs, cargo area floor mats.
Volvo	V70, C70	Seat paddings, natural foams, cargo floor trays, dashboards, and ceilings.
Ford	Mondeo CD 162, Focus	Floor trays, door inserts, door panels, B-pillars, and boot-liners.

Furthermore, natural fibre composites have been employed to develop load-bearing components such as beams, roofs, multifunctional panels, water tanks, and pedestrian bridges for structural and infrastructural purposes [19].

In Malaysia, most studies focus on the potential application of natural fibres in general. As an example, [20, 21] published a review on the potential usage of vegetable fibres, and in particular, oil palm empty fruit bunch (EFB), as a roofing material in order to be an energy-efficient approach to sustainable building. [22] reported that natural fibres such as oil palm, sugar palm, pineapple leaf, coir, coconut shell, rice husk, banana pseudostem, kenaf, rubber wood, bagasse, and bamboo are potentially used in industries such as automotive, furniture, and building construction and in a move to use them in the aerospace industry.

The variety of NFPC applications is expanding quickly across several engineering disciplines. Many automotive businesses, like the Proton company, have given the various types of natural fibre-reinforced polymer composite a significant amount of attention in a variety of vehicle applications [23]. To sum up, synthetic fibre is already recognised as having superior properties to other materials, as opposed to natural fibre composite, which is yet relatively unexplored.

1.4 Problem Statement

In the realm of structural engineering, the search for materials that are both lightweight and eco-friendly while retaining fire resistance poses a significant challenge. It is well-established that manipulating the core material and its design can significantly alter the overall properties of the composite. Different core designs exhibit varying capabilities in terms of specific energy absorption. Recent data confirm the exceptional performance potential of cores made of natural fibre-reinforced composites. However, an evident research gap exists, as only limited studies have investigated the behaviour of sandwich composite structures incorporating natural fibres under compression loading. This deficiency underscores the active and underexplored nature of this research area.

Hence, this study aims to address this knowledge gap by focusing on the design of a double cell wall square interlocking core structure fabricated using flax fibre reinforced with polylactic acid (PLA). This innovative core design will be compared to a corrugated honeycomb core sandwich structure, also manufactured from flax fibre reinforced with polylactic acid (PLA). Through comprehensive testing and analysis, this research seeks to provide new insights into the mechanical properties of sandwich structures and their fire resistance capabilities. In doing so, this research aims to contribute to the development of sustainable, fire-resistant structural materials, fostering advancements in this actively evolving research field.

1.5 Objectives

The objectives of this research are:

1. To investigate the tensile properties of flax composites and their sensitivities to various manufacturing temperatures.

2. To fabricate the square interlocking core and honeycomb core structures made of flax/polylactic acid composite.

3. To study compression properties of empty and foam-filled square interlocking core structures made of flax/polylactic acid composite, and compare the energy absorption capability with the current widely used sandwich structures.

4. To study compression properties of empty and foam-filled corrugated honeycomb core structures made of flax/polylactic acid composite.

5. To compare the energy absorption capability of double cell wall square interlocking core and corrugated honeycomb core reinforced-foam structures.

6. To investigate the fire performance of square interlocking and honeycomb core structures made of flax/polylactic acid composite.

1.6 Scope and Limitation of the Study

This study aims to investigate the compression properties under quasi-static compression load and fire resistance of sandwich structures utilising flax fibre-reinforced composites as core and skin materials. It will encompass material characterisation, composite fabrication, compression testing, fire performance assessment, and comparative analysis with synthetic materials. By assessing the structural and fire properties of flax fibre-based sandwich structures, this research seeks to contribute to sustainable and fire-resistant structural solutions in various industries. While conducting this study, several limitations were encountered that are important to acknowledge. First, the onset of the COVID-19 pandemic significantly impacted the research environment, leading to resource constraints and logistical challenges. These limitations affected our ability to carry out certain experiments as originally planned. For instance, due to limitations in the machine's capabilities and availability, we were unable to vary the pressure during the manufacturing process, resulting in the production of samples solely at a fixed pressure level. Additionally, when employing the slotting technique for square interlocking core manufacturing, we encountered difficulties in achieving a consistent thickness of 1.4 mm. The inherent characteristics of the material made it prone to bending or breaking, necessitating the use of thicker sections (3 mm) to ensure the successful production of samples. These limitations should be considered when interpreting the results and may have implications for the generalisability of our findings.

1.7 Thesis Layout

This thesis is structured into five chapters.

Chapter 1 contains a brief overview of sandwich structures along with their applications. The potential application of natural fibre-reinforced polymer composites, the motivation for the study, and the rationale behind the need to study the mechanical properties of sandwich structures made of natural fibre are also presented.

Chapter 2 presents a comprehensive literature review on relevant areas associated with the topics in this research. This chapter comprises the background, properties, and applications of natural fibres, followed by an introduction to the sandwich structure and an extensive review of the mechanical properties of cellular core structures, such as cellular foam, corrugated, and honeycomb core structures. The chapter then discussed different types of fabrication processes of core structures, NFCs material characterisations, and mechanical properties of NFCs core sandwich structure and fire properties of the sandwich structure. Finally, the key findings are drawn.

Chapter 3 describes the methodology of the research work proposed. The chapter starts by discussing the material used and the fabrications process of composite panels using a hot press machine under three different pressing temperatures. Then, sandwich structures, square interlocking, and honeycomb core structure manufacturing processes are also presented. Finally, tensile, mechanical, and fire characterisation testing of the sandwich structure is discussed.

The following Chapter 4 presents the results and discussions of the research findings. The first part of the chapter investigates the sensitivity of flax/PLA to the variations in manufacturing temperature, mechanical properties, and specific energy absorptions of square interlocking and honeycomb core structures with and without foam-filled. A comparison between both sandwich structures and their fire performance is discussed.
Chapter 5 represents the summary of the results and discussions of the experimental work, and this chapter also discusses potential future directions for the study.

CHAPTER 2

LITERATURE REVIEW

2.1 Introduction

The interest in using natural fibre-reinforced composites is currently at its highest. Numerous studies have been conducted due to their positive benefits related to environmental issues. Even though they have limitations for some load requirements, this drawback has been countered through fibre treatment and hybridisation. Sandwich structure, on the other hand, is a combination of two or more individual components with different properties, which, when joined together, can result in better performance. Sandwich structures have been used in a wide range of industrial material applications. They are known to be lightweight and good at absorbing energy, providing superior strength and stiffness-to-weight ratios, and offering opportunities, through design integration, to remove some components from the core element.

Today, many industries use composite sandwich structures in a range of components. Through the good design of the core structure, one can maximise the strength properties while having a low density. However, the application of natural fibre composites in sandwich structures is still minimal. Therefore, this chapter reviewed the possibility of using a natural fibre composite in sandwich structure applications. It addressed the mechanical properties and energy-absorbing characteristics of natural fibre-based sandwich structures tested under various compression loads. The results and potential areas of improvement to fit into a wide range of engineering applications are discussed.

2.2 Natural Fibre Composites: Background, Properties, and Applications

The utilisation of natural fibres as alternative materials in many industrial sectors has been of major global interest in moving towards a greener environment and sustainability. These natural fibres, e.g., kenaf, sugar palm, flax, jute, hemp, etc., have been incorporated with polymeric resins to form new materials called natural fibre composites (NFCs) [24-28]. These natural fibres can be mixed with bioplastics such as PLA, phenolics, and starch to produce green composites [29-34]. In general, these NFCs are constituted from thermoset or thermoplastic resins to offer specific qualities and properties for various applications [35-37]. From this point of view, it can be seen that the application of NFCs has grasped the attention of material researchers and engineers due to the advantages they offer (Table 2.1) [38]. On top of this, the current environmental issues have expedited the growing interest among industries for innovating with NFCs for various products.

Table 2.1: Benefits and drawbacks of natural fibre composites (NFCs).

Benefits	Drawback
Very good sound, acoustic, and electrical insulating properties.	Moisture absorption, causing fibres to swell.
Reactivity materials provide sites for water absorption and are also available for chemical modification.	Restricted maximum processing temperature.
Biodegradability: as a result of their tendency to absorb water, natural fibres biodegrade under certain circumstances through the actions of fungi and\or bacteria.	Lower durability, fibre treatments can improve this drawback.
Combustibility: products can be disposed of through burning at the end of their useful service life, and energy can simultaneously be generated.	Poor dimensional stability as a consequence of the hygroscopicity of fibres, products, and materials.
Very good mechanical properties, especially tensile strength. In relation to their weight, the best fibres attain strength similar to Kevlar.	Variability in quality, dependent on unpredictable variables such as weather.
The abrasive nature of natural fibres is much lower compared to glass fibres, which leads to advantages in regards to the technical aspects, material recycling, or processing of composite materials.	Less fire retardance.
Plant fibres are renewable raw materials with unlimited availability.	Lower strength properties, particularly impact strength.

From the aforementioned statements, NFCs have been suggested to substitute for the previous traditional composites, including glass, basalt, carbon, and aramid fibre composites [38]. This could be happening due to the NFCs themselves, which have low manufacturing costs, higher productivity, as well as good mechanical strength and stiffness. Generally, the performance of NFCs depends on the fibre type. For instance, bast fibres tend to show superior flexural strength, while leaf fibres tend to offer excellent impact properties [39]. Thus, the understanding of natural fibre properties and forms is crucial for achieving successful improvement outcomes [40-42]. Chandrasekar et al. [43] found that flax fibre-reinforced epoxy composites exhibited higher bending and impact strengths. Of equal importance, an accurate aspect ratio should be considered because natural fibres can exist in different forms, such as entangled yarn, bundles, and elementary fibre [44]. There are various factors that influence the mechanical performances of natural fibre, e.g., fibre content, temperature, humidity, fibre treatment, and fibre type.

Typically, natural fibres such as flax and hemp have a high potential for substituting traditional synthetic fibres. On the other hand, natural fibres are considered challenging materials since their mechanical properties vary widely, depending on their source, storage method, and nature [45]. The most prominent issues during the fabrication of NFCs include poor water resistance, low durability, and poor fibre–matrix adhesion. The poor interfacial adhesion between natural fibres and their polymer matrix is because of natural fibres' composition: hemicellulose, pectin, and lignin [38, 46] [32,42]. These components exhibit hydrophilicity, whereby a matrix is usually hydrophobic, causing the natural fibre filler to be easily removed, cracked, fractured, and cratered. Moreover, this phenomenon happens due to fibres and matrices that are not strongly bonded with each other. Figure 2.1 briefly explains how the high moisture absorption of natural fibres diminishes the overall mechanical performance of NFCs. The lack of interfacial bonding and the absorption of moisture resulted in NFCs being less efficient for stress transfer and having low durability.

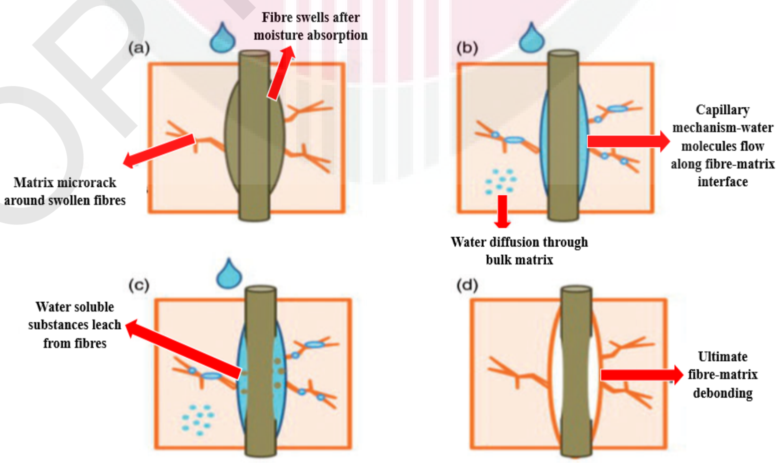

Figure 2.1: Effect of water absorption of natural fibre on mechanical properties of composite laminate [47]

NFCs also have thermal degradation problems, as the composite laminate is exposed to overheating. To solve the issue, fibre treatment is one of the methods that can be considered to improve the surface topography of fibres for industrial uses. These treatments provide a better interlocking system between fibre and matrix due to good surface roughness and fibre–matrix compatibility [48]. Improvements in interfacial bonding automatically improve the overall performance of natural fibre composites. Subsequently, the NFCs can fulfil a wider range of applications. There are three main fibre treatments for improving the quality of NFCs: alkali, silane, and acetyl [49]. Alkali treatment, or mercerisation, aids in the removal of lignin and hemicellulose [46], whereas silane treatment provides a coating layer on the surface of the natural fibres [50]. For acetylation, the mercerisation process is carried out to remove the hemicellulose, natural fats, lignin, and waxes from the acetylating cellulose [51]. In this case, the process can yield a higher potential of hydroxyl groups and other reactive functional groups on the fibres' surface. Subsequently, the NFCs are comparable with glass fibre composites, especially in impact strength properties.

Still, the progress of NFCs has continued to snowball since efforts for promoting the recyclability of crop wastes into goods to replace synthetic fibres were initiated. Natural fibres are highly promising for application as sandwich structures, either the face sheet sandwich or the inside core structure. They can replace the aluminium honeycomb, NOMEX, glass fibres, and other traditional materials in sandwich structures, which are highly useful in aerospace, automobile, civil, and marine applications [52]. These NFCs are produced by hand lay-up, compression moulding, and vacuum bagging techniques to attain good, finished sandwich products. The application of NFCs in sandwich structures could provide better mechanical properties and move resistance performance towards more extended durability [53].

2.3 Sandwich Core Structure

There are several types of sandwich cores that have been studied in recent years. All studies targeted the development of a lightweight structure with good strength and stiffness. Today, researchers are seeking an archetypal lightweight cellular core that can be used in sandwich structures, e.g., stochastic and periodic cells. Gibson and Ashby [54] suggested that foam (open or closed cells), classified as a random microstructure, is one of the most used stochastic materials. On the other hand, Wadley [55] asserted that the periodic structures produced from a chain of unit cells in an array could be grouped into three categories: honeycomb structures, prismatic topologies, and lattice truss structures. Table 2.2 shows the classification of cellular materials as cores for sandwich structures.

Table 2.2: Classification of cellular materials as sandwich structures cores [56].

Cellular Materials					
Periods				Stochastic	
Three Dimensions (Lattice)		Two Dimensions			
Truss	Textile	Honeycombs	Prismatic	Open-cell	Closed-cell
Pyramidal 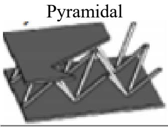	Diamond Collinear 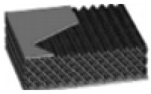	Square 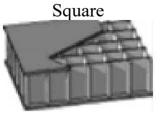	Diamond 	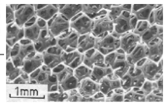	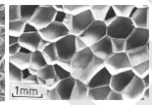
Tetrahedral 	Diamond Textile 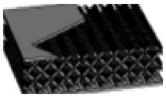	Hexagonal 	Triangular 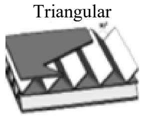		
3D Kagome 	Square Textile 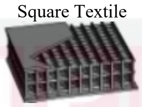	Triangular 	Navtruss 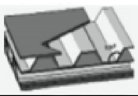		

2.3.1 Cellular Foams

A number of techniques can be used in foaming various forms of solids. According to Liu and Chen [57], the phases of foaming polymer foams include bubble nucleation, expansion, and solidification. Ashby et al. [54] stated that metal foams that have solid metals in them are usually produced from aluminium with gas pores. Cellular foams with pores can be open- or closed-cells. Gong and Kyriakides [58] explained that cellular materials are beneficial because of their ease of manufacturing and for alternating the densities by a small percentage (~2–10 %) of the base material's density. Detailed studies on the manufacturing process of cellular foams have been extensively performed by many researchers [59, 60]. Though metal foams have a higher density than polymer foams, they are similar in the sense that they can sustain large compressive strains and can be used in energy-absorbing applications.

Extensive studies have been performed on the energy-absorbing capability of cellular foam-based core structures. An investigation of the compressive response of three polymeric foam materials, i.e., expanded polystyrene (EPS), high-density polyethylene (HDPE), and polyurethane (PU), under quasi-static testing (medium and high strain rate conditions), was made by Ashraf et al. [61]. They discovered that EPS and HDPE materials showed an increasing value of crush stress plateaus and a decreasing strain value when the strain rate was increased. The materials also exhibited an increasing value of material density. The PU material, on the other hand, displayed large-scale fractures and emission at intermediate rates. This caused a depletion in the strength of the crush plateau in comparison with low-rate tests.

Subhash et al. [62] examined the function of polymeric structural foams with varying porosity levels, low density (<1 g/cm^3), and high density (>1 g/cm^3) under low and high strain rate loadings. It was found that an increase in foam density also led to an increase in Young's modulus, yield strength, maximal stress, and strain to failure. In contrast, the high-density foams showed an increasing consistency in deformity and resulted in a ductile-like fracture form, as the low-density foams failed as a result of the prior disintegration of large porous cells. In addition, Saha et al. [63] carried out a test on two polymeric foams: cross-linkedpolyvinyl chloride (PVC) and polyurethane (PUR). This was done under compression loading at varying strain rates. The analysis showed that peak stress and energy absorption were largely dependent on the microstructure, density, foam materials, and strain rate.

Chen et al. [64] investigated several advanced foam-filled multi-cell composite panels (FMCPs) made from glass fibre-reinforced polymer (GFRP) skins, GFRP lattice webs, and polyurethane (PU) under quasi-static compression. This study investigated four parameters: the effects of the skin and lattice-web thickness, the foam-cell width and height, and the foam density. The analysis showed great reductions in the peak crushing force and bearing loads for the FMCP with trapezoidal cells. Importantly, the FMCP with double-layer dislocation cells exhibited a specific energy absorption capacity and the highest mean crushing load. A study on the response of sandwich panels made of uniform (UD) and several graded density (GD) foam cores and skins produced from aluminium (AL), stainless steel (ST), and carbon fibre (CF) was conducted by Sun et al. [65]. The UD and CF were noted as having the highest specific energy absorption in comparison with the other panels, while specimens produced with GD_0.16_D were recorded as having the highest energy absorption when compared with the other panels, with less than 485 J impact, as shown in Figure 2.2.

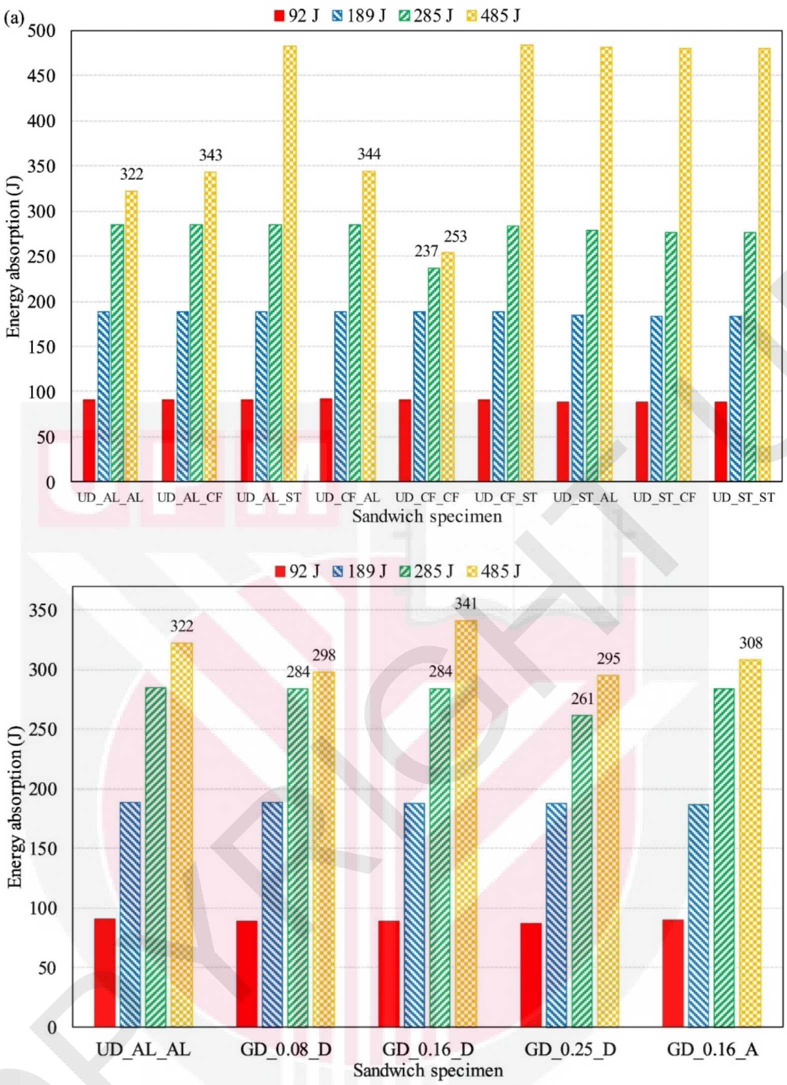

Figure 2.2: Energy absorption of sandwich panels under different impact energies: (a) sandwich panels with different face sheets and (b) sandwich panels with homogeneous and various graded foam cores [65].

2.3.2 Corrugated Core

Recent studies have shown that tremendous attention is being given to metallic sandwich structures, which are now regarded as protective structures in fields such as aerospace, marine, and transportation [66, 67]. This is because the plastic deformation absorbs the impact energy in a situation where the structure suffers from an unexpected crash. Several sandwich structures with various cores, such as foams [68], honeycomb [56], and truss [69], were recommended by scholars to make the structures more crashworthy.

Dayyani et al. [70] proposed that corrugated structures would have an impact on engineering applications. This is because they have exceptional structural characteristics, including extreme anisotropic behaviour and high stiffness-to-weight ratio, resulting from their geometric properties.

Several experimental and numerical studies on the quasi-static or dynamic behaviour of sandwich structures have been carried out. A trial of an aluminium honeycomb-corrugation hybrid core sandwich construction was performed by Han et al. [71]. This led to the combination of aluminium honeycomb with corrugated aluminium that resulted in appreciably enhanced compressive strength and absorption of energy, mainly in the low-density regime. Zhang et al. [72] explored the effect of varying thicknesses on the dynamic behaviours of sandwich steel plates and graded corrugated cores. They considered three different core arrangements of sandwich plates with identical core density: BBBB, AACC, and ABBC, where A referred to 0.762 mm, B referred to 0.508 mm, and C referred to 0.254 mm. The results and elucidation revealed that the ABBC absorbed the smallest plastic energy in the back substrate and the most in the core. In addition, Hou et al. [73] carried out a number of experimental studies and numerical simulations on multilayered corrugated sandwich panels under quasi-static crushing loading conditions. The study concluded that there was an extension of the plateau stage, as well as that the addition of more layers led to an increasing value of energy absorption before densification.

A comparison of the specific compressive response of composite corrugation cores, conventional honeycomb, and foam materials was investigated by Rejab and Cantwell [74]. They reported that the compressive components of thick corrugated cores were like those of aluminium honeycomb. Furthermore, Yan et al. [75] noted increments in the compressive strength and energy absorption capacity of a hybrid sandwich by 211 % and 300 %, respectively. Meanwhile, an increase in value for specific energy absorption by 157 % was caused by a foam filling into the empty corrugated sandwich core. Similarly, Damghani and Gonabadi [76] assessed the role of foam-core relative density on the impact properties of sandwich panels. They discovered that an increase in the foam core would invariably lead to a rise in the impact resistance and energy absorption. In addition, Yang [77] reported that specific energy absorption was partly dependent on the thickness of the corrugated core layer. Moreover, a study on scaling effects in the compression response of sandwich structures was carried out by Zhou et al. [78]. In the study, the authors used both carbon and glass fibres, as well as varying the corrugation thickness and the number of unit cells. The results showed that the tested cores had no notable scaling effects, and as the corrugation got thicker, the compression strength was increased.

2.3.3 Honeycomb

Honeycomb refers to a lightweight structure that requires a number of cells to be fused together to form a structure. Aluminium, Nomex, or thermoplastics, such as propylene, are examples of materials used for honeycomb structures [79]. As previously reported, it was shown that hexagonal honeycomb structures offered an outstanding mechanical performance, allowing them to be used as sandwich core structures [80, 81].

Furthermore, as noted by Côté et al. [82], the presence of bonded skins affected the compressive response of the core with a relative density of 0.20, more than the cores with 0.03 and 0.10 relative densities. They also made a comparison between steel square honeycomb and aluminium hexagonal honeycomb. The hexagonal honeycomb showed lower peak stress and increased rapid softening and exceeded the peak load when compared with the square honeycomb.

In addition, the compressive properties of composite sandwich structures with a grid-reinforced honeycomb core were studied by Sun et al. [83]. Here, they used a honeycomb core, a grid core, and a combination of the two cores. The report showed that the combination of the cores exhibited an increased stiffness, as well as better energy absorption and critical load. This can be observed when comparing it with the honeycomb core and the grid core individually (see Figure 2.3).

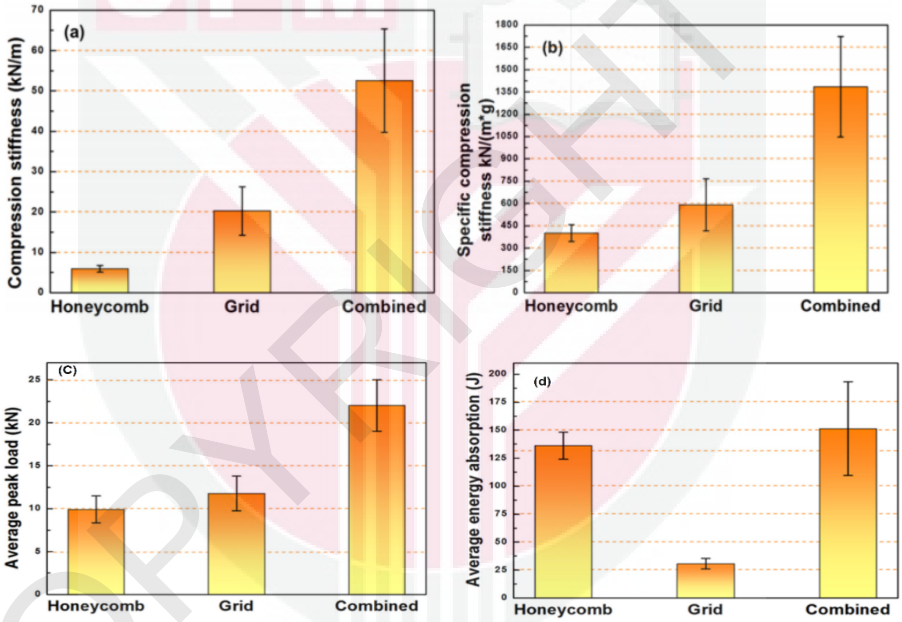

Figure 2.3: Average properties of sandwich specimens: (a) compression stiffness, (b) specific compression stiffness, (c) peak load, and (d) energy absorption [83].

Furthermore, Xiong et al. [84] also examined an egg honeycomb grid core and a pyramidal honeycomb grid core regarding their compression and energy absorption. An assessment of these carbon fibre-reinforced honeycomb cores showed that the advanced honeycomb core exhibited higher energy absorption than the lightweight square honeycombs of equal density, as shown in Figure 2.4.

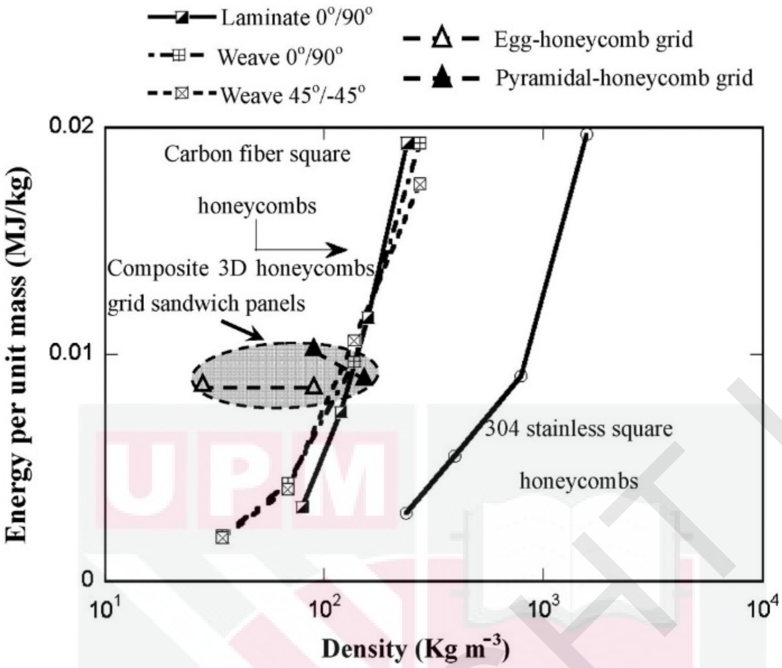

Figure 2.4: A comparison between the energy absorption capacities per unit mass of competing metallic and composite grids sandwich panels, as reported in [84].

2.4 Fabrication Process of Core Structure

Table 2.3 presents the number of the fabrication processes of composite cores. It is seen that the sandwich core structure could be fabricated from NFCs to produce good quality and more robust products. Even so, the fabrication of the NFC core is quite challenging. To ensure the NFC cores are well fabricated, the parameter settings must be optimised to eliminate any possible defects. In general, injection moulding and compression moulding are among the suitable manufacturing techniques to fabricate the core of the sandwich structure. Recently, zaman et al. [85] developed a thin-walled structure using NFCs via injection moulding, which has the potential to be used to manufacture cores for sandwich structures. Some studies also put out that NFC core could be associated with several issues, such as porosity and uneven wall thickness.

Table 2.3: Core fabrication techniques

Type of Materials	Fabricating Process	Parameter Control	Refs.
Synthetic composites	Injection moulding	Hexagonal core geometries (lengths of cell walls, wall thickness, and the internal cell angle)	[86]
Synthetic composites	Pre-preg	Geometries	[87]
Synthetic composites	Hand lay-up	Temperature loadings	[88]
		Corresponding thermal strains and stresses	
NFCs	Compression moulding process	Core geometries	[89]
NFCs		Material	[90]
Synthetic composite		Process (forming temperature, speed, and the forming angle)	[91]
		Geometry of core	[92]
NFCs	Solidification	Weight	[93]
		Geometry	[84]
NFCs	Hot press process	Temperature	[94]
		Pressure	
Synthetic composites		Consolidation time	

Even though the NFC core technology is still in the infancy stage to identify its capabilities, many studies have been conducted to manufacture NFC cores using the compression moulding technique to solve the porosity issues. Even so, the main disadvantages of fabricating via compression moulding are de-bonding of the cell wall interface, buckling of the cell wall, and fracture. Stocchi et al. [93] compared NFCs honeycomb core properties from two different manufacturing processes. Jute fibre-reinforced vinyl ester composites were used to manufacture honeycomb cores by moulds with fixed inserts and lateral compression. The honeycomb core fabricated from lateral compression had higher performance due to the technique that removed excess resin and air. On the counterpart, the lateral compression technique entailed additional time to produce hexagonal cores. Rao et al. [95] found that sinusoidal cores and hexagonal cores from sisal fibre-reinforced polypropylene composites were higher than commercial cores using compression moulding and roll forming methods in terms of specific modulus and strength. Table 2.4 depicts the summary of the specific mechanical properties of the sisal-polypropylene core.

Table 2.4: Specific mechanical properties of sisal-polypropylene core [95].

Material, Cell Size (mm)	Density (kg/m³)	σ/ρ(Nm/kg)	τ/ρ(Nm/kg)	E/ρ(Nm/kg)
Sisal-Polypropylene sinusoidal core (≃ 12)	49(±12.0)	52.56×10^3	12×10^3	1.82×10^6
Sisal- Polypropylene hexagonal core (≃ 12)	37(±3.0)	56.04×10^3	10×10^3	1.73×10^6
Nomex (phenolic) (≃ 10)	48(±3.0)	45.83×10^3	27×10^3	2.29×10^6
Aluminium (5056) (≃ 10)	151(±7.6)	41.89×10^3	32×10^3	10.54×10^6
Polypropylene core (≃ 6)	145(±3.2)	25.27×10^3	8×10^3	0.80×10^6

In addition, the fabrication of flax fibre reinforced with linear low-density polyethylene (LLDPE) composites was conducted via compression moulding to form a corrugated shape [90]. The process was initiated by the layering process of dry flax fibre mat and LLDPE film in a moulding slot and ended with compression action at 170 ^oC. However, Rao et al. [95] implemented the extrusion process to produce a better-corrugated sheet than the previous compression moulding technique. This was due to the increase in edge constraints. Apart from those mentioned techniques, a flax fibre-reinforced polylactic acid (PLA) composite honeycomb core was also manufactured by Zuhri et al. [89] using the slotting method. In the first place, the composite was prepared by the lamination process to form a sheet. Later, the square and triangular honeycombs were produced by the slotting technique. The research was supported by FEA results to show that progressive failure could happen within the honeycomb design slots. Thus, the fabrication technique of NFC cores plays a significant role in producing higher-quality sandwich structures.

2.5 NFC material characterization

Natural fibres have various origins, and as such, their characteristics differ, disallowing their use in recent structures. According to Nishino et al. [96], factors that determine their properties, such as shape, strength, and size of natural fibres include their place of origin, maturity, retting process, and the cultivation environment. This variation will also cause complexity in the properties of the natural fibre composite. The variation in the characteristics of NFCs means that each has its own strengths and weaknesses. Hence, a proper design that involves the hybridisation of two different cellulosic fibres portends excellent enhancement of the properties of the hybrid composite. Due to their cellulosic nature, this type of hybrid fibre composite provides more flexibility and serves as a better economical choice [97]. Despite their advantages, some factors might hinder the natural fibres' performance during the hybridisation process. These include fibre loading, fibre selection, fibre form, fibre orientation, fibre arrangement, matrix selections, porosity, and interfacial strength [98-103].

The hybridisation effect of NFCs to improve their mechanical properties has become an area of interest to researchers in recent times. For instance, Alavudeen et al. [104] presented a study on the mechanical properties of kenaf/banana hybrid composites. It was shown that the kenaf/banana composites offered better mechanical properties compared to the individual fibre-based composites. In a similar study by Venkatesh et al. [105], the addition of bamboo fibre to sisal-unsaturated polyester composites enhanced their mechanical properties compared to the sisal-unsaturated polyester composites on their own**.** Moreover, Wu et al. [106] hybridised silk fibre with flax fibre and studied their mechanical properties. The study showed that the hybrid exhibited excellent flexural and impact strengths over that of other NFCs. In addition, an examination of the mechanical properties of sisal and banana fibre-reinforced polylactide acid (PLA) composite was carried out by Gupta et al. [107]. According to their study, the treated fibres gave better mechanical properties than pure PLA and untreated fibre bio-composites.

In recent times, a few researches have been carried out on the hybridisation of natural fibres in composite manufacturing with respect to their energy absorption characteristic. For instance, an examination of external basalt layers' influence on the mechanical degradation of flax composites when situated in critical environments was performed [108]. They reported that the external basalt laminate when added to a flax composite, improved mechanical stability in the static and dynamic loads. Flax-based composites were able to increase their energy absorption capability with their increasing ageing time;

meanwhile, the hybrid of the basalt and flax was unable to vary their impact strength significantly. Similarly, Živković et al. [109][120] analysed the effect of moisture absorption on the impact properties of basalt, flax, and hybrid of flax/basalt fibre composites under both dry and conditioned states. The authors observed significant energy-absorbing improvements for hybrid composites compared to those single composites counterparts, especially in conditioned samples. On the other hand, Senthil Kumar et al. [110] examined a hybridisation of banana and coconut fibres and the effect of their layering pattern. The individual composites and their hybrids were compared, and the results showed that the coconut fibre as the outer layer exhibited the utmost damping behaviour and, therefore, better energy absorption capability.

In addition, Wu et al. [106] investigated a hybrid of flax and silk fibre-reinforced composites. It was reported that when compared with the individual composites, this hybridisation increased energy absorption. In another study, it was found that hybridisation of ramie/jute fibre-reinforced composite with a volume fraction of ramie fibre about 55 % improved the energy absorption and impact resistance compared to individual fibre [111].

2.6 Methodology standards

Presently, various industries encounter a broad array of testing techniques for evaluating material characteristics. ISO standards have gained acceptance within the European Union and most European nations. Nevertheless, the more comprehensive ASTM International standards enjoy global utilization across multiple sectors, primarily due to the relatively constrained test procedures within ISO [112]. It's important to note that, often, both ASTM and ISO standards are designed to achieve identical testing goals but diverge in the technical methodologies employed, thus rendering the test results from the two methods not directly commensurable [112]. In the literature, ASTM standards play a vital role in the field of materials science and engineering, particularly in tensile and compression testing. Notable standards include ASTM E8 for metallic materials and ASTM D638 for plastics, which are crucial for characterizing tensile properties. For compression testing, ASTM E9 guides the evaluation of metallic materials, while ASTM C39 focuses on concrete specimens. Additionally, standards such as ASTM D695, ASTM E74, ASTM E139, ASTM D1621, ASTM D1623, and ASTM D7078 are employed to assess the mechanical properties of various materials, including rigid plastics, thin plastic sheeting, non-metallic materials, rigid cellular plastics, and composite materials[113].

As for polymers and polymer composites tensile testing is carried out in accordance with standardized procedures, such as ISO 527-4, ISO 527-5, ASTM D 638, ASTM D 3039, and ASTM C 297. These tests generate stress-strain diagrams that are essential for determining the tensile modulus. Tensile testing also provides data on tensile strength (at yield and at break), tensile modulus, tensile strain, elongation, and the percentage of elongation at yield, as well as at break[114]. While there exist inherent disparities between the ISO 527-2 and ASTM D638 methodologies for polymers, it's worth noting that the test results may align, and contingent upon the specific material being examined [112]. Furthermore, for compression testing, the relevant standards are ASTM D695, ISO 604, ASTM D3410, ISO 14126 and ISO844[115] are specialized standards designed for the in-plane compression of fibre-reinforced composites, offering measurements for compressive modulus, compressive yield stress, compressive strength at failure, and compressive strain at failure [114, 116].

2.7 Mechanical Properties of NFC Core Sandwich Structures

Natural fibre composites in engineering applications have increased in recent years due to their advantages over conventional mineral fibre composites. The benefits include low density, high specific strength, increased toughness compared to glass fibre, increased sound absorption, improved biodegradability, environmentally cleaner, and rapidly renewable [117]. Several natural fibre-reinforced polymer composites have been studied recently to be used in sandwich structure applications. The natural fibre composite is used as both skins and core materials for sandwich panel constructions. For example, Du et al. [118] investigated sandwich panels containing paper-reinforced polymer (PRP) composite as skin material and natural fibre incorporated into the structure as a core. The authors claimed that the cell size and height of the honeycomb core had greatly affected the mechanical properties of the sandwich structure. The findings indicated that the sandwich structure studied here can replace the existing commercial products. In a recent work by Du et al. [119], they produced bio-based sandwich-structured composites with both skin and core materials made from biofibre and polylactic acid (PLA) matrix. Then, subsequently, an assessment of the flexural properties and failure modes of the structures was carried out. The results showed that 50 % of fibre had the highest compressive properties, and thus, the flexural properties and failure mode of the composites met the automotive load floor requirements. Stocchi et al. [93] fabricated a novel honeycomb core made of jute-reinforced vinyl ester composite manufactured by lateral compression moulding. In contrast to the commercially available cores, the developed cores possessed high compression strengths. Furthermore, Petrone et al. [90] developed an eco-friendly honeycomb core for sandwich panels by combining flax fibre with polyethylene matrix; the analyses involved both reinforced and un-reinforced cores. The authors reported a significant improvement in reinforced cores (continuous-unidirectional and short-random) compared to un-reinforced ones in terms of mechanical properties. In addition, improvement in damping value was also achieved by filling the core with wool fibre, resulting in minimal weight increment. More works and investigations on the mechanical behaviour of natural fibre were reported in [120].

Manipulating the core material and its design can change the behaviour of the sandwich structure, both in terms of compression and impact properties. For example, Jusoh et al. [121] stated that more experimental works should be conducted on the corrugated core sandwich structure made of natural fibres. It is evident that, based on the information in the literature, the type of core materials can significantly alter the overall properties of the composite. This can be seen in recent work done by Zuhri et al. [89], where two different types of flax-based core structures were compared. The core materials were flax/polypropylene (flax/PP) and flax/polylactide (flax/PLA); the finding showed that sandwich structure with flax/PP core offered higher strength and excellent energy-absorbing characteristics over those offered by the flax/PP core, (see Figure 2.5).

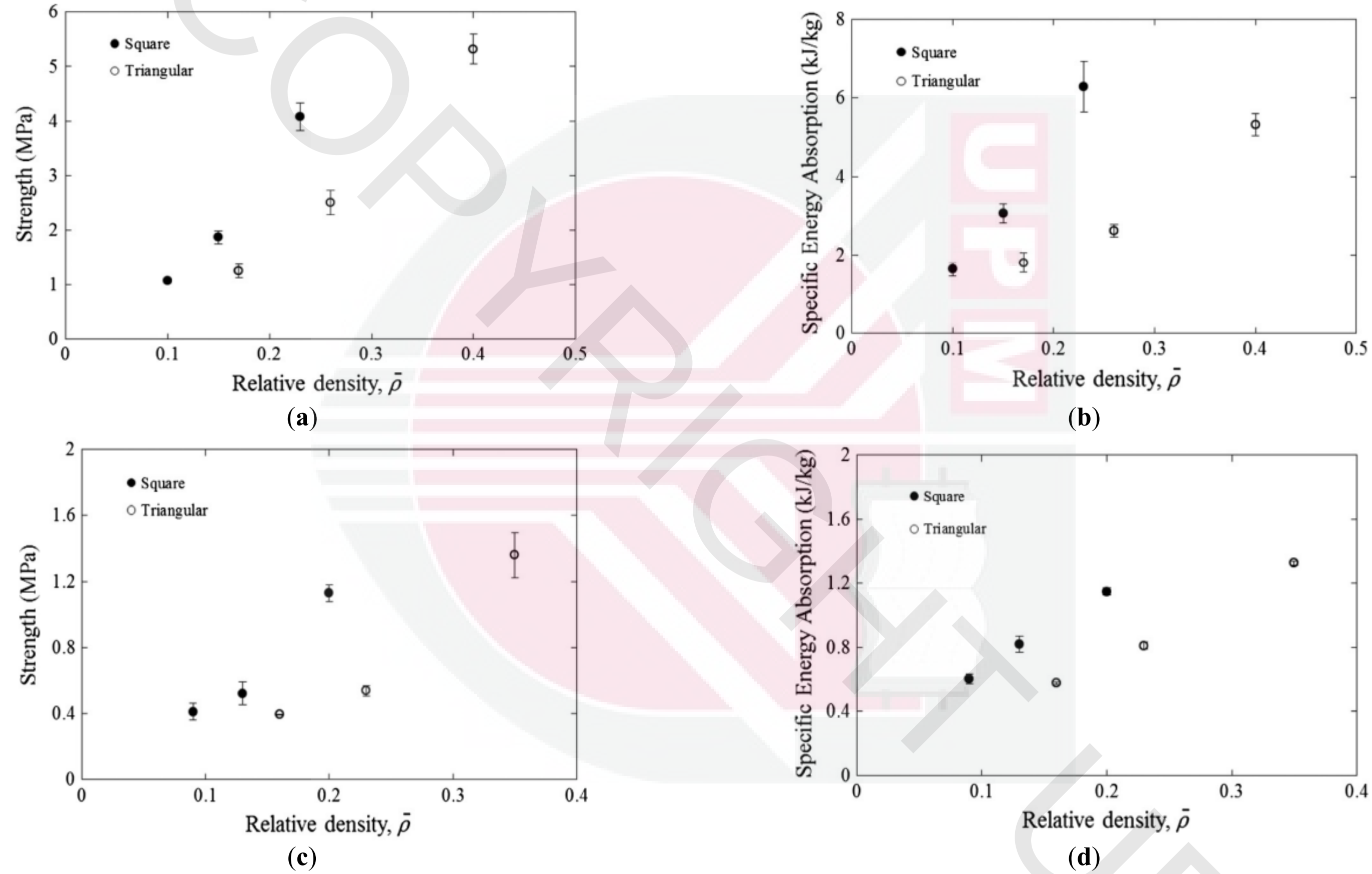

Figure 2.5: The compression strength and energy absorption of (a, b) flax/PP and (c, d) flax/PLA interlocking structures [89]

Also, a comparison of the capacity of bamboo and foam as core materials was investigated by Zuhri et al. [122]. The results revealed that the energy-absorbing capacity of the bamboo structure increased as the diameter-to-thickness ratio decreased. Moreover, the combination of bamboo-foam composite structure offered higher energy absorption capacity than the sum of the individual foam and bamboo, which was due to the constraint of the foam. In a similar study, eco-friendly corrugated cores made of flax fibre, combined with polyethylene matrix, were studied under a low-velocity impact [90]. The authors reported that continuous fibre reinforcement polymer gave better results than short fibre composite in response to impact loading. The presence of skin increased energy absorption because of energy dissipation. However, Petrone et al. [90] studied polymeric honeycombs reinforced with short and continuous flax fibre. They concluded that the energy absorption was increased with the core thickness, and the effect of the presence of skin on the energy absorption was minimal. In addition, sisal fibre reinforced with polymer matrix in the form of core structures was investigated by Rao et al. [95]. The design of the core significantly affected the properties of the sandwich structure. A similar result was found in a finding by Roslan et al. [123], who carried out a compression test on the square and triangular honeycomb core structures based on bamboo/epoxy composite. The different designs of cores had varying capabilities of specific energy absorption. Therefore, it was evident, based on the data, that the core made of natural fibre-reinforced composites can offer an excellent result. Table 2.5 summarises selected papers on the development of cores from natural fibres.

2.8 Cone calorimeter properties of sandwich structure

Sandwich panels are used in many aircraft interior applications, such as floors, sidewalls, ceilings, and storage compartments. These types of sandwich panels may be used in similar applications in other types of transport vehicles. Due to the need for more environmentally friendly materials, natural fibre composites are regaining the attention that has once been shifted to synthetic products. Although synthetic fibre composite materials, such as glass fibres, carbon fibres, and aramid, are high-performance materials, they are questionable when cost and environmental concerns come into consideration. Studies have indicated that sandwich structures containing natural fibres such as flax may be a viable alternative to synthetic fibre as a reinforcement in polymer composites due to improvement in their mechanical properties [57, 124, 125]. Although the mechanical properties of sandwich panels made of natural fibre have been invested in a wide range recently, less work has been done on their flammability properties, which has recently become a major issue in a wide range of industries, including aerospace, transportation, and construction [126, 127]. Research on fire reactions of the sandwich structure under cone calorimeter has been reported extensively in the literature; for example, Najmi et al. [128] conducted the fire reaction to Nomex honeycomb, which was later sandwiched with glass fibre composites. The authors reported that the top skin of the sandwich structure played an important role in delaying the ignition time. Furthermore, painting the skin of the sandwich structure offers excellent resistance to volatile gases escaping from the composites. Other studies reported that the ignition time was affected by the initial mass of the samples tested [129-131]. In addition, Makovicka et al. [129] stated that treated composites by fire retardant (FR) take a longer time to burn in comparison to untreated composites; however, other properties remain the same. A recent study on flax/PLA and flax/PP composites was done by Pornwannachai et al. [132, 133], where authors revealed that adding FR to flax/PLA and flax/PP composites increased fire resistance to some level, but increasing FR above 0.9 % might have an adverse effect on their fire performance. Furthermore, FR has reduced the mechanical properties of the composites, and this loss was more severe in flax/PLA than in flax/PP; a similar conclusion was made by Kandare et al. [134]. In a similar study by Kandare et al. [135], the authors stated that treated flax/PLA composites had lower flammability than flax/PP composites due to the interaction of the FR with flax/PLA during the thermal decomposition and no chemical interaction with flax/PP. Furthermore, Dutta et al. [136] studied the influence of flax/PP composite orientations on fire performance, such as ignition temperature, burning time, and heat release rate. According to the authors, increasing the sample's angle increased the critical heat flux; however, increasing the sample's angle to equal to or greater than 60° made it insensitive, making the sample difficult to ignite. The time to ignition, on the other hand, did not vary significantly across sample orientations. In addition, the orientation of the cone heater (horizontal (H) and vertical (V)) and fibre type had a significant effect on the composite fire performance [137]. Extensive work on the fire performance of laminated composite structures based on natural fibre was reported [135, 138-144]. However, the majority of this work was in laminated composites, with a relatively little study on the cellular core of sandwich structures made of natural fibre [145, 146]. In today's market, biodegradable core materials for sandwich structures are in high demand, and structural analyses have been conducted for decades. However, to date, investigations on the fire performance of various cores and sandwich structures have received very little attention. The current research focuses on an experimental evaluation of the fire reaction of two sandwich core shapes, square interlocking, and honeycomb core structures.

2.9 Summary

Natural fibres reinforced polymer composite materials are replacing synthetic materials to a great extent due to their eco-friendly, non-toxic, and biodegradable nature. This thesis explored the potential use of natural fibre-based composite to be applied in the sandwich structures application. A brief overview of the classifications of cellular materials as cores for sandwich structures, e.g., cellular foams, corrugated, and honeycomb cores, is given. An assessment of the individual fibres, as well as a combination of two fibres, are reviewed. Also, the mechanical behaviour of the fibres under static and dynamic loads is discussed. The following research conclusion can be made as: 1) limited emphasis on natural fibre-reinforced composites: most existing research has primarily concentrated on improving the performance of synthetic fibres and hybrid composites with natural fibres, particularly in terms of their dynamic and static load-bearing capabilities. However, there is a notable lack of comprehensive investigations into the mechanical characteristics of sandwich structures exclusively made of natural fibres, 2) neglected focus on natural fibre composites (NFC) characterisation in sandwich structures: the current research landscape has predominantly directed its efforts towards characterising NFC materials themselves. Consequently, there is a significant research gap in the analysis of the mechanical properties of sandwich structures made solely from natural fibres. Understanding how NFCs perform within sandwich configurations is essential for various applications and industries, and 3) understudied area of fire performance in sandwich structures: another critical research gap lies in the evaluation of the fire performance of various core materials and sandwich structures. While research on the fire resistance of materials, in general, has garnered some attention, there is a significant deficiency in exploring the fire reaction of specific core shapes commonly employed in sandwich structures, such as square interlocking and honeycomb cores. Investigating the fire performance of these core types is essential for enhancing safety in applications where sandwich structures are used. Therefore, experimental studies of sandwich core shapes, square interlocking, and honeycomb core structures on their mechanical and fire reaction are still active fields of research. Table 2.5 summarises selected papers on the development of core structures from natural fibres.

Table 2.5: Summary of selected papers on the natural fibres-based core developments.

Author	Mechanical Test	Design/Parameter	Finding
Stocchi et al. [93]	• Compression test • Flexural modulus	• Honeycomb core • Fixed inserts (6 mm cell wall) • Lateral insert (10 mm cell wall)	• Lateral-based compression had better results with the capability to produce thinner walls and remove excess resin, including trapped air bubbles. • Resulted in cores with the same specific compression strength but higher compression strength compared to commercially available counterparts. • Specific: 0.085MPa/Kg and 0.05MPa/Kg for 6 mm and 10 mm cell cores, respectively. • 6mm-cell core with 15.5MPa; 10mm-cell core with 13.5 MPa. • Flexural modulus for 10 mm-cell core: higher dispersion of about 40 % than mean value (115.48±1.35 MPa).
Rao et al. [95]	Four-point flexural tests	• Sinusoidal core • Hexagonal core	• Sinusoidal core (6.5 MPa) higher than hexagonal core (5.2 MPa). • Static failure stress (40 %).
Zuhri et al. [89]	Compression test	• Square core • Triangular core	• Core design and specific strength. • 2 mm thickness: square possessed higher strength than triangle cores (flax/PLA). • 2.3 mm thickness: triangle core possessed higher strength (flax/PP). • Square structure offered better strength and energy absorption characteristics than triangular structure.
Du et al. [119]	Creep test	• Relative humidity (20–50%)	• Static failure stress (40 %)
Chen et al. [147]	Flexural creep test	• Expanded core (31.75 mm) • Corrugated core (19.05 mm)	Creep flexural deflection rates. • Expanded honeycomb characterised by higher rates compared to corrugated honeycomb cores.

Table 2.5: Continued

Roslan et al. [123]	Compression test	• Triangle core • Square core Configuration setup • 0-degree orientation • 45-degrees orientation • 90-degrees orientation	Triangular core superior to its counterpart with higher energy absorption rates and/or capability, and hence desirable in strength and stability applications.
Oliveira et [148]	Three-point bending test	• Bamboo core with different dimensions • Aluminium skin sheets	• Sandwich panels with 30 mm bamboo rings exhibited greater strength, modulus, and skin stress. • Sandwich panels with 20 mm bamboo rings have a higher shear stiffness and resistance. • Sandwich panel with aluminium skin showed a clear debonding failure.
Shuguang Li et al. [149]	Compression test	• Single- and double-layers corrugated lattice sandwich structures made of jute. Configuration set up: • 90/90 • 45/45	• The fibre angle and length-to-diameter ratio of the struts had the most significant influence on the mechanical properties of the structure of the single layer. • 90/90 had better compressive strength and modulus than 45/45 fibre orientation by around 83 % and 60 %, respectively. • The two-layer structure's compression performance significantly influenced by the design of the core and the existence of the intermediate support plate. • The compressive strength and Young's modulus increased by 75 % and 27 % due to the middle plate.
Chanda et al.[145]	Cone calorimeter test	Flax/PLA, core structure • Corrugated • Honeycomb	Honeycomb with open cell has a better performance than corrugated core in terms of time to ignite (10 s) and time to peak (65 s). Both core structures had almost similar initial mass loss and heat release.

CHAPTER 3

METHODOLOGY

3.1 Introduction

In this chapter, details of the experiments conducted during the course of this study is presented. This includes the mechanical testing and fabrication techniques used to investigate the characteristics of sandwich structures made of flax/PLA composite (with and without foam). The first part of this chapter describes the materials used. It is then followed by the specimen preparation process for the various parameters investigated. The experimental arrangement adopted, including tensile and quasi-static compression testing, as well as the fire testing, are outlined. A detailed research framework is shown in the following flow chart (see Figure 3.1).

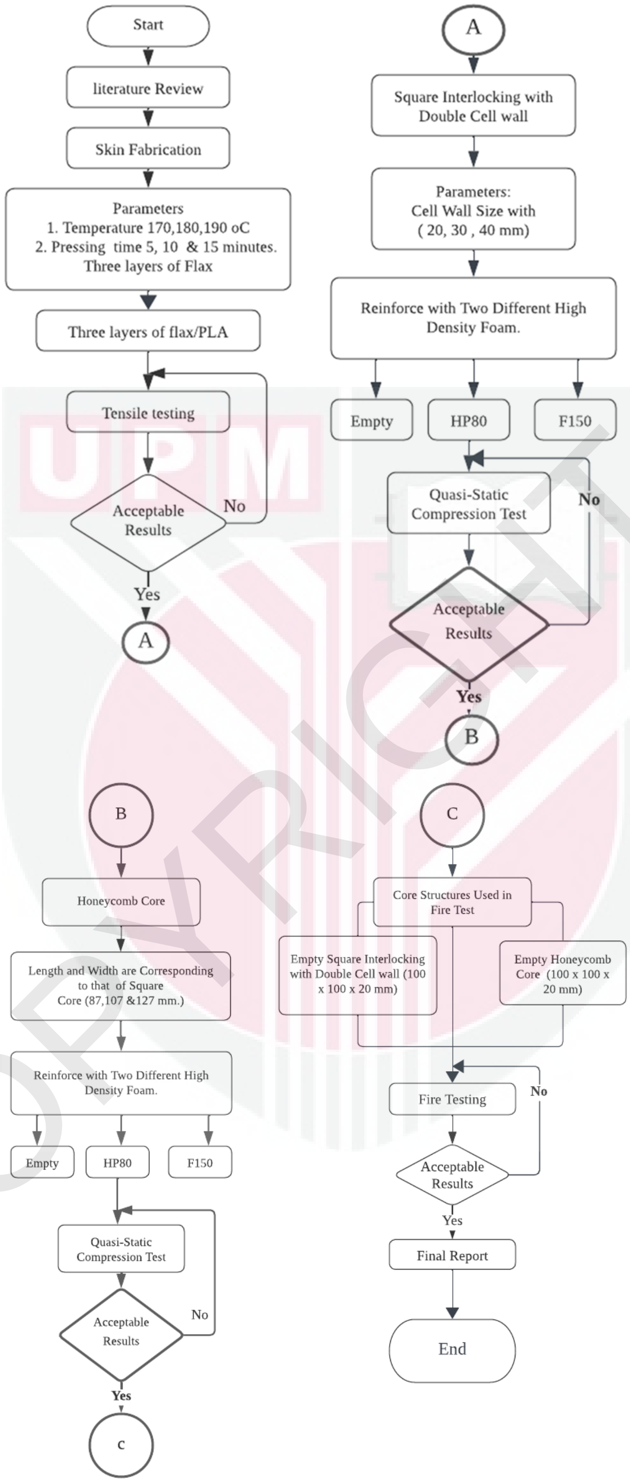

Figure 3.1: Detailed Research Framework

3.2 Materials

The materials used in this study were Biotex flax fibre, in the weave style of 2 × 2 twill and a surface density of 400 $g \cdot m^{-2}$ and biodegradable polylactic acid (PLA) film supplied by Easycomposite, United Kingdom, and PSG Group Ltd United Kingdom respectively. Epoxy adhesives (BBT-7892A resin and BBT-7892B hardener) were used to bond the double cell wall square cores to the skins. The mix ratio of adhesive used was 5:1 by weight. The epoxy resin and the hardener were supplied by Berjaya Bintang Timur Sdn. Bhd. Finally, the Divinycell HP80 and F150 PVC foams were provided by Diab Group, Sweden. These foams are closed-cell type with an average density of 80 kg/m^3 and 150 kg/m^3, respectively, with a thickness of 20 mm.

3.3 Fabrication of composite panel

To prepare the composite panels, the flax fibre, and PLA film were arranged alternately between the two identical flat platen aluminium moulds. Then, the moulds were placed under a hot press machine and pressed following the chosen manufacturing parameters reported in [89, 150-152]. Here, the temperatures used were (T_c) 170, 180, and 190 °C, while the pressing times were 5, 10, and 15 minutes for each temperature. The pressure was set to 10 bar based on the machine's capability. Next, the composite panels were taken out from the machine when it was already cooled down. The manufacturing process cycle composite laminate panel is illustrated in Figure 3.2.

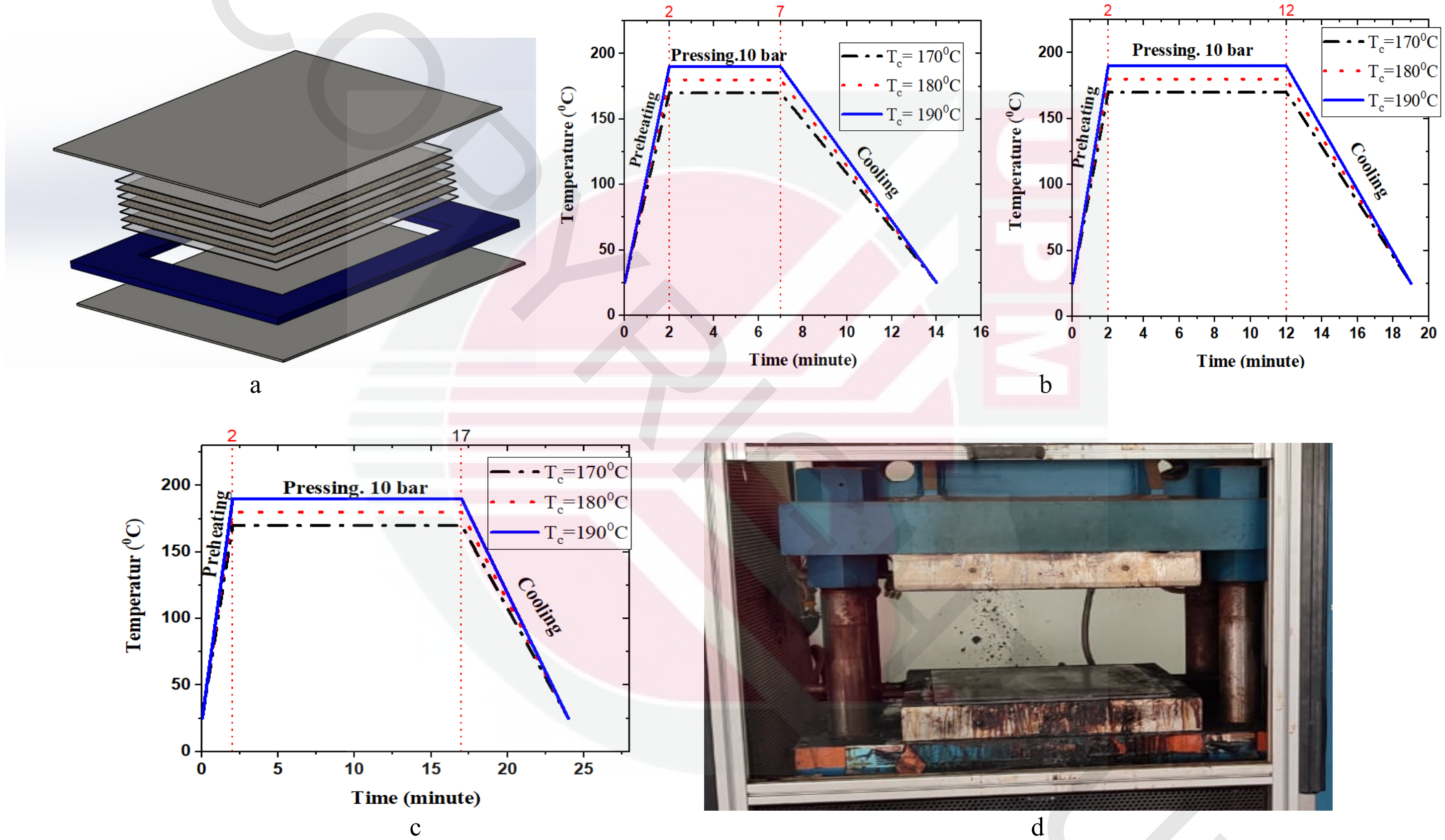

Figure 3.2: Manufacturing process cycle of flax/PLA composite

Following this, the flax/PLA composite panels were cut based on the ASTM3039 standard size for tensile testings [153]. The total specimen length was equal to 250 mm, 150 mm for the gauge length, and 50 mm for each grip length. Figure 3.3 shows the schematics diagram of the tensile specimen.

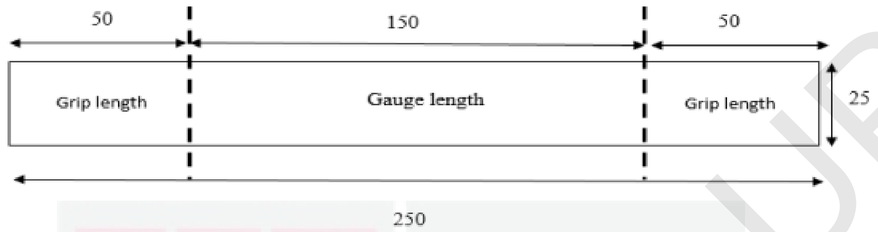

Figure 3.3: Tensile specimen based on ASTM D3039 standards

3.4 Fabrication of Sandwich Structures

3.4.1 Square interlocking core structure

Three types of double cell wall square core sandwich structures were fabricated at different stages: (a) manufacturing composite panel using hot press machine, (b) cutting of composite panel using bench saw, (c) cutting of HP80 and F150 foams, and finally (d) bonding of core to skins using adhesive material. The square core sandwich structures were fabricated with double cell walls and different cell sizes of 20 mm (SC20), 30 mm (SC30), and 40 mm (SC40).

At stage (a), a hot press machine was used to manufacture the composite panels. The composite panels were produced with an approximately 40 % volume fraction using a stacking procedure, where the flax fibre and PLA film were arranged alternately (similar as previously done in Section 3.3). Here, three plies of flax fibre and 18 PLA film plies were used. The arranged materials were placed into two-matched flat moulds with a dimension of 300 mm × 300 mm. Next, the moulds were placed in a hot press machine and pressed for 10 minutes at a temperature of 180 °C and a pressure of 10 bar. Then, the composite panels were taken out of the machine when they had already cooled down. This produced a flax/PLA laminate with a nominal thickness of 1.4 mm. Both skins and core were made using the same method with the same manufacturing parameters.

At stage (b), the composite panels produced in the previous stage were then cut into rectangular strips using a bench saw machine to fabricate the core structures. Here, a simple slotting technique was applied to fabricate three types of square interlocking cores. The overall sizes of these cores were approximately 81 x 81 x 20 mm, 102 x 102 x 20 mm, and 121 x 121 x 20 mm, representing the cell sizes of 20 mm, 30 mm, and 40 mm, respectively. The detailed design of the double cell wall square interlocking core is presented in Figure 3.4 and Table 3.2.

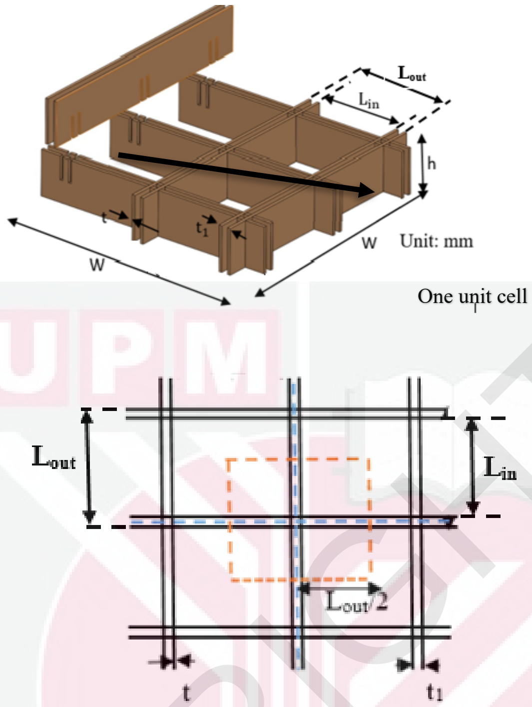

Figure 3.4: The details design of the double cell wall square interlocking cores

Following this stage, the two types of foam, HP80 and F150, were cut into blocks with dimensions of length and width equal to L_{in} and h and t_1 and h. The foam blocks were then inserted into the empty core at the centre part, stage (c). Finally, the core with foam was bonded to the skins with epoxy adhesive at stage (d). Figure 3.5 shows an example of an empty and filled-foam square sandwich structure.

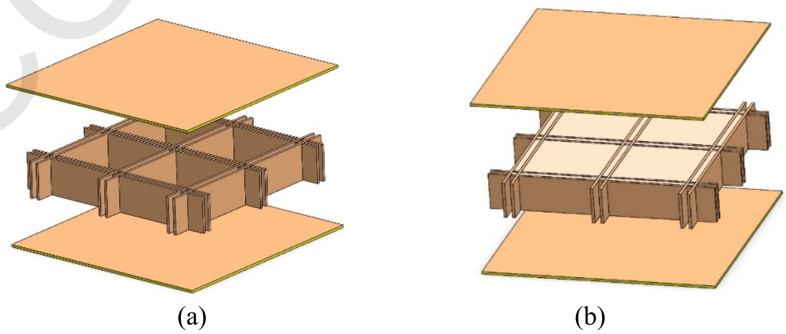

Figure 3.5: Illustration of (a) empty and (b) filled-foam of square core structure

A total of 36 samples of double cell wall square interlocking core structures were manufactured, as summarised in Table 3.1. All cores were characterised by different densities and double cell wall sizes, as shown in Table 3.2. The relative density of the core material was estimated from the proportion of the composite to the unit cell volume. The empty double cell wall square core sandwich structure relative density $\overline{v}_s$ was calculated using Equation 3.1.

$$\overline{v}_s = \frac{v}{v_s} = \frac{n\left(\frac{L_{out}}{2} - \frac{t_1}{2}\right) th}{L^2 h}$$

Equation 3.1

$$\overline{v}_s = \frac{4t(L_{out} - t_1)}{(L_{out})^2}$$

Here t, t_1, and L_{out} are defined in Table 3.2, where n represents the number of the cell wall of a unit cell, here n=8 to reduce the double-wall unit cell formula to a single wall unit cell $n = 4$ and t_1=0. For foam filled square core sandwich structures, the relative density can be defined as the average relative density $\overline{\rho}_c$, given by [154]:

$$\overline{\boldsymbol{\rho}}_c = \overline{\mathbf{v}}_s + (1 - \overline{\mathbf{v}}_s)\boldsymbol{\rho}_f / \mathbf{p}_s \quad \text{Equation 3.2}$$

Where ρ_f and p_s are the densities of foam and square core materials, respectively.

Table 3.1: Summary of the total samples square interlocking flax/PLA core structures

Core Code	Type of Core	Samples
SC20		4
SC30	Empty core(without foam)	4
SC40		4
SC20HP80	Filled with HP80 foam	4
SC20F150	Filled with F150 foam	4
SC30HP80	Filled with HP80 foam	5
SC30F150	Filled with F150 foam	3
SC30HP80	Filled with HP80 foam	3
SC30F150	Filled with F150 foam	3

Table 3.2: Dimensions of the square interlocking flax/PLA core structures and their relative densities

Core ID	Height, h (mm)	Cell size (mm)		Thickness (mm)		Relative density ($\overline{\rho}$)		
		L_{in}	L_{out}	t_1	t	Empty	Filled-foam core	
							HP80	F150
SC20	20	20	24.5	3	1.4	0.20	0.44	0.55
SC30	20	30	34.5	3	1.4	0.15	0.45	0.58
SC40	20	40	44.5	3	1.4	0.12	0.47	0.62

3.4.2 Honeycomb core structure

A trapezoidal corrugated-core mould with 45^0 profiles was used to fabricate the honeycomb cores. The measurements of the mild steel moulds were 300 x 300 mm, as shown in Figure 3.6. Each unit cell measured 10 mm in height and 20 mm in width. The female mould (lower profile) was used for placing the raw material, while the male mould (upper profile) pressed the material to create the shape of a trapezoidal profile.

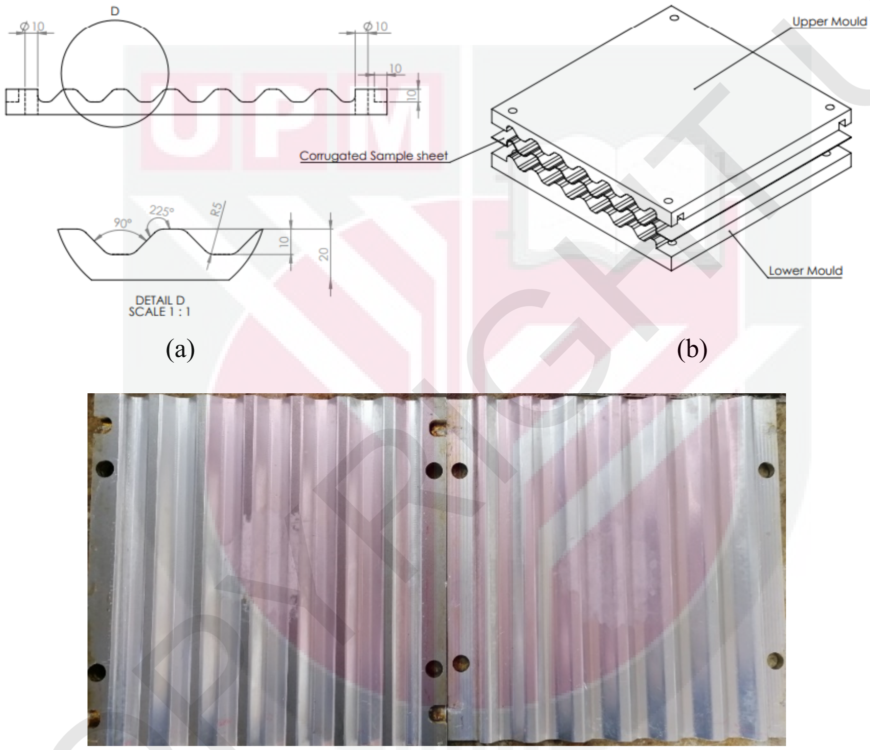

(c)

[Unit: mm]

Figure 3.6: Detailed design of corrugated mould

Initially, flax fibre and PLA film were prepared by cutting them into the required dimension, which was 300 mm x 300 mm (based on the designed moulds). The material was then arranged between the male and female moulds and later placed in a hot press machine for approximately 7 minutes under the temperature of 170 °C and a pressure of 10 bar. Then, the moulds were placed in a cooling press machine for 5 minutes. The moulds were then taken out from the cooling press to remove the corrugated core from the moulds. This yielded a corrugated core with a nominal thickness of approximately 1 mm. The summary of the fabrication process of the corrugated core profile is shown in Figure 3.7.

Figure 3.7: Fabrication process of corrugated core profile

The fabricated corrugated core profile was then cut into strips using a bench saw machine to prepare the honeycomb core. Following this, the strips were bonded using an epoxy to form the desired honeycomb core (see Figure 3.8).

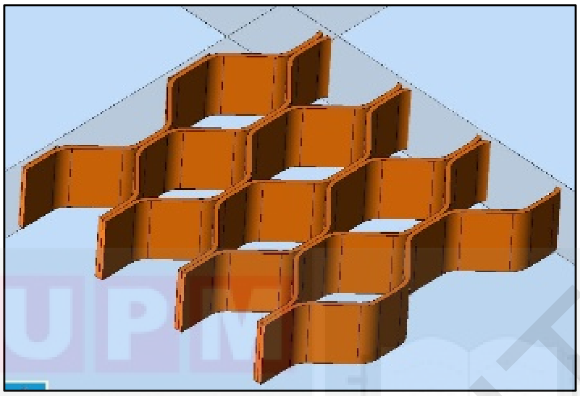

Figure 3.8: Illustration of the assembly of honeycomb core structure

Figure 3.9 shows three different lengths of honeycomb core, i.e., 80 mm (HC1), 100 mm (HC2), and 120 mm (HC3), and all having the same height of 20 mm. Notably, three identical samples for each parameter were tested for the quasi-static compressing loading.

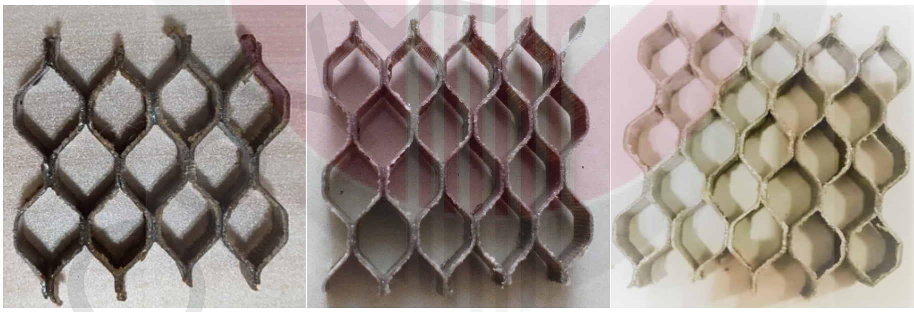

(a) (b) (c)

Figure 3.9: Schematic top view and photograph of honeycomb cores of different lengths

Later, two different high-density foams were used to assess the effect of foam on the honeycomb cores' mechanical properties. The foams were similar to that being used for the square interlocking core and presented in Table 3.1. Initially, the HP80 and F150 PVC foams were cut into the desired shape to be occupied in the empty cells (see Figure 3.10). The core and the foam were then bonded to two skins using an epoxy resin. At least three identical samples were tested for each case under the quasi-static compression testing.

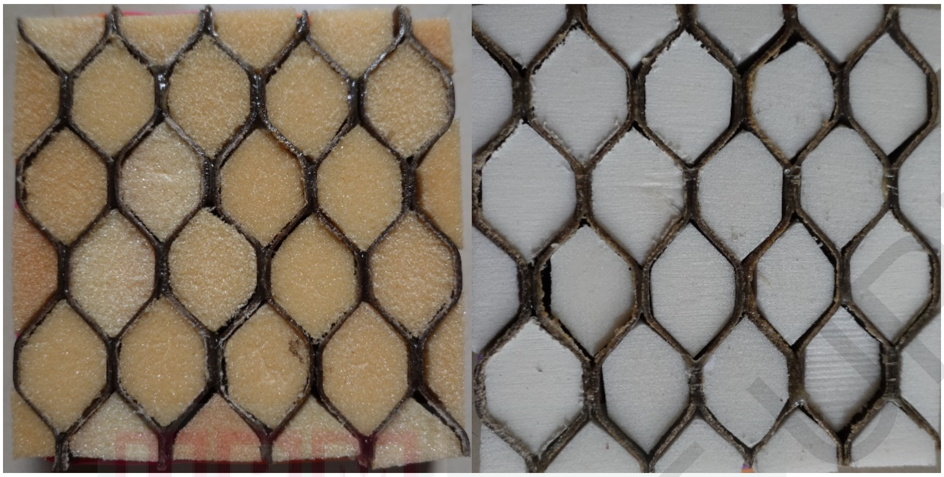

Figure 3.10: Photos of filled-foam honeycomb sandwich structure

3.5 Fire Test Methodology

3.5.1 Fabrication of composite structure

The flax/PLA was put on an aluminium mould to prepare the composite structure. The mould was then placed in a hot press machine and compressed for 10 minutes at 180 ^{0}C. Based on the machine's capabilities, the pressure was set to 10 bars. After that, the composite was removed from the machine once it had cooled down. A laminated composite with a nominal thickness of 1.4 mm resulted as a result of this process (see Figure 3.12a). Finally, the composites were cut to the dimensions 100 mm x 100 mm using a bench saw machine to construct the sandwich structure's skin. This composite panel was also utilised to create square cores as well as skins for square and honeycomb structures.

3.5.2 Fabrication of square core structure

To fabricate a square interlocking core, the fabricated flax/PLA composites presented in Figure 3.11 were cut into strips (100 mm by 20 mm) in Figure 3.11 b. A simple slotting technique was employed to prepare the double-cell all-square interlocking core, as shown in Figure 3.11 c and d. The complete fabrication process of 100 mm x 100 x 20 mm (length x width x height) square interlocking core sandwich structures is shown in Figure 3.11 d.

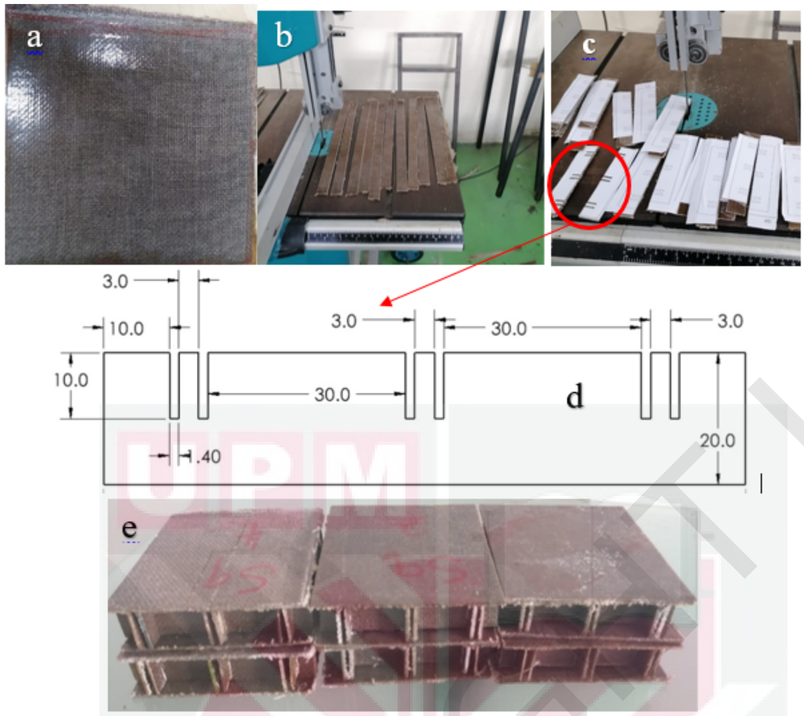

Figure 3.11: Process of fabricating square interlocking core structure

3.5.3 Fabrication of honeycomb core structure

Three layers of flax fibres and 18 plies of PLA film were first prepared by cutting them into the desired dimensions of 300 mm x 300 mm (based on the designed mould). The material was then arranged between the male and female moulds before being placed in a hot press machine for approximately 7 minutes at 170 °C and 10 bar pressure. After that, the moulds were placed in a 5-minute cooling press machine. As a result, a corrugated core with a nominal thickness of 1 mm was created. To prepare the honeycomb core of the sandwich structure, the samples were cut into strips using a bench saw machine. Following that, the strips were glued together with a 5:1 epoxy adhesive to create the desired honeycomb with dimensions of 100 mm x 100 mm x 20 mm (length x width x height). Figure 3.12 shows the complete process of fabrication of the honeycomb core sandwich structure.

Figure 3.12: Photos of the complete process of fabrication of honeycomb core sandwich structure

3.6 Mechanical characterization

3.6.1 Tensile testing

With the aid of Instron 3039 and 4505 testing machines, the tensile test was carried out at a crosshead displacement rate of 2 mm/min. An extensometer was attached to the specimen with an initial gauge length (L_g) of 50 mm. To produce accurate results, the tests were run on at least five samples. The data taken from the machine was in the form of load against displacement to calculate the tensile properties of flax/PLA composites. Figure 3.13 shows the experimental setup for the tensile testing. Equation 3.1 was used to calculate the tensile strength.

$$\sigma = \frac{P}{A} \quad \text{Equation 3.3}$$

Where P =Load (N) and A cross-section area of the specimen (m^2).

The Young's modulus (E) and strain (ε) were calculated using Equations 3.4 and 3.5, respectively.

$$E = \frac{\sigma}{\epsilon} \quad \text{Equation 3.4}$$

$$\varepsilon = \frac{\delta L}{L_g} \quad \text{Equation 3.5}$$

Where σ = strength (MPa), δL = elongation length (mm), and L_g = gauge length (mm).

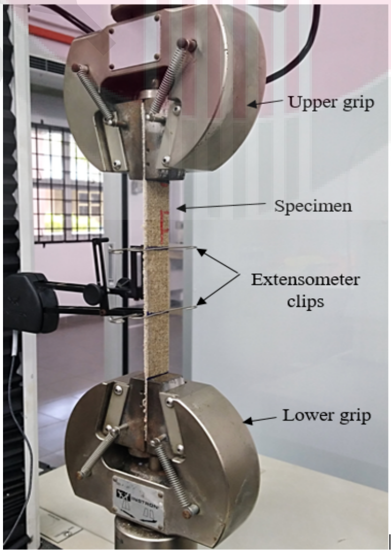

Figure 3.13: Tensile test setup

3.6.2 Quasi-static compression testing

At a crosshead displacement rate of 2 mm/min, quasi-static compression tests were performed according to the ISO844[115] standard using an Instron 4505 testing machine. The specimen was put between the two circular platens, and a load was applied to it until the structures were completely crushed (see Figure 3.14). The machine data were in the form of load versus displacement. The stress-strain value was calculated from the experimental data to calculate the compressive strength of the sandwich structures. The area under the load-displacement graph was then used to calculate the energy absorption values. The calculation here is based on the trapezoidal rule, which was been used in previous works [155]. The energy absorption capability (in terms of specific properties) was calculated using Equation 3.3 by dividing the absorbed energy values by the core mass.

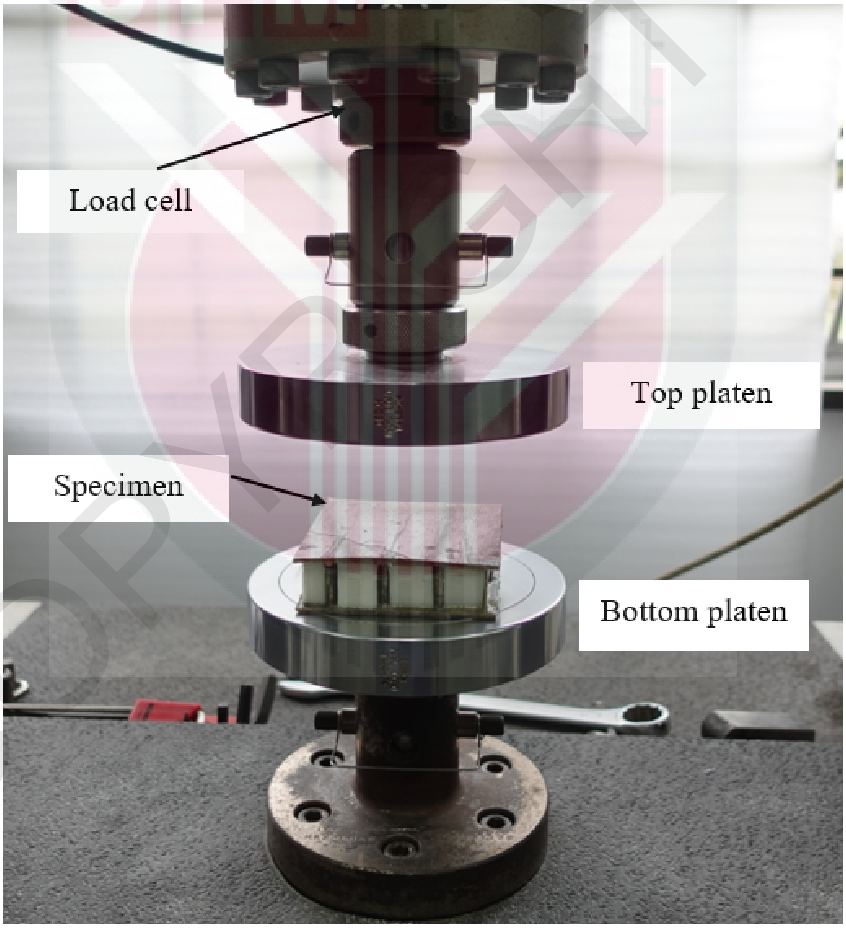

Figure 3.14: Photograph of Instron machine used for the compression test

3.6.3 Cone calorimeter testing

A cone calorimeter (FESTEC International Co., Ltd., Korea) (Figure 3.15) was employed to evaluate the combustion properties of sandwich composite structures at three heat fluxes (35, 50, and 70 kW/m^2) according to ISO5660 standard [156]. The data reported in this study included the following measurements: heat release rate (kW/m^2) (HRR), peak heat release rate (PHRR) (kW/m^2), time to PHRR (s), total heat released (THR) (MJ/m^2) and mass loss rate (%). Before testing, all the samples were conditioned at 50 % relative humidity for at least 24 h at 23 ºC [157]. The samples were tested on the standard 13 mm thick low-density refractory blanket with samples of 100 mm x 100 mm wrapped in aluminium foil to avoid heating over the samples' side. Flame-out was recorded as the flame was extinguished, and testing was stopped as the flame-out time was recorded. The heat release rate was determined based on the oxygen depletion principle, utilising the fact that heat release per unit mass of oxygen consumed was approximately independent of the type of fuel and had a value of 13.1 MJ/kg, with an error of 5 %.

Figure 3.15: (a) Cone calorimeter tester; (b) combustion process after spark [157]

CHAPTER 4

RESULTS AND DISCUSSION

4.1 Mechanical properties of flax/PLA composites

4.1.1 Influence of processing temperature

The sensitivity of manufacturing temperature and pressing time on the tensile properties of flax/PLA composites are presented in Figure 4.1 to 4.3. Tensile stress traces at three different temperatures and 5 minutes of pressing time are shown in Figure 4.1. According to Figure 4.1, all curves began to increase in a similar manner, beginning linearly stress $< 15MPa$ and continuing nonlinearly stress $\geq 15MPa$ until they reached their maximum tensile stress ($20MPa < stress < 25MPa$). Following this, the composites failed in a catastrophic manner results breaking across the flax/PLA composites samples due to a sharp drop in the tensile stress values. It is apparent that flax/PLA composites manufactured at 170 and 180 °C had a greater tensile stress of roughly 23.5 MPa than composites manufactured at 200 °C, which only had a tensile stress of 16.8 MPa. Furthermore, a composite manufactured at 170 °C had a higher failure strain of 0.16 compared to composites at 180 and 200° C, which failed at 0.07 and 0.05, respectively. A similar trend and tensile stress values were agreed with the data published in [158, 159].

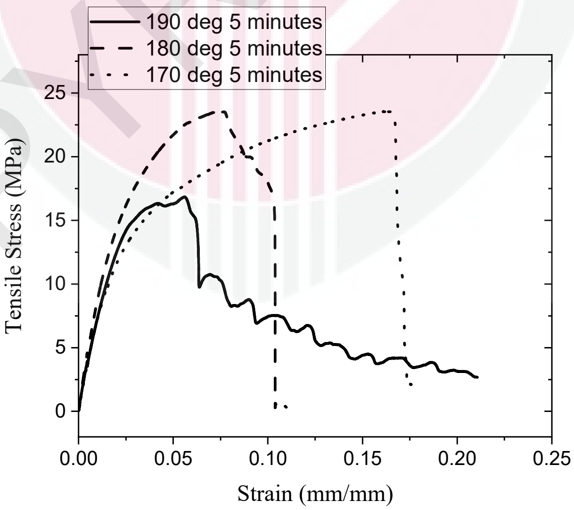

Figure 4.1: Tensile stress-strain curves at 5 minutes pressing time

Tensile stress values at 170 °C were reduced by around 17 % and the failure strain by 50 % as pressing time increased from 5 to 10 minutes (see Figure 4.2). Furthermore, Figure

4.2 demonstrated that at a temperature of 180 °C, the tensile stress showed no noticeable difference in terms of tensile stress and failure strain compared to 5 minutes of pressing time. In contrast, at 190 °C, the tensile increased by around 24 %, and however, the failure strain remained at 0.05.

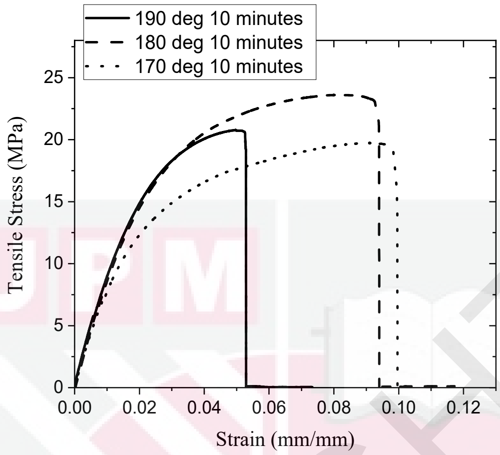

Figure 4.2: Tensile stress-strain curves at 10 minutes pressing time

Figure 4.3 presents the tensile stress-strain curves of flax/PLA composites manufactured at 170 to 190° C with a pressing time of 15 minutes. It can be observed that the flax/PLA composite exhibited a similar trend to the stress-strain curve. Here, the tensile strength at a temperature of 180 °C was slightly higher compared to the 170 °C and 190 °C, respectively.

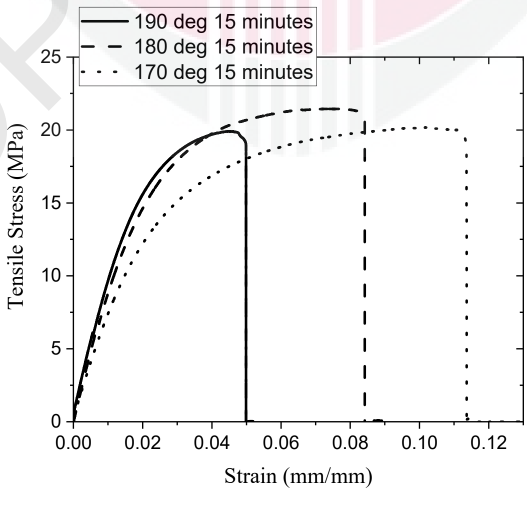

Figure 4.3: Tensile stress-strain curves at 15 minutes pressing time

On close observation, it was found that the tensile strain value decreased as the temperature increased. Table 4.1 presents the tensile properties of the flax/PLA composites. In the table, the temperature of 190 °C with a pressing time of 15 mins exhibited the highest tensile modulus of 4.07 GPa. Overall, most of the temperatures are having their tensile modulus values under 3 GPa. In a comparison between all temperatures, it was found that 180 °C offered higher strength than 170 °C and 190 °C at each pressing time. The flax/PLA composites were observed to experience a failure of fibre breakage, whereas, at 170 °C, delamination during the test occurred. These results agreed well with recent literature presented in [160-162]. They reported that the decrease in mechanical properties of flax fibre at high processing temperatures (above 180 °C) was mainly related to the evolution of the cell wall structure and organisation. Additionally, multiple failure modes involving matrix cracking, delamination, and fibre breakage were observed, while fibre breakage was the main failure mode when using high processing temperatures [161]. Hence, all subsequent square interlocking cores were manufactured at a temperature of approximately 180 °C.

Table 4.1: The tensile properties of flax/PLA composites with different manufacturing temperatures

Manufacturing Temperature (°C)	Pressing Time (min)	Tensile Strength, σ (MPa)	Tensile Modulus, E (GPa)
170	5	21.97	1.29
	10	20.68	1.98
	15	19.22	1.87
180	5	26.81	2.04
	10	23.61	2.64
	15	20.99	2.70
190	5	22.64	2.22
	10	20.77	3.23
	15	19.20	4.07

4.2 Compression properties of square interlocking core structure

4.2.1 Core without foam filling

Figure 4.4 presents the stress-strain curve of 20 mm, 30 mm, and 40 mm cell wall size of flax/PLA composite square core structures. Taking the graph for the square core structure of 20 mm cell size as an example shows the mechanical behaviour of the square core under quasi-static compression loading. Initially, the trace increased linearly with the strain up to the maximum point (or peak stress) at about 3.5 MPa. Under the linear elastic region, it was observed that the core structure deformed into a symmetrical structure at the x-axis, where a buckling shape occurred. In this case, the cell wall buckled towards the right side of the structure, and as the loading continued, the cores started to lose their stability and decrease their load-resistant capability. During this stage (nonlinear plastic), the composite materials faced their typical fibre breakages at the middle area of the cell wall. Further loading resulted in a progressive decrease of stresses between the strain of around 0.2- 0.55. Figure 4.8b shows that one side of the break cell wall had fallen into the second cell wall. The break of the outer cell wall was believed to hold the inner cell wall from having sudden failure under the plastic region. Finally, the continued force caused the structure to reach its densification stage, which means it completely failed. The images of failure deformations are shown in Figure 4.8. The flax/PLA composite core structures failed into a few failure types, such as buckling and their typical fibre breakage. An inspection of the failure modes throughout compression loading revealed that all specimens tested had similar failure; buckling to fibre breakage of the vertical double cell walls.

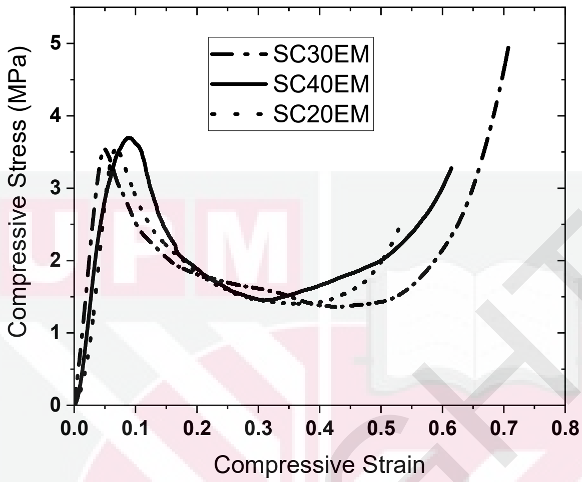

Figure 4.4: Compressive strain-compressive stress curves of empty square core structure with three different cell sizes

4.2.2 Effect of foam filling

To demonstrate the effect of foam filling in the core structures, the stress-displacement curves for empty and foam-filled sandwich structure cores are plotted in Figure 4.5 to Figure 4.7, and related images referring to the stress-strain curves are shown in Figure 4.8. As can be seen in Figure 4.8, in both cases, the deformation pattern and the failure mode due to crushing were almost identical. However, the presence of foam in the core, on the other hand, clearly reduced the local densification. Furthermore, Figure 4.5 indicates an initial non-linear response upon loading. This might be due to skins not being completely parallel to each other, then stress-strain curves increased linearly until the peak stresses were achieved. Following this, some of the core walls bent slightly (local buckling), subsequently reducing the strength of the core structures. As the compressive loading continued, the stress then dropped suddenly to a very low level due to the buckling of core cell walls. However, the stresses of the foam-filled core structure dropped after it reached the peak load and were much smaller than the empty sandwich structure core (Figure 4.6 and Figure 4.7). The response of the samples then became increasingly nonlinear, with the compressive loading gradually decreasing as the sandwich lost stability due to simultaneous local buckling and delamination between the sandwich skin and core, which later propagated to become a buckling failure all over the cell walls of the sandwich cores. Finally, cell walls continued to fold until the sandwich was fully densified, resulting in debonding between the skins and the core at the sample edges in the majority of the sandwich structures.

Overall, cores filled with F150 foam outperformed the empty and cores filled with HP80 foam counterparts by different percentages. Due to the fact that the F150 had a higher density than its counterpart, it needed a higher load to break, as can be seen in Table 4.2. For example, Figure 4.5 shows that the SC20F150 core panel had a strength of 8 MPa, greater than the strength of the SC20EM and SC20HP80 core panels by almost 125.7 % and 25.7 %, respectively. These results were in good agreement with the data reported by Zhou et al. [163]. However, the failure strains were not significantly different between the samples; for instance, SC20F150 and SC20HP80 failed at approximately 0.09, and SC203M failed at approximately 0.07; this might be due to inadequate bonding between the foam and the cell walls.

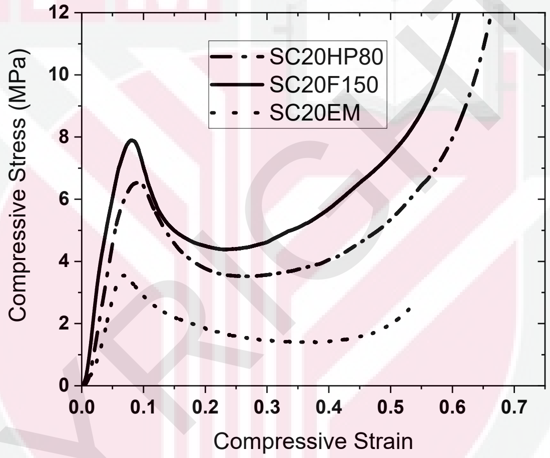

Figure 4.5: Stress-strain curve of 20 mm cell size core, empty, and foam-filled (HP80 and F150 foam)

Similarly, SC30F150 outperformed SC30EM and SC30HP80 by 81 % and 12 %, respectively, as portrayed in Figure 4.6. It is also clear that, in contrast to the core with a cell size of 20 mm, the failure strain was pronounced in this case, with SC30F150 having a better strain failure by 1.2 compared to failure strain of 0.07 and 0.05 for SC30HP80 and SC30EM, respectively, because SC230F150 had a higher relative density.

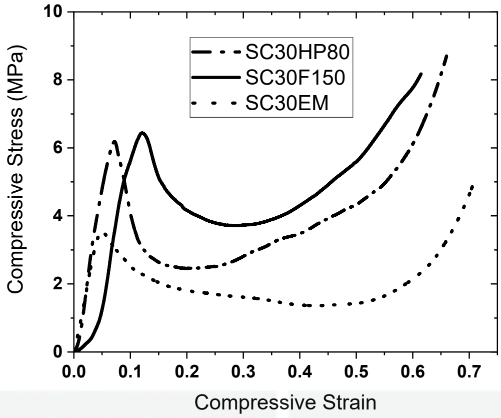

Figure 4.6: Stress-strain curve of 30 mm cell size core, empty and foam-filled (HP80 and F150 foam)

Furthermore, SC40F150 had a strength of 5.4 MPa, higher than those obtained in SC40EM and SC40HP80 sandwich structures by 39.5 % and 34.6 %, respectively, as shown in Figure 4.7. According to Figure 4.7, cores filled with F150 PVC foams outperformed the other samples in terms of compressive strength, regardless of the core cell size. This is because a core filled with F150 PVC foam had a higher relative density in comparison with a core filled with HP80 PVC foam.

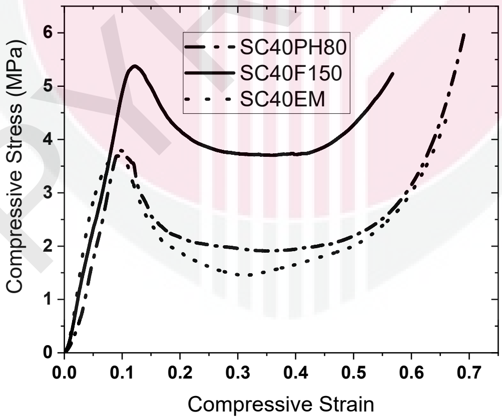

Figure 4.7: Stress-strain curve of 40 mm cell size core, empty, and foam-filled (HP80 and F150 foam)

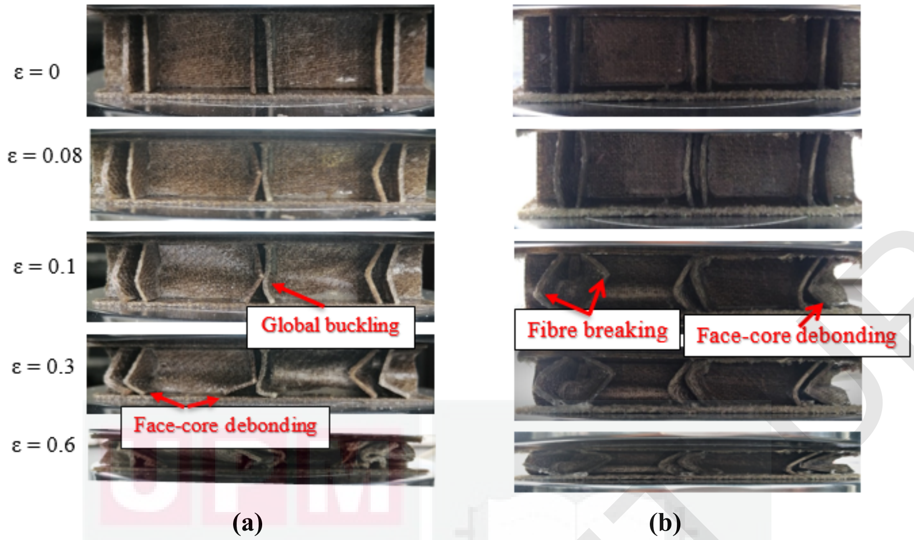

Figure 4.8: Progress failure modes in the core flax/PLA composites structure with (a) foam-filled core structure and (b) empty core structure

4.2.3 Effect of varying cell size

Furthermore, a comparison between empty and foamed-filled cores with respect to varying the cell size of the core structure is shown in Figure 4.9. It is seen from Figure 4.9a, the SC20HP80 core exhibited relatively higher strength than SC30HP80 and SC40HP80 core structures, by around 9 % and 75 %, respectively. On the other hand, the SC30HP80 core outperformed the SC40HP80 by around 60 %. A similar trend was observed for the case of cores filled with F150 foam, as shown in Figure 4.9b, where SC20F150 possessed higher strength than SC30F150 and SC40F150 by 22 % and 63 %, respectively, while SC30F150 core outperformed SC40F150 by 41 %. These findings were consistent with those published in [164], which concluded that smaller cell sizes had greater compressive strength than larger cell sizes. In contrast, SC40EM and a specific density of 0.11 exhibited a strength of 4.5 MPa, higher than the sandwich structures of SC20EM and SC30EM by around 8.4 % and 6.3 %, respectively (see Figure 4.9c). In addition, it can be stated that filling the square core with high-density foam has a greater impact on the mechanical performance of the square core sandwich structure than the cell size of the sandwich structure. The current findings have been compared to those found in the literature and are summarised in Table 4.2.

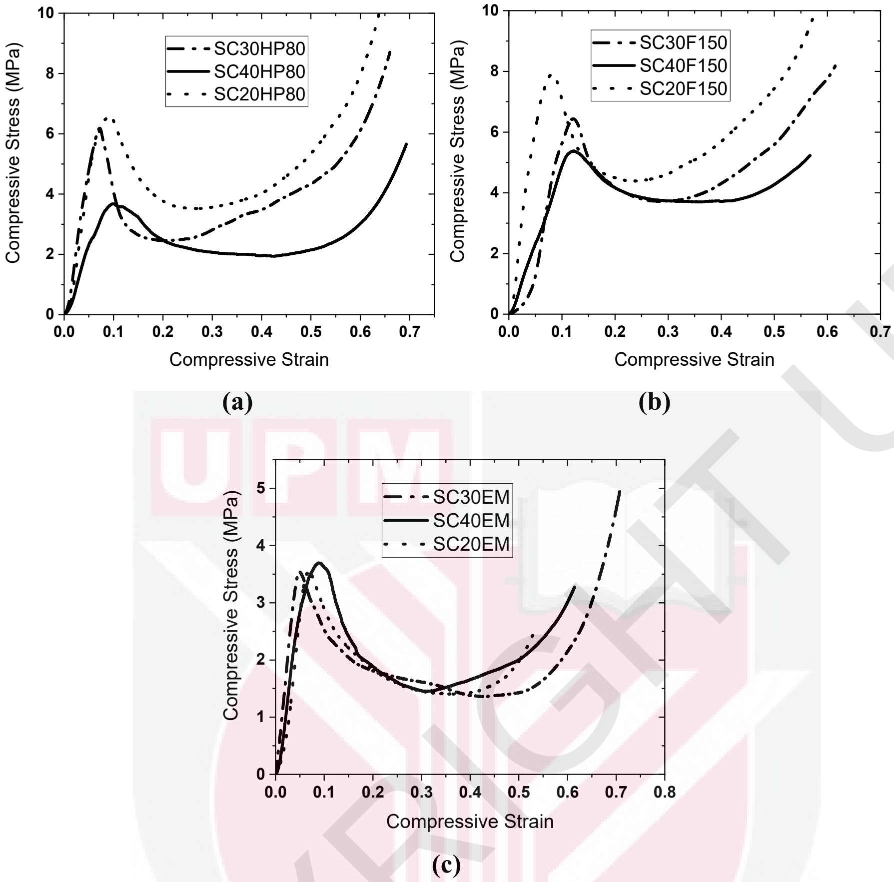

Figure 4.9: Stress-strain curves of (a) SC20HP80, SC30HP80 and SC40HP80 (b) SC20F150, SC30F150, and SC40F150, and (c) SC20EM, SC30EM, and SC40EM

4.2.4 Energy absorption capability

Moreover, the performance of the studied cores was compared in terms of their specific energy absorptions (SEA) (see Figure 4.10). It can be observed that SC20F150 offered superior mechanical properties compared to any core studied in this work. It is clear from Figure 4.10 that SC20F150 exhibited the highest SEA of 8.85kJ/kg compared to the rest of the samples; this supports the findings of Zuhri et al. [164]. For example, SC20F150 outperformed SC30F150 and SC40F150 by 12 % and 9 %, respectively. In addition, SC20HP80 exhibited a SEA of 8.1 kJ/kg, which was higher than that obtained by SC30HP80 and SC40HP80 by 9.4 % and 7.6 %, respectively. However, the SC40EM had a SEA of 7.9, which was higher than its SC20EM and SC30EM counterparts by around 47 % and 13 %, respectively. In the case of an empty core, the influence of cell size variation has a substantial effect on the SEA values, as the SEA increased with increasing cell size; however, the greater the increase in cell size, the less effect can be observed. In addition, the incorporation of foam with an empty core has greatly enhanced the SEA of SC20. Nonetheless, these values marginally decreased as cell size increased.

Furthermore, while SC30F150 had slightly higher SEA values than SC40 (both with and without foam), there was no significant difference between SC30 and SC40. In addition, current data have been compared with previous researchers in terms of their strength and specific energy absorption values (SEA), as shown in Table 4.2. The current data was found to be 36-94 % and 14-128 % higher than those reported by Mozafari et al. [165, 166] and more than 7 and 10 times higher than those reported by Zuhri et al. [89] and Zhang et al. [167] for core with square, triangular, and corrugated Y-shapes, respectively. However, it should be noted that cores studied in the literature have only one cell wall. As a result, it is shown that filling the core with high-density foam improved the energy absorption ability of the square core structure. The SEA results obtained in this study were compared to those reported in the literature (see Table 4.2.)

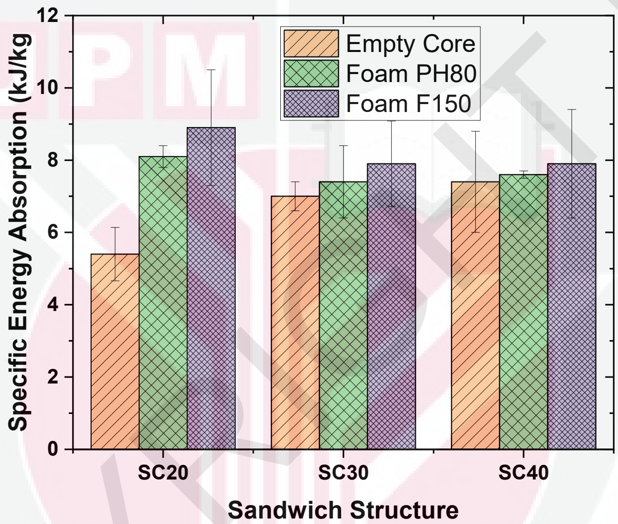

Figure 4.10: Comparison of specific energy absorption with different core parameters

Table 4.2: Comparison of properties between current flax/PLA composite structures with published works

Type of core	Type of material	Relative density	Compressive Strength (MPa)	SEA (kJ/kg)	Ref
Square (20 mm cell size)	Flax/PLA				
	Cell size: 20 mm				
	- Empty core				
	- Filled with HP80 foam	0.19	3.54	5.38	
	- Filled with F150 foam	0.44	6.37	8.13	
		0.55	8	8.85	
	Cell size: 30 mm	0.14	3.62	7.00	Current
	- Empty core	0.45	5.84	7.45	
	- Filled with HP80 foam	0.58	6.55	8.05	
	- Filled with F150 foam				
	Cell size: 40 mm				
	- Empty core	0.11	3.52	7.40	
	- Filled with HP80 foam	0.47	3.64	7.55	
	- Filled with F150 foam	0.62	4.9	7.90	
Honeycomb (16.45 mm cell size)	3003 aluminium				
	polyurethane foams (PU)				
	- Empty core	--	1.00	5.87	[165]
	- Filled with (PU) F16 kg/m^3	--	1.70	4.56	
	- Filled with (PU) F52 kg/m^3	--	2.00	6.51	

Table 4.2: Continued

Y-shape core (110 × 20 × 34 mm)	304 stainless steel sheets.				
	Aluminium alloy foam (AlSi7).				
	- Empty (core member thickness)	0.036	0.78	0.39	
	- Empty (core thickness)	0.072	2.89	0.62	[166]
	- Filled (core member thickness 0.4)	0.115	13.78	7.79	
	- core member thickness	0.148	17.40	6.96	
	- **All core thicknesses are 0.4*				
Corrugated core	Core made of 304 stainless steel.				
	Aluminium foam with three different densities.				
	- Empty core		13.40		
	- Foam density of 297 kg/m^3		25.60	5.42	[75]
	- Foam density of 432 kg/m^3	-	31.50	10.42	
	- Foam density of 540 kg/m^3		41.70	11.72	
				13.92	
Square	Flax/PLA	0.13	0.5	0.90	
	Flax/PP	0.15	1.9	3.00	
Triangular	Flax/PLA	0.23	0.54	0.8	[89]
	Flax/PP	0.26	2.5	2.70	
	**All tested with empty cores*				
Corrugated	Glass fibre with foam inserted.				
	Carbon fibre with foam inserted.			0.60	[167]
	Hybrid of glass and carbon (50:50) with foam inserted.	-	-	0.82	
	*Eco foam GP330			0.65	

4.3 Quasi-static compression properties of honeycomb core structure

4.3.1 Core without foam filling

The mechanical behaviour of an empty honeycomb was investigated using quasi-static compressive testing. The test findings of the specimens under compression are presented in Figure 4.11, which depicts the samples' stress-strain curves. Initially, empty honeycomb exhibited similar features, specifically the four typical regions of linear, nonlinear, plateau, and densification regions. It was observed that all traces increased linearly until the stress achieved its compressive strengths (peak stresses). HC1 achieved the least strength by around 3.8 MPa; however, the strength increased as the length and width of the honeycomb structure increased until it reached 4.1 MPa for HC3 samples, but this increment is insignificant, as shown in Figure 4.11. These results demonstrated that varying the lengths and widths had only a small effect on the honeycomb structure's strength. Similar behaviour was observed for the failure strain, where it increased from around 0.08 for HC1 to 0.15 for HC3. Furthermore, as the compressive load continued, the compressive stress rapidly dropped to reach a considerable value (smaller than the peak stress) of around 70 %, 50 %, and 58 % for HC1, HC2, and HC3, respectively. Additionally, as the load continued, the stress-strain curve remained almost unchanged during the plastic deformation until they reached their densification points. Surprisingly, HC1 and HC2 reached their densification points earlier than HC3; later on, curves gradually increased, resulting in increments in the stresses and strain values. In addition, in the deformation process of the empty honeycomb (Figure 4.12) with the increase of compressive strain, the honeycomb cell walls gradually thickened due to delamination of the cell wall and fibre breaking of the cell wall, resulting in a decrease in the space enclosed by the honeycomb cell walls. To conclude the deformations process, delamination of the cell wall was the mean failure in almost all the samples tested here, followed by fibre breaking and, finally, delamination of the skin and the edge cell wall of the honeycomb.

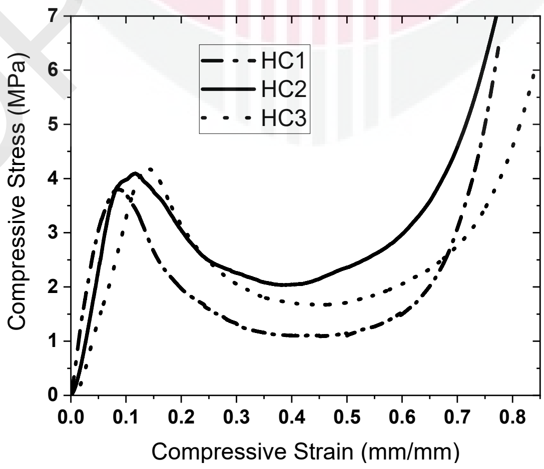

Figure 4.11: Stress-strain curve of empty honeycomb core

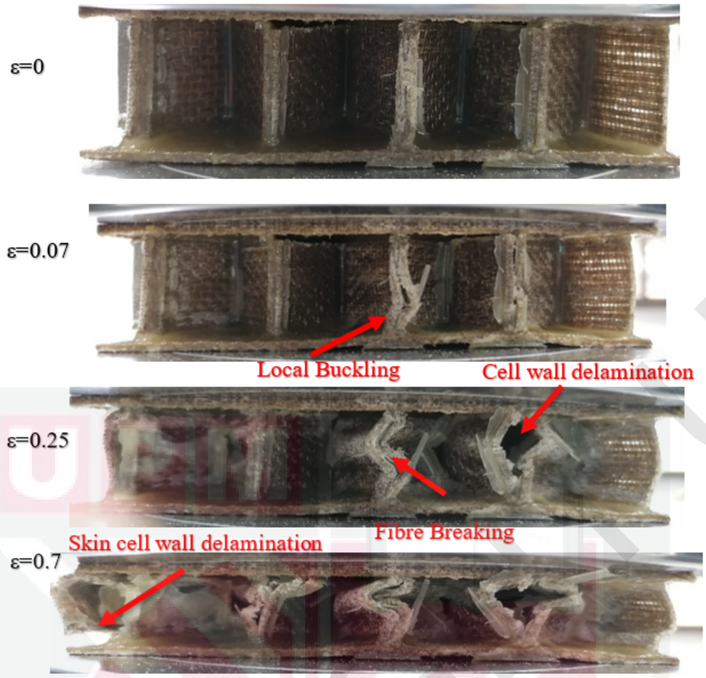

Figure 4.12: Progress failure modes in the core flax/PLA composites structure with empty core structure

4.3.2 Foam filling core

The mechanical behaviours of foam-filled honeycomb were investigated using quasi-static compressive testing. The findings in Figure 4.14 depict the samples' stress-strain curves. Initially, foam-filled honeycomb exhibited similar features to empty honeycomb cores, specifically the four typical regions of linear, nonlinear, plateau, and densification. Figure 4.14a can be utilised as an example to show the behaviour of empty and foam-filled honeycomb core structures under compression load. One can see from the figure that all traces increased linearly until the stress achieved its compressive strength (peak stress). Unlike filled foam honeycomb, empty honeycomb samples reached their peak stress of 4.0 MPa at lower strain values of about 0.08. However, with a foam-filled honeycomb, the compressive strength increased from 4.0 to 6.8 MPa, and the corresponding strain increased from 0.08 to 0.15 compared to the empty honeycomb. Furthermore, as the compressive load continued, the compressive stress rapidly dropped and reached a considerable value (smaller than the peak stress). In this stage, the foam-filled honeycomb samples exhibited a lesser drop in their stresses to around 5 MPa to 0.34 strain as compared to the empty honeycomb's 1.5 MPa and 0.37 strain, respectively. This can be attributed to the absorbent foam filling where the foam acted as a support and connection to the walls of the honeycomb, and the structural integrity could also be well ensured.

Moreover, due to the foam filling, the densification stage of the honeycomb happened forward. The densification strain of absorbent-foam-filled honeycomb started at strain 0.403, and as the load continued, the stress-strain curve gradually increased, resulting in an increase in the stresses and strain values. At this stage, a similar trend was observed, however, with a gradual increase in stress and strain. Besides, the filling of absorbent foam slowed the process of the increase of wall thickness for foam-filled honeycomb, making the honeycomb and absorbent foam squeezed each other, which explained the earlier occurrence of the densification stage (Figure 4.13). To conclude the deformations process, delamination of the cell wall was the mean failure in almost all the samples tested here, followed by fibre breaking and, finally, delamination of the skin and the edge cell wall of the honeycomb.

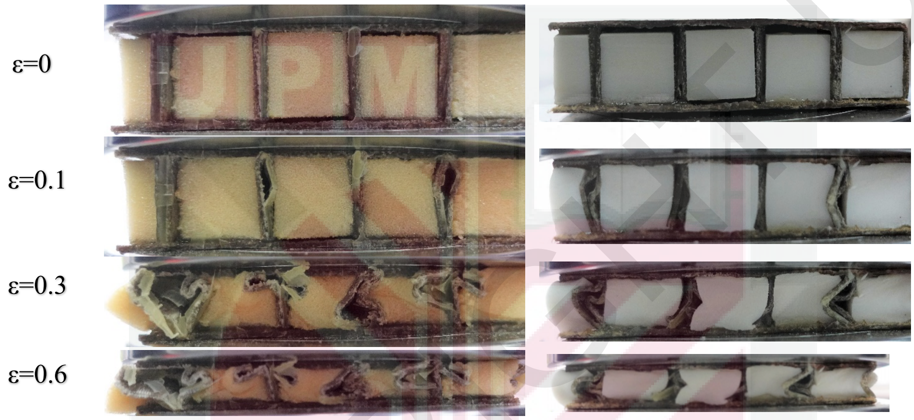

Figure 4.13: Progress failure modes in the core flax/PLA composites structure with foam-filled cores (a) HP80 core structure and (b) F150 core structure

4.3.3 Effect of foam-filled core

Figure 4.14 displays the stress-strain curve of the filled-foam honeycomb core structure. Initially, both HP 80 and F150 had compression and greatly enhanced properties compared to the empty honeycomb core (see Figure 4.14). In comparison between the three honeycomb structures, one can observe that honeycomb filled with F150 foam outperformed the rest of the samples studied here. Figure 4.14a shows HC1F150 having a compressive stress of 6.34 MPa at a strain of 0.15 compared to HC1HP80, which had 5.30 MPa at a strain of 0.11, while Figure 4.14b shows HC2F150 had 6.3 MPa compared to 5.9 MPa for HC2HP80 at a strain of 0.15 and 0.11, respectively. Moreover, Figure 4.14c depicts similar values to that in Figure 4.14b. It is worth mentioning that F150 foam had a higher density foam than HP80; this explained the reason behind the honeycomb filled with F150 having a very short pleated region. Therefore, lower densifications were observed in all three graphs. Both cores filled with either F150 or HP80 failed in a similar manner; however, for the core filled with HP80, the delamination and fibre breaking were more pronounced due to the high density of the former, as shown in Figure 4.12 and Figure 4.13.

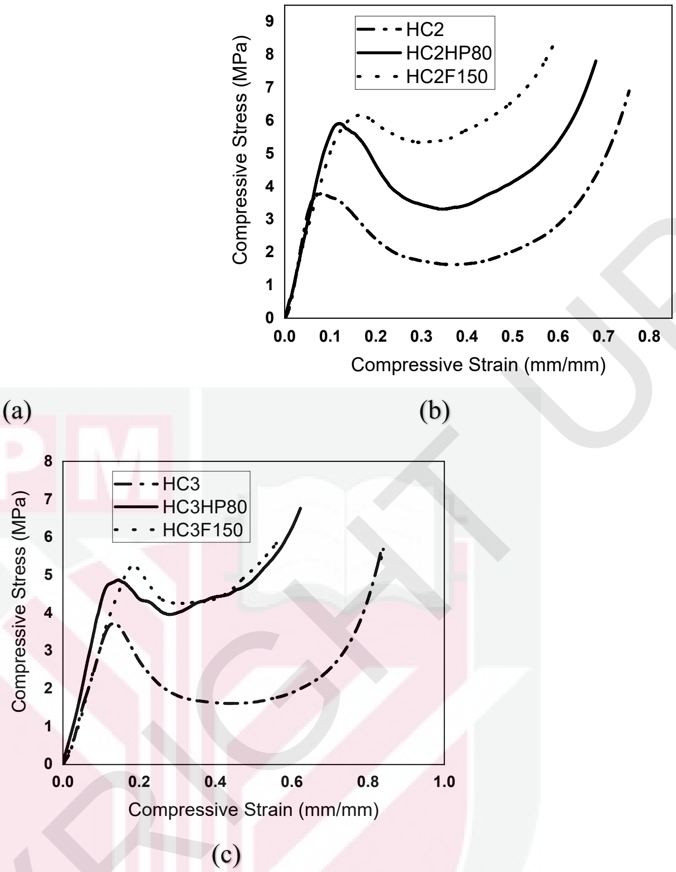

Figure 4.14: Typical stress-strain graphs (a) HC1 with and with foam-filled, (b) HC2 with and with foam-filled, and (c) HC3 with and with foam-filled

4.3.4 Effect of varying core lengths and width

Figure 4.15 shows the effect of varying the length of empty honeycomb core sandwich structures. It is found that HC3 and HC3 had similar compression strength of around 4.1 MPa compared to HC1 with 3.8 MPa. A similar trend to this was found in [168]; the authors mentioned that increasing the length of the honeycomb can significantly improve the compressive strength. However, increasing the height can decrease the compressive strength. Furthermore, adding HP80 foam into the three empty honeycomb cores further improved the compressive strength, as presented in Figure 4.16. It can be noticed that HC2HP80 and HC3 increased by around 50 %, whereas HC1HP80 increased by 40 %. In addition, adding HP 80 foam slightly improved the elastic strain for all samples; for example, HC3HP80 reached its maximum strength at 1.8, which is an 18 % improvement over HC3; additionally, HC1HP80 and HC2HP80 reached their highest strength at around a similar strain, which was a 25 % improvement over their empty counterparts.

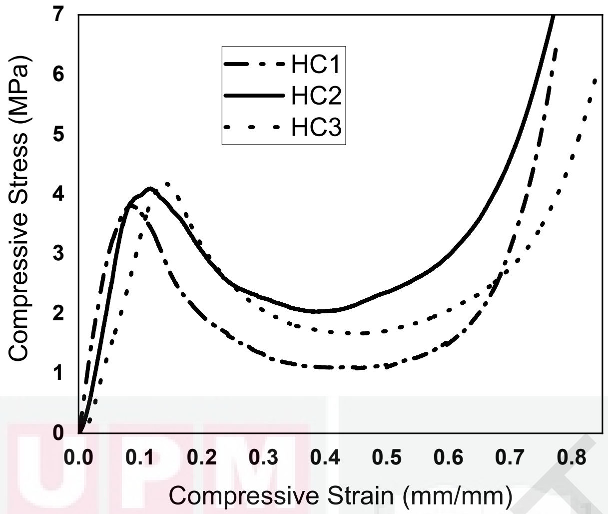

Figure 4.15: Stress-Strain curves of empty honeycomb core structure with different core sizes

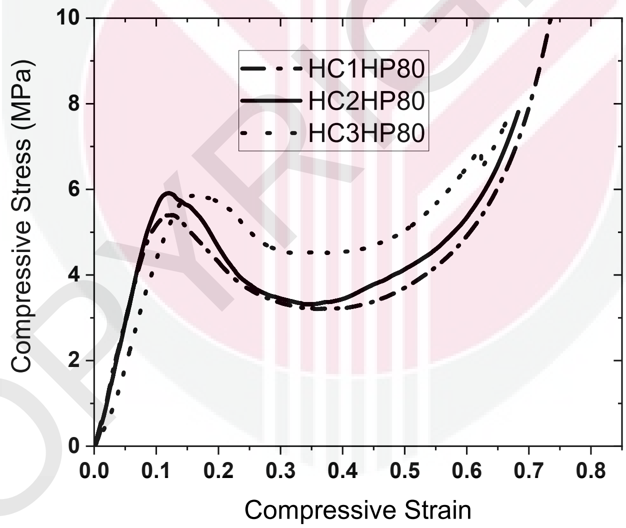

Figure 4.16: Stress–strain curves of HC2 and HC2 filled with HP80 foam

Figure 4.17 shows that HC1F150 had almost similar strength to HC2F150 at around 6.2 MPa, better than HC3F150 by around 15 %. However, HC3F150 had an elastic strain of 0.2, which is 33 % more than the elastic strain of the HC1F150 and HC2F150. It is worth mentioning that HC1F150 outperformed the rest of the samples studied here. Furthermore, HC2HP80 had almost similar values compared to those of HC3 and HC3HP80.

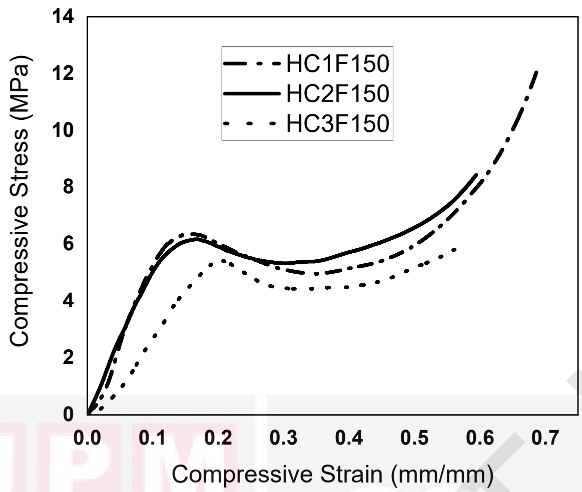

Figure 4.17: Stress–strain curves of HC2 and HC3 filled with F150 foam

4.3.5 Energy absorption capability with and without foam

Figure 4.18 shows the specific energy absorbing capability (SEA) of both empty and foam-filled honeycombs. One can see that the HC2HP80 honeycomb had better SEA values of 10 kJ/kg, higher than the other samples tested here. Furthermore, the HC1HP80 had around 8.7kJ/kg SEA value, similar to those of the HC3 and HC2F150 honeycomb structures, as well as higher than the rest of the samples except for HC2HP80. An additional note: while comparing the SEA values of an empty honeycomb core structure, one can see that the SEA values increased as the length and width increased. HC3 structures, for example, outperformed both HC1 and HC2 structures by around 8.8 % and 6.5 %, respectively, whereas HC2 structures outperformed HC1 structures by around 5 %.

Surprisingly, all empty honeycomb core structures showed higher SEA values than foam-filled core structures, particularly HC3HP80 and HC3F150 of around 16 % and 22.5 %, respectively. It should be observed that the SEA values honeycomb core structure filled with F150 foams had the lowest SEA values compared to the other samples since the high density of F150 resisted the load, resulting in an earlier densification strain.

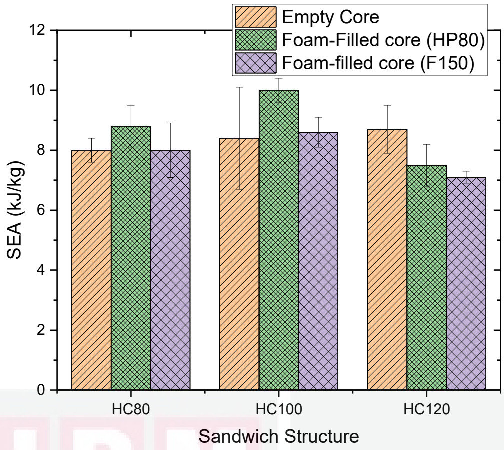

Figure 4.18: Comparison of specific energy absorption of honeycomb cores

4.4 Comparison between square core and honeycomb core structures

The stress-strain curves of both sandwich constructions were displayed in Figure 4.19-4.21 to compare the compression properties of square interlocking and honeycomb core structures. Figure 4.19 compares the stress–strain curves for three different cell sizes of interlocking square core, SC20EM, SC30EM, and SC40M, to honeycomb cores with three different lengths and widths, HC1, HC2, and HC3. The figures show that the honeycomb core structure had somewhat greater strength in most cases, with the exception of HC3 and SC40EM, which had approximately similar strains. Furthermore, when the cell size, length, and width increased, the strength gap between the two core structures began to close until they were almost similar.

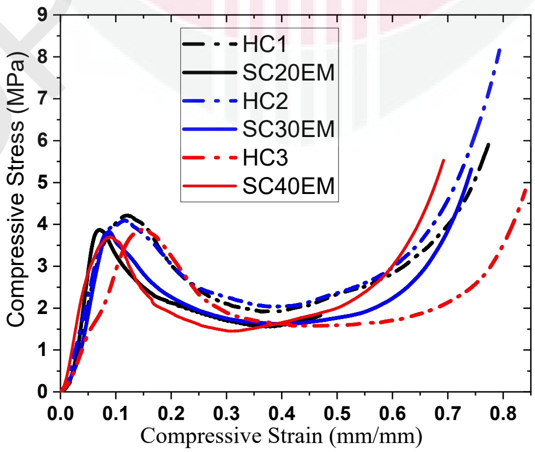

Figure 4.19: A compressive strength of both empty square interlocking and empty honeycomb core structure

In contrast, for the case of foam–filled core structure, the square interlocking core structure outperformed the honeycomb core structure except for the case of SC40HP80 and HC3HP80, in which the HC3HP80 was superior by almost 45 % to the square interlocking core structure, as shown in Figure 4.20. Similarly, the foam-filled square interlocking core continued to have better strength, especially for the case HC1F150 and SC20F150. However, almost similar strength was observed for the rest of the cases (see Figure 4.21). It is worth mentioning that, in all the cases, the square core tended to fail at lower strain in comparison to the honeycomb structure, which can be attributed to the geometry of the core cell structure.

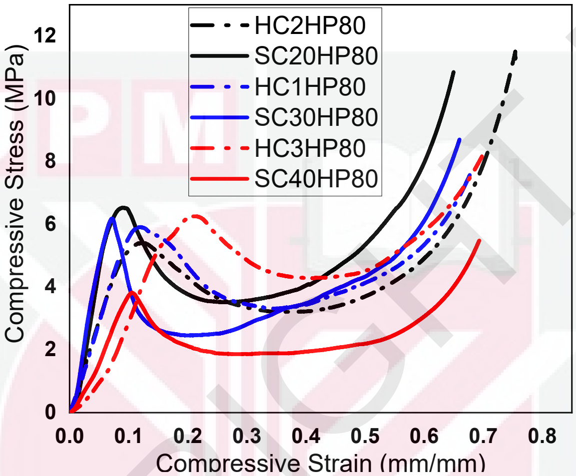

Figure 4.20: A strength of both square interlocking and honeycomb cores structure filled with HP80 foam

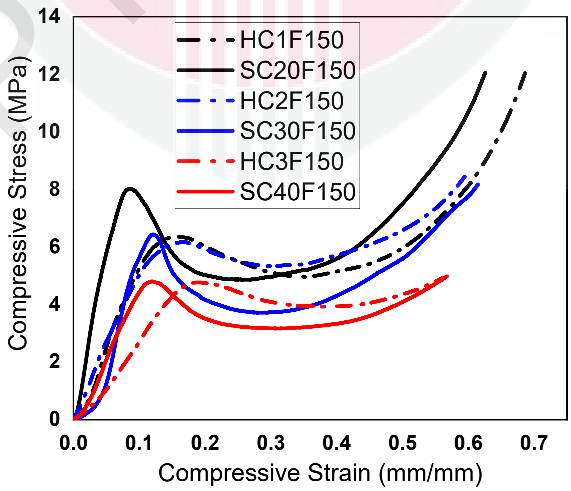

Figure 4.21: A strength of both square interlocking and honeycomb cores structure filed with F150 foam

Figure 4.22 depicts a comparison of the SEA values of square interlocking and honeycomb core sandwich structures. As can be seen, honeycomb cores had higher SEA values than square cores in most cases; for example, HC2HP80 had 10 (kJ/kg), higher than any case studied here. Furthermore, when compared to empty square cores, empty honeycomb cores showed higher SEA values in all scenarios; a similar trend was found for cores filled with HP80 foam. In contrast, square cores packed with F150 foam outperformed their honeycomb core counterparts, with the exception of HC100, where the honeycomb was shown to have a higher SEA.

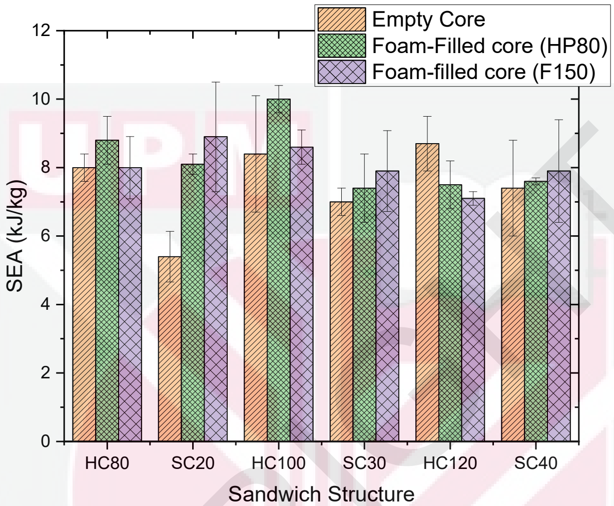

Figure 4.22: A strength of both square interlocking and honeycomb cores structure

4.5 Cone calorimeter properties of square and honeycomb cores structure

The time series of all cone calorimeter measurements on both square and honeycomb core structures were investigated to facilitate the comparison of the evolution of all variables (HRR, THR, Mass loss %, and TSP). Figure 4.23-4.25 show the heat release curves of the two sandwich structures during burning based on the principles of oxygen consumption calorimetry. Tests at 35kW/m^2 indicated that the sample needed around 25 seconds to reach the pyrolysis temperature and ignite, as shown in Figure 4.23. After ignition, the HRR curve presents a steep increase due to the heat released by the ignition of volatiles from the composite interface until it reached its first peak at around 95 seconds with HRR of 273kW/m^2 and 266kW/m^2 for square interlocking and honeycomb cores structure, respectively. The HRR was then subsequently reduced by the char formation that eventually broke due to the continuous heat radiation, allowing the heat to pass to the next layer (core structure). Hence, the HRR of both structures dropped sharply by around 50 % in just 105 seconds. As the heat radiation continued, the HRR curves started increasing gradually until they reached their second peak at around 214 kW/m^2 and 273 kW/m^2 for honeycomb and square interlocking core structures, respectively. Unlike the first peak, here, both structures reached their second peak at different durations, for example, the honeycomb core structure reached its second beak around 1 minute earlier compared to its square core structure. This could be attributed to the double cell wall of the interlocking core, which can form effective char formations, hence reducing the compositional delays and the eventual time to reach the HRR second peak.

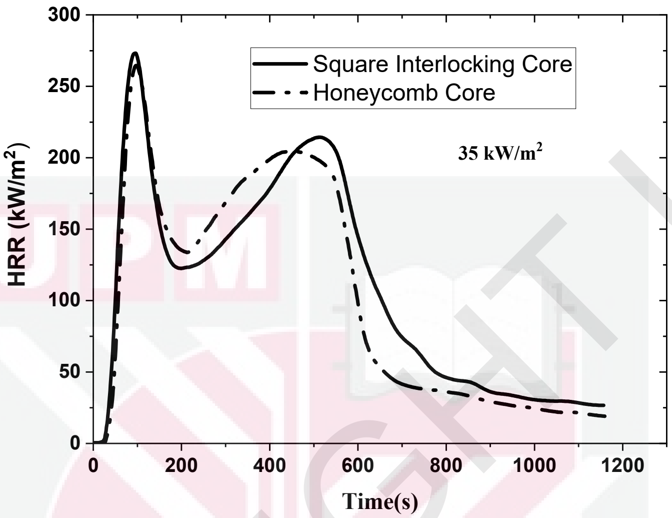

Figure 4.23: The heat release rate vs time at 35 kW/m²

Finally, the HRR of both core structures went to a very low level at around 700 seconds after the end of flaming combustion. Both core structures lost their structural integrity significantly while the flax fibre retained its initial shape to some extent, as can be seen in Figure 4.26, despite the bonding methods between the flax fibre and PLA played a vital role in the final structural integrity of the residue. This is due to the fact that both cores were prepared through a hot press machine, and the PLA subsequently melted during combustion, resulting in a greater structural failure.

A similar trend was observed as the heat flux increased to 50 and 70 kW/m², as shown in Figure 4.24 and Figure 4.25. The figures show that both structures reached a pyrolysis temperature and ignited at 18 s and 3 s, respectively. One minute later, the HRR curves sharply increased until they reached their first peak at approximately 410 kW/m² and 368 kW/m² for honeycomb and square core structures, respectively. As the ignition of volatiles reached the core structures, the HRR curves dropped sharply to almost the same level at around 175 kW/m². After around 70 s, the core structure ignited, and the HRR curves were gradually increased until reaching the HHR second peak. Similar to the first case (35 kW/m²), here, the square interlocking core reached its HRR peak earlier with less HRR compared to the honeycomb core structure. In contrast, under 70 kW/m², the second HRR peak was higher than its first peak, and that was due to the amount of mass that the sample contained in its core. Once again, the honeycomb core had a higher heat release rate than the square interlocking counterpart.

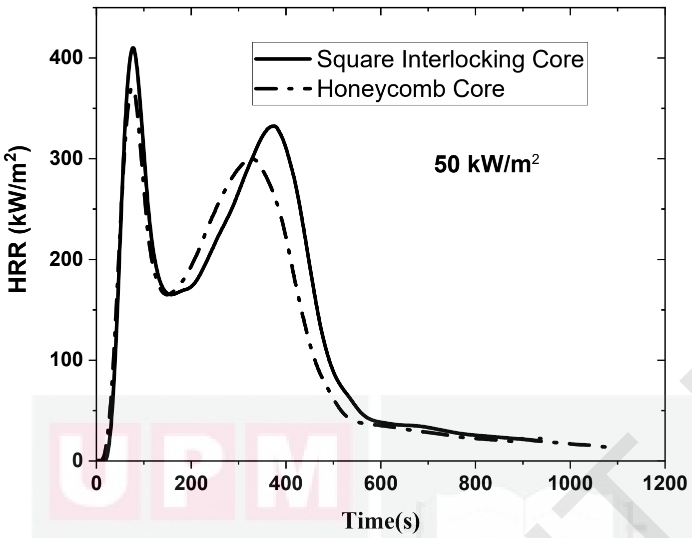

Figure 4.24: The heat release rate vs time at 50 kW/m²

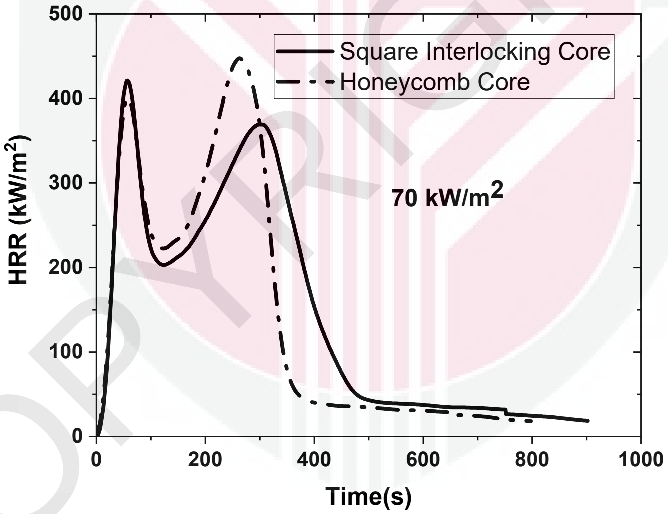

Figure 4.25: The heat release rate vs time at 70 kW/m²

The research data has been compared with data from the literature and presented in Table 4.3. In terms of time to ignite and peak of HRR, the tested samples outperformed similar research in the literature in [145] by more than 15 s and 50 %, respectively. Despite these composite laminates and cellular core structures' data published in the literature, used fire retardants, the developed square, and honeycomb core structure exhibited significantly superior fire resistance at different heat flux levels. This suggested that the developed structure's inherent properties or design may naturally resist ignition more effectively.

Table 4.3: Cone calorimeter data measured for flax/PLA square interlocking and honeycomb core structures subjected to an applied heat flux of 35, 50, and 70 kW/m²

Sample	Heat Flux kW/m²	Time to Ignite (s)	Peak HRR kW/m²	T_{PHRR} (s)	*FIGRA kW/s	*THR kW/m² 300s-600s	TSR m²/m²
Honeycomb	35	45	277	95	2.9	43.3 - 99	856.0
Interlocking core		28	285	95	3.0	42.3 - 97.8	657.8
[133]							970 ±59
- Flax/PP	35	31 ± 2	452 ±8	75 ±3	6.0	98 ±3	870 ±145
- FR1-flax/PP		36 ±3	284 ±8	61 ±1	4.7	70 ±3	1015 ±126
- FR3-flax/PP		36 ±3	305 ±7	61 ±1	5.0	83 ±2	1736 ±187
- FR4-flax/PP		46 ±2	46 ±2	67 ±5	4.4	87 ±2	58 ±2
- Flax/PLA		34 ±1	287 ±18	57 ±1	2.5	58 ±2	
Honeycomb	50	25	395	74	5.3	62.68 - 107	828.5
Interlocking core		30	435	76	6.5	61.0 - 117.05	1378.0
[134]							
- FE		35	616	173	124	96	3038
- FE-APP		32	485	211	12	87	3232
- BFE		29	907	49		278	5338
- BFE-APP		30	354	234		263	5617
[145]	50						
- Plywood 2-layered corrugated core		22.8	428.7	36			
- Plywood 2-layered corrugated core		21.4	449	34			
- Flax-FRPP corrugated core		11.5	430.4	55			
- Plywood corrugated sandwich		20.2	396.4	32			
- Flax-FRPP corrugated sandwich		16	469.5	42.5			
- Plywood honeycomb core		23	376.5	100			
- Flax-FRPP honeycomb core		15	458.7	127.5			
- Plywood honeycomb sandwich		21	435	35			
- Flax-FRPP honeycomb sandwich		16.5	485.2	42.5			
Honeycomb	70	13	458	260	1.7	90.5 - 110.0	1071.5
Interlocking core		13	460	57	8.0	79.4 - 119.0	910.0

*THR = THR (the 1st 300s – 1st 600s); *FIGRA = Peak HRR divided by the T_{PHRR} (s) of the 1st peak of all samples except the Honeycomb under 70 kW/m² heat flux where the value was calculated from the 2nd peak as the HRR value is higher than that for the first peak.

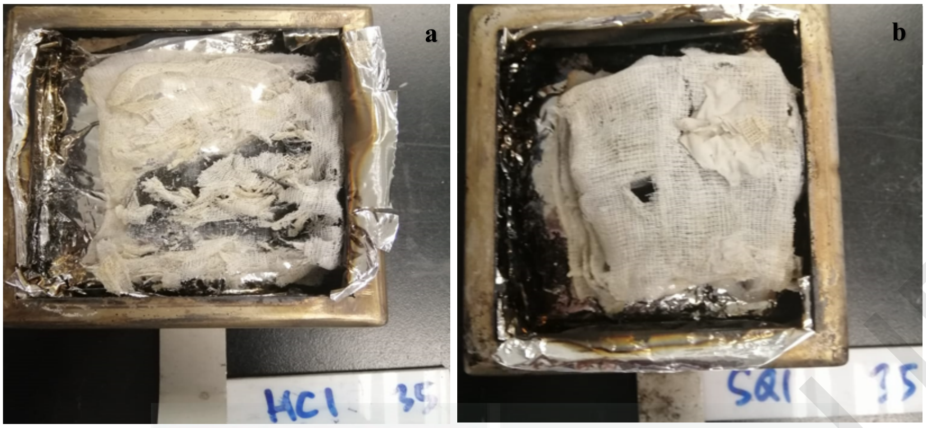

Figure 4.26: Photos after the test of both core sandwich structures (a) honeycomb and (b) square

Interestingly, the HRR first peak was practically the same in all cases because the first layer of the sandwich structure (skin) was characterised by the same thickness in all samples. However, the HRR of the second peak differed because the second layer (core structures) mainly responsible for the HHR second peak were different.

It is believed that the thickness of the cell wall of the core structure has a significant impact on HRR values, thus resulting in lower peak values for the honeycomb core samples, except for one case when compared to the square interlocking core. The composite layers were quite thinner and tended to have greater HRR peaks [169].

Furthermore, Figure 4.27 shows the mass versus time graphs for heat fluxes of 35, 50, and 70 kW/m^2. As illustrated in Figure 4.26c, both structures lost mass rapidly as the heat flux increased, with the honeycomb structure losing its mass slightly earlier than the square interlocking core at around 300 s and the square interlocking core losing mass at 400 s. However, when exposed to a heat flux of 35 kW/m^2 and 50 kW/m^2, both core structures lose their mass at the same time, approximately 700 s and 500 s, respectively (Figure 4.27a and b). Furthermore, all the samples experienced about 90 % to 95 % loss in their masses during the burning stage. The peak of mass loss was observed at the time of peak HRR, and the mass loss % curves also peaked as the different layers were gradually ignited.

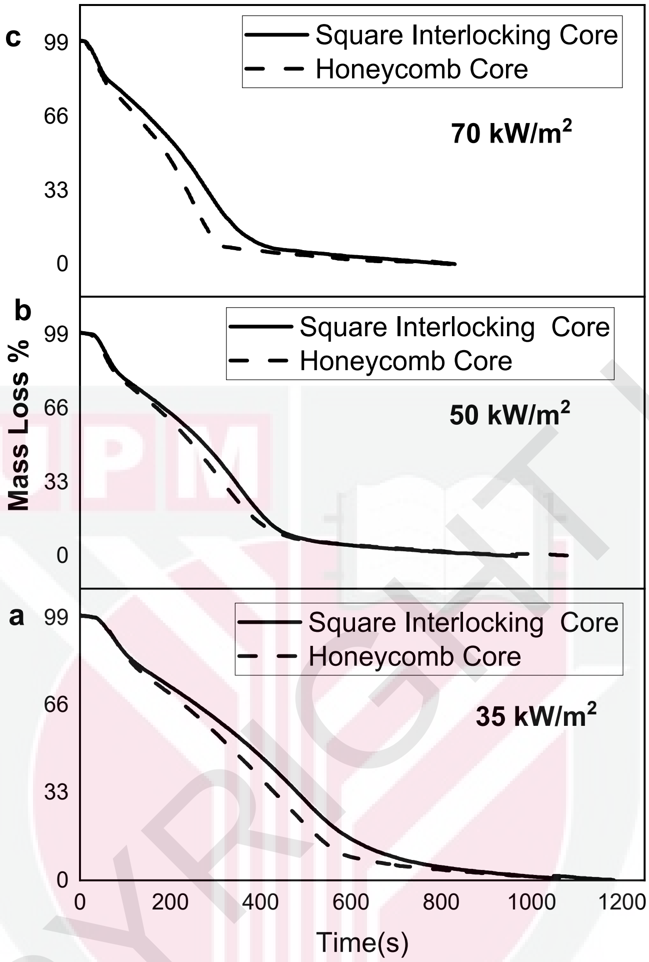

Figure 4.27: Mass loss % under three different heat fluxes

Similarly, in all three cases, the total heat release (THR) was somewhat greater for the square interlocking core structure, with THR of around 120 MJ/m^2, while the honeycomb core structure had 110 MJ/m^2, as shown in Figure 4.28.

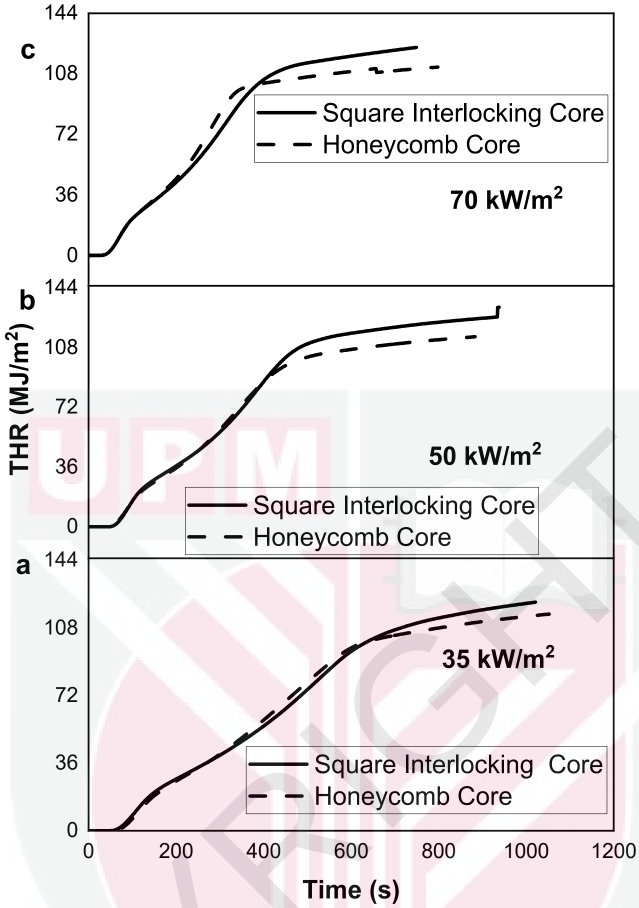

Figure 4.28: Total heat rate under three different heat fluxes

Figure 4.29 illustrates the total smoke production of the two cores, and it can be observed that the square interlocking core structures had a significantly lesser amount of smoke production when compared to the honeycomb core structure when exposed to 35 kW/m^2 and 70 kW. The maximum TSPs of the square interlocking core structure were 5.5, 12, and 7.8 m^2 under the three heat fluxes of 35, 50, and 70 kW, respectively. However, the honeycomb core produced less amount of smoke when exposed to flux heat of 50 kW/m^2. The maximum TSPs of the honeycomb cores were 7, 7.1, and 9.2 m^2 under the three heat fluxes of 35, 50, and 70 kW/m^2.

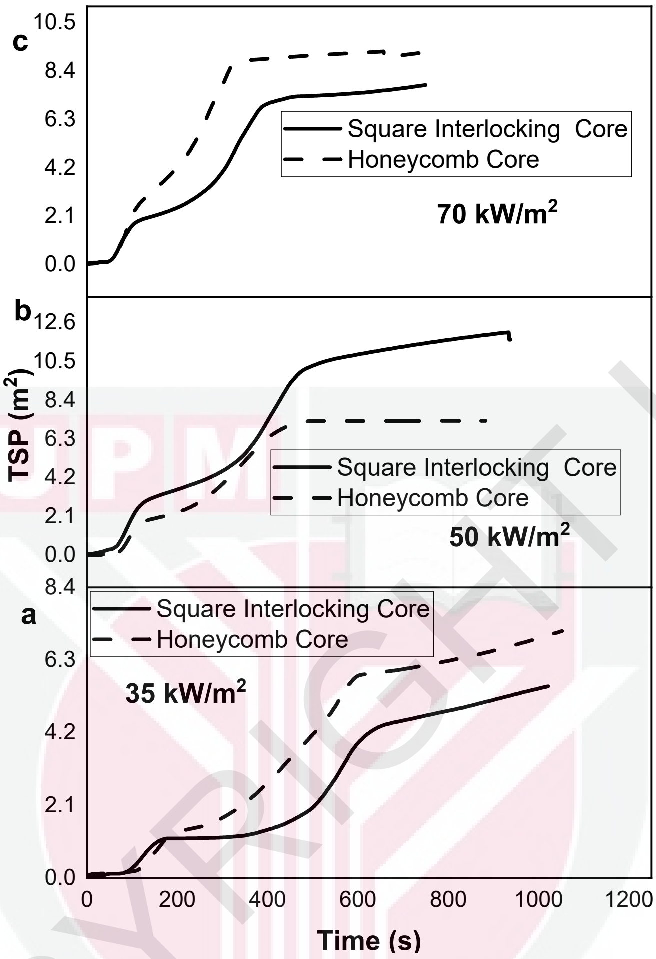

Figure 4.29: Total smoke production rates under three different heat fluxes

CHAPTER 5

CONCLUSION AND RECOMMENDATIONS

5.1 Conclusion

The aim of this study is to manufacture a range of sandwich structures made from flax/PLA composite and to investigate their mechanical properties. This study investigated the double cell wall square and honeycomb core structures with and without HP80 and F150 foam-filled. Quasi-static compression tests were performed in order to evaluate the mechanical response, energy absorption, and failure modes of the structures. In addition, a bench-scale cone calorimeter was employed to measure the fire reaction properties of the flax/PLA composites along with the subsequent effects of the core structures. Based on the findings of this study, the following conclusions can be drawn:

- Manufacturing temperature is an important consideration in the manufacturing process of natural fibre composites that influences composite performance. The results of this study showed that flax/PLA manufacturing temperatures above 190 °C degraded the tensile properties of the flax/PLA composites. It was also found that the flax/PLA composites under the manufacturing temperature of 180 °C offered better tensile strength value at all pressing times.

- Testing on double cell wall square core revealed that the variations in cell size were more prominent for the case of the empty core structure, where increasing the cell size considerably improved both the strength and SEA by 8.4 % and 6.3 %, respectively. Incorporating foam with an empty core was more prominent than cell size variation in all the samples studied here. Adding foam to the empty core structure improved the literal support to the core cell wall, resulting in a considerable delay in cell wall buckling and a significant improvement in strength and SEA values relative to the empty core structure. The failure mode was dominated by buckling failure of the vertical cell wall as well as the debonding between the skin and the core.

- Average SEAs of foam-filled and empty honeycomb core structures had no significant difference, around 8.7 kJ/kg and 8.2 kJ/kg, respectively. In contrast, its loading capabilities were clearly pronounced, in which the foam-filled core outperformed the empty counterparts by around 33 %. Finally, the results for empty and foam-filled cores were significantly superior to aluminium cores published in the literature.

- Both the honeycomb and the interlocking square core sandwich showed nearly identical THR for the first 600 seconds, fire growth rate (FIGRA), and time at the peak of HHR when exposed to a heat flux of 35 kW/m^2. On the other hand, the honeycomb core had a lower HHR peak and a longer ignition in most of the cases. In contrast, the interlocking square core produced less smoke (TSR), 23.2 %, than the honeycomb sandwich structure. When the heat flux was increased to 50 kW/m^2, the honeycomb structure outperformed the interlocking core structures in terms of PHRR peak and FIGRA values, and unlike the previous case, the honeycomb produced less smoke (approximately 39 %). However, when compared to the interlocking structure, the honeycomb structure ignition time and HRR time were 5 s and 2 s earlier, respectively. Both cores had nearly the same values of THR. Under 70 kW/m^2, the honeycomb performed differently from the first scenarios, with the second HRR peak being greater than the first peak. Although the fire properties of both core structures were nearly identical, honeycomb had a 15 % lower SPR and 78 % lower FIGRA because the FIGRA value was computed from the second peak as the HRR value, which was higher than the value for the first peak. Results showed that the skin was the major factor in increasing the HRR, therefore, further improvement is needed for this structure to be used in engineering applications.

5.2 Recommendations

The following recommendations are made for this research:

1. The other properties, such as dynamic mechanical analysis, can also be studied for the fabricated sandwich structure.

2. The microstructure analysis can also be investigated for the fabricated sandwich structures.

3. Further improvement on the fire properties of fabricated samples by applying fire retardant before testing.

REFERENCES

[1.] Gay, D. and Hoa, S.V.(2007). Composite materials: design and applications.: CRC press.

[2.] Birman, V. and Kardomateas, G.A., (2018). Review of current trends in research and applications of sandwich structures. *Composites Part B: Engineering.* **142**: p. 221-240.

[3.] Petras, A. (1999). Design of sandwich structures. University of Cambridge

[4.] Vinson, J.R.,(1999).The behavior of sandwich structures of isotropic and composite materials.: *CRC Press.*

[5.] Mansor, M., Nurfaizey, A., Tamaldin, N., and Nordin, M.,(2029). Natural fiber polymer composites: Utilization in aerospace engineering, in Biomass*, Biopolymer-Based Materials, and Bioenergy*. 2019, Elsevier. p. 203-224.

[6.] Ilyas, R., Sapuan, S., Norizan, M.N., Atikah, M., Huzaifah, M., Radzi, A., Ishak, M., Zainudin, E., Izwan, S., and Azammi, A.N.,(2019). Potential of natural fibre composites for transport industry: A review. in *Prosiding Seminar Enau Kebangsaan*.

[7.] Boegler, O., Kling, U., Empl, D., and Isikveren, A.,(2015). Potential of Sustainable Materials in Wing Structural Design. *Deutsche Gesellschaft für Luft- und Raumfahrt-Lilienthal-Oberth eV.*

[8.] Kling, U., Empl, D., Boegler, O., and Isikveren, A., (2015). *Future Aircraft Structures Using Renewable Materials.* Paper. **370118**: p. 64.

[9.] Black, S.,(2017). *Looking to lighten up aircraft interiors-with natural fibers?*.

[10.] John, M.J., Anandjiwala, R., Wambua, P., Chapple, S.A., Klems, T., Doecker, M., Goulain, M., and Erasmus, L.(2008). Bio-based structural composite materials for aerospace application*s. South African International Aerospace Symposium.*

[11.] Haris, M., Laila, D., Zainudin, E., Mustapha, F., Zahari, R., and Halim, Z., (2011). Preliminary review of biocomposites materials for aircraft radome application. in *Key Engineering Materials*. Trans Tech Publ.

[12.] Subash, T. and Pillai, S.N., (2015). Bast fibers reinforced green composites for aircraft indoor structures applications. *Journal of Chemical and Pharmaceutical Sciences. 7:* p. 305-307.

[13.] Red, C., (2012). Composites in aircraft interiors*, 2012-2022. Composites World*.

[14.] Eloy, F., Costa, R., De Medeiros, R., Ribeiro, M., and Tita, V.,(2015). Comparison between mechanical properties of bio and synthetic composites for use in aircraft interior structures. *in Meeting on Aeronautical Composite Materials and Structures, São Carlos, Brazil.*

[15.] Manan, N., Majid, D., and Romli, F.,(2016). Mould design and manufacturing considerations of honeycomb biocomposites with transverse fibre direction for aerospace application. in *IOP Conference Series: Materials Science and Engineering*. IOP Publishing.

[16.] Arockiam, N.J., Jawaid, M., and Saba, N.,(2018). Sustainable bio composites for aircraft components, in Sustainable Composites for Aerospace Applications, Elsevier. p. 109-123.

[17.] Omrani, E., Menezes, P.L., and Rohatgi, P.K., (2016). State of the art on tribological behavior of polymer matrix composites reinforced with natural fibers in the green materials world. *Engineering Science and Technology, an International Journal.* **19**(2): p. 717-736.

[18.] Mohammed, L., Ansari, M. N., Pua, G., Jawaid, M., & Islam, M. S. (2015). A review on natural fiber reinforced polymer composite and its applications. *International journal of polymer science*, *2015*.

[19.] Abidin, N. M., Sultan, M. T., Hua, L. S., Basri, A. A., Md Shah, A. U., & Safri, S. N. (2019). A brief review of computational analysis and experimental models of composite materials for aerospace applications. *Journal of Reinforced Plastics and Composites*, *38*(23-24), 1031-1039.

[20.] Ilyas, R. A., Sapuan, S. M., Norizan, M. N., Atikah, M. S. N., Huzaifah, M. R. M., Radzi, A. M., ... & Jumaidin, R. (2019). Potential of natural fibre composites for transport industry: A review. In *Prosiding Seminar Enau Kebangsaan* (Vol. 2019, pp. 2-11). Persatuan Pembangunan dan Industri Enau Malaysia (PPIEM) Bahau, Negeri.

[21.] Kaliwon, J., Ahmad, S.S., and Aziz, A.A.,(2018). OIL PALM EMPTY FRUIT BUNCH (EFB) AS ENERGY EFFICIENT ROOFING MATERIAL. *academia.edu.*

[22.] Sapuan, S. M., Sahari, J., Ishak, M. R., & Sanyang, M. L. (Eds.). (2018). *Sugar palm biofibers, biopolymers, and biocomposites*. CRC Press..

[23.] Mohammed, L., Ansari, M.N., Pua, G., Jawaid, M., and Islam, M.S., (2015). A review on natural fiber reinforced polymer composite and its applications. *International Journal of Polymer Science*. **2015**.

[24.] Jaafar, C.A., Zainol, I., Rizal, M.M., and Sultan, U.,(2018). Preparation and characterisation of epoxy/silica/kenaf composite using hand lay-up method. in *27th Scientific Conference of the Microscopy Society Malaysia (27th SCMSM 2018)*. Melaka Malaysia.

[25.] Ayu, R.S., Khalina, A., Harmaen, A.S., Zaman, K., Isma, T., Liu, Q., Ilyas, R., and Lee, C.H.J.P., (2020). Characterization study of empty fruit bunch (EFB) *fibers reinforcement in poly (Butylene) succinate (PBS)/starch/glycerol composite sheet.* **12**(7): p. 1571.

[26.] Syafiq, R., Sapuan, S. M., Zuhri, M. Y. M., Ilyas, R. A., Nazrin, A., Sherwani, S. F. K., & Khalina, A. (2020). Antimicrobial activities of starch-based biopolymers and biocomposites incorporated with plant essential oils: A review. *Polymers,* 12(10), 2403..

[27.] Sabaruddin, F. A., Paridah, M. T., Sapuan, S. M., Ilyas, R. A., Lee, S. H., Abdan, K., & Abdul Khalil, H. P. S. (2021). The effects of unbleached and bleached nanocellulose on the thermal and flammability of polypropylene-reinforced kenaf core hybrid polymer bionanocomposites. *Polymers*, 13(1), 116.

[28.] Omran, A. A. B., Mohammed, A. A., Sapuan, S. M., Ilyas, R. A., Asyraf, M. R. M., Rahimian Koloor, S. S., & Petrů, M. (2021). Micro-and nanocellulose in polymer composite materials: A review. *Polymers*, 13(2), 231..

[29.] Ilyas, R. A., Sapuan, S. M., Ishak, M. R., & Zainudin, E. S. (2018). Development and characterization of sugar palm nanocrystalline cellulose reinforced sugar palm starch bionanocomposites. *Carbohydrate polymers,* 202, 186-202.

[30.] Ilyas, R. A., Sapuan, S. M., Atikah, M. S. N., Asyraf, M. R. M., Rafiqah, S. A., Aisyah, H. A., & Norrrahim, M. N. F. (2021). Effect of hydrolysis time on the morphological, physical, chemical, and thermal behavior of sugar palm nanocrystalline cellulose (Arenga pinnata (Wurmb.) Merr). *Textile Research* Journal, *91(1-2), 152-167.*

[31.] Ilyas, R. A., Sapuan, S. M., Atiqah, A., Ibrahim, R., Abral, H., Ishak, M. R., & Ya, H. (2020). Sugar palm (Arenga pinnata [Wurmb.] Merr) starch films containing sugar palm nanofibrillated cellulose as reinforcement: Water barrier properties. *Polymer Composites,* 41(2), 459-467.

[32.] Jumaidin, R., Khiruddin, M. A. A., Saidi, Z. A. S., Salit, M. S., & Ilyas, R. A. (2020). Effect of cogon grass fibre on the thermal, mechanical and biodegradation properties of thermoplastic cassava starch biocomposite. *International Journal of Biological Macromolecules*, 146, 746-755..

[33.] Ilyas, R. A., Sapuan, S. M., Ibrahim, R., Abral, H., Ishak, M. R., Zainudin, E. S., & Jumaidin, R. (2019). Effect of sugar palm nanofibrillated cellulose concentrations on morphological, mechanical and physical properties of biodegradable films based on agro-waste sugar palm (Arenga pinnata (Wurmb.) Merr) starch. *Journal of Materials Research and Technolog*y, 8(5), 4819-4830..

[34.] Rozilah, A., Jaafar, C. A., Sapuan, S. M., Zainol, I., & Ilyas, R. A. (2020). The effects of silver nanoparticles compositions on the mechanical, physiochemical, antibacterial, and morphology properties of sugar palm starch biocomposites for antibacterial coating. *Polymers*, 12(11), 2605..

[35.] Ilyas, R., Sapuan, S., Norrrahim, M.N.F., Yasim-Anuar, T.A.T., Kadier, A., Kalil, M.S., Atikah, M., Ibrahim, R., Asrofi, M., and Abral, H.,(2020).

Nanocellulose/starch biopolymer nanocomposites: Processing, manufacturing, and applications, *in Advanced Processing, Properties, and Applications of Starch and Other Bio-Based Polymers*., Elsevier. p. 65-88.

[36.] Ilyas, R. A., Sapuan, S. M., Ibrahim, R., Abral, H., Ishak, M. R., Zainudin, E. S., & Jumaidin, R. (2020). Thermal, biodegradability and water barrier properties of bio-nanocomposites based on plasticised sugar palm starch and nanofibrillated celluloses from sugar palm fibres. *Journal of Biobased* Materials and Bioenergy, 14(2), 234-248.

[37.] Syafri, E., Yulianti, E., Asrofi, M., Abral, H., Sapuan, S. M., Ilyas, R. A., & Fudholi, A. (2019). Effect of sonication time on the thermal stability, moisture absorption, and biodegradation of water hyacinth (Eichhornia crassipes) nanocellulose-filled bengkuang (Pachyrhizus erosus) starch biocomposites. Journal of Materials Research and Technology, 8(6), 6223-6231.

[38.] Shahroze, R., Chandrasekar, M., Senthilkumar, K., Senthilmuthukumar, T., Ishak, M., and Asyraf, M., (2019). A review on the various fibre treatment techniques used for the fibre surface modification of the sugar palm fibres. in *Proceedings of the Seminar Enau Kebangsaan (pp. 48-52)*.

[39.] Tawakkal, I.S.M., Talib, R.A., Abdan, K., and Ling, C.N.J.B., (2012). Mechanical and physical properties of kenaf-derived cellulose (KDC)-filled polylactic acid (PLA) composites. *BioResources*, **7**(2): p. 1643-1655.

[40.] Dumanlı, A. G., & Windle, A. H. (2012). Carbon fibres from cellulosic precursors: a review. *Journal of Materials Science,* 47, 4236-4250

[41.] Ilyas, R. A., Sapuan, S. M., Ibrahim, R., Abral, H., Ishak, M. R., Zainudin, E. S., & Jumaidin, R. (2019). Sugar palm (Arenga pinnata (Wurmb.) Merr) cellulosic fibre hierarchy: A comprehensive approach from macro to nano scale. *Journal of Materials Research and Technology*, 8(3), 2753-2766..

[42.] Vickers, N. J. (2017). Animal communication: when i'm calling you, will you answer too?. *Current biology*, 27(14), R713-R715..

[43.] Chandrasekar, M., Shahroze, R. M., Ishak, M. R., Saba, N., Jawaid, M., Senthilkumar, K., & Siengchin, S. (2019). Flax and sugar palm reinforced epoxy composites: effect of hybridization on physical, mechanical, morphological and dynamic mechanical properties. *Materials Research Express*, 6(10), 105331.

[44.] Mohd Nurazzi, N., Khalina, A., Chandrasekar, M., Aisyah, H. A., Ayu Rafiqah, S., Ilyas, R. A., & Hanafee, Z. M. (2020). Effect of fiber orientation and fiber loading on the mechanical and thermal properties of sugar palm yarn fiber reinforced unsaturated polyester resin composites. *Polimery*, 65.

[45.] Huzaifah, M. R. M., Sapuan, S. M., Leman, Z., & Ishak, M. R. (2019). Comparative study of physical, mechanical, and thermal properties on sugar palm fiber (Arenga pinnata (Wurmb) Merr.) reinforced vinyl ester composites obtained from different geographical locations. *BioResources*, 14(1), 619-637.

[46.] Jaafar, C. N. A., Rizal, M. A. M., & Zainol, I. (2018). Effect of kenaf alkalization treatment on morphological and mechanical properties of epoxy/silica/kenaf composite. *Int. J. Eng*. Technol, 7, 258-263.

[47.] Azwa, Z. N., Yousif, B. F., Manalo, A. C., & Karunasena, W. (2013). A review on the degradability of polymeric composites based on natural fibres. *Materials & Design*, 47, 424-442.

[48.] Ilyas, R. A., Sapuan, S. M., Asyraf, M. R. M., Atikah, M. S. N., Ibrahim, R., Dele-Afolabi, T. T., & Hazrol, M. D. (2020). Introduction to biofiller-reinforced degradable polymer composites. *In Biofiller-Reinforced Biodegradable Polymer Composites* (pp. 1-23). CRC press.

[49.] Chandrasekar, M., Ishak, M. R., Sapuan, S. M., Leman, Z., & Jawaid, M. (2017). A review on the characterisation of natural fibres and their composites after alkali treatment and water absorption. *Plastics, Rubber and Composites*, 46(3), 119-136..

[50.] Hamidon, M. H., Sultan, M. T., Ariffin, A. H., & Shah, A. U. (2019). Effects of fibre treatment on mechanical properties of kenaf fibre reinforced composites: a review. *Journal of Materials Research and Technology*, 8(3), 3327-3337.

[51.] Kabir, M. M., Wang, H., Lau, K. T., & Cardona, F. (2012). Chemical treatments on plant-based natural fibre reinforced polymer composites: An overview. *Composites Part B: Engineering*, 43(7), 2883-2892.

[52.] Johari, A., Ishak, M., Leman, Z., Yusoff, M., Asyraf, M., Ashraf, W., and Sharaf, H.,(2019). Fabrication and cut-in speed enhancement of savonius vertical axis wind turbine (SVAWT) with hinged blade using fiberglass composites. *in Seminar Enau Kebangsaan. Institute of Tropical Forestry and Forest Products (INTROP), Universiti.*

[53.] Johari, A. N., Ishak, M. R., Leman, Z., Yusoff, M. Z. M., & Asyraf, M. R. M. (2020). Creep behaviour monitoring of short-term duration for fiber-glass reinforced composite cross-arms with unsaturated polyester resin samples using conventional analysis. *Journal of Mechanical Engineering and Sciences, 14*(4), 7361-7368.

[54.] Ashby, M. F., Evans, T., Fleck, N. A., Hutchinson, J. W., Wadley, H. N. G., & Gibson, L. J. (2000). Metal foams: a design guide. Elsevier.

[55.] Wadley, H. N. (2006). Multifunctional periodic cellular metals. Philosophical Transactions of the Royal Society A: *Mathematical, Physical and Engineering Sciences*, 364(1838), 31-68..

[56.] Zhu, F., Wang, Z., Lu, G., & Nurick, G. (2010). Some theoretical considerations on the dynamic response of sandwich structures under impulsive loading. *International Journal of Impact Engineering,* 37(6), 625-637.

[57.] Alsubari, S., Zuhri, M. Y. M., Sapuan, S. M., Ishak, M. R., Ilyas, R. A., & Asyraf, M. R. M. (2021). Potential of natural fiber reinforced polymer composites in sandwich structures: A review on its mechanical properties. *Polymers*, 13(3), 423.

[58.] Gong, L., Kyriakides, S., & Jang, W. Y. (2005). Compressive response of open-cell foams. Part I: Morphology and elastic properties. *International Journal of Solids and Structures*, 42(5-6), 1355-1379.

[59.] Ray, S. S. (2013). Environmentally friendly polymer nanocomposites: types, processing and properties. *Elsevier*.

[60.] Gong, L., & Kyriakides, S. (2005). Compressive response of open cell foams Part II: Initiation and evolution of crushing. *International Journal of Solids and Structures,* 42(5-6), 1381-1399.

[61.] Ashraf, W., Ishak, M. R., Zuhri, M. Y. M., Yidris, N., Yaacob, A. M. B., & Asyraf, M. R. M. (2019, April). Investigation of different facesheet materials on compression properties of honeycomb sandwich composite. *In Seminar Enau Kebangsaan* (Vol. 1, pp. 129-132).

[62.] Subhash, G., Liu, Q., & Gao, X. L. (2006). Quasistatic and high strain rate uniaxial compressive response of polymeric structural foams. *International Journal of Impact Engineering*, 32(7), 1113-1126..

[63.] Saha, M. C., Mahfuz, H., Chakravarty, U. K., Uddin, M., Kabir, M. E., & Jeelani, S. (2005). Effect of density, microstructure, and strain rate on compression behavior of polymeric foams. *Materials Science and Engineering: A,* 406(1-2), 328-336.

[64.] Chen, J., Fang, H., Liu, W., Zhu, L., Zhuang, Y., Wang, J., & Han, J. (2018). Energy absorption of foam-filled multi-cell composite panels under quasi-static compression. *Composites Part B: Engineering*, 153, 295-305.

[65.] Sun, G., Wang, E., Wang, H., Xiao, Z., & Li, Q. (2018). Low-velocity impact behaviour of sandwich panels with homogeneous and stepwise graded foam cores. *Materials & Design,* 160, 1117-1136.

[66.] Evans, A. G., Hutchinson, J. W., Fleck, N. A., Ashby, M. F., & Wadley, H. N. G. (2001). The topological design of multifunctional cellular metals. *Progress in materials science,* 46(3-4), 309-327.

[67.] Lu, G., & Yu, T. X. (2003). Energy absorption of structures and materials. *Elsevier*.

[68.] Hou, W., Zhu, F., Lu, G., & Fang, D. N. (2010). Ballistic impact experiments of metallic sandwich panels with aluminium foam core. I*nternational journal of impact engineering*, 37(10), 1045-1055..

[69.] Liu, H., Liu, H., Yang, J., & Zhao, S. (2013). Cantilever sandwich beams with pyramidal truss cores subjected to tip impact. *Science China Technological Sciences*, 56, 181-187.

[70.] Dayyani, I., Shaw, A. D., Flores, E. S., & Friswell, M. I. (2015). The mechanics of composite corrugated structures: A review with applications in morphing aircraft. *Composite Structures*, 133, 358-380.

[71.] Han, B., Qin, K., Yu, B., Wang, B., Zhang, Q., & Lu, T. J. (2016). Honeycomb–corrugation hybrid as a novel sandwich core for significantly enhanced compressive performance. *Materials & Design*, 93, 271-282.

[72.] Zhang, L., Hebert, R., Wright, J. T., Shukla, A., & Kim, J. H. (2014). Dynamic response of corrugated sandwich steel plates with graded cores. *International Journal of Impact Engineering*, 65, 185-194..

[73.] Hou, S., Shu, C., Zhao, S., Liu, T., Han, X., & Li, Q. (2015). Experimental and numerical studies on multi-layered corrugated sandwich panels under crushing loading. *Composite Structures*, 126, 371-385..

[74.] Rejab, M. R. M., & Cantwell, W. J. (2013). The mechanical behaviour of corrugated-core sandwich panels. *Composites Part B: Engineering*, 47, 267-277.

[75.] Yan, L. L., Yu, B., Han, B., Chen, C. Q., Zhang, Q. C., & Lu, T. J. (2013). Compressive strength and energy absorption of sandwich panels with aluminum foam-filled corrugated cores. *Composites Science and Technology*, 86, 142-148.

[76.] Devi, S. R., Valarmathi, B., & Kumar, R. M. (2017). Growth Aspects, Structural and Optical Properties of 2-aminopyridinium 2, 4 Dinitrophenolate Single Crystal. *Mechanics, Materials Science & Engineering Journal,* 9.

[77.] Yang, X., Ma, J., Shi, Y., Sun, Y., & Yang, J. (2017). Crashworthiness investigation of the bio-inspired bi-directionally corrugated core sandwich panel under quasi-static crushing load. *Materials & Design,* 135, 275-290.

[78.] Zhou, J., Guan, Z. W., & Cantwell, W. J. (2016). Scaling effects in the mechanical response of sandwich structures based on corrugated composite cores. *Composites Part B: Engineering,* 93, 88-96.

[79.] Zarei, H., & Kröger, M. (2008). Optimum honeycomb filled crash absorber design. *Materials & Design*, 29(1), 193-204.

[80.] Abbadi, A., Koutsawa, Y., Carmasol, A., Belouettar, S., & Azari, Z. (2009). Experimental and numerical characterization of honeycomb sandwich composite panels. *Simulation Modelling Practice and Theory*, 17(10), 1533-1547.

[81.] Kaman, M. O., Solmaz, M. Y., & Turan, K. (2010). Experimental and numerical analysis of critical buckling load of honeycomb sandwich panels. *Journal of composite materials,* 44(24), 2819-2831.

[82.] Cote, F., Deshpande, V. S., Fleck, N. A., & Evans, A. G. (2004). The out-of-plane compressive behavior of metallic honeycombs. *Materials Science and Engineering:* A, 380(1-2), 272-280.

[83.] Sun, Z., Shi, S., Guo, X., Hu, X., & Chen, H. (2016). On compressive properties of composite sandwich structures with grid reinforced honeycomb core. *Composites Part B: Engineering*, 94, 245-252.

[84.] Xiong, J., Vaziri, A., Ghosh, R., Hu, H., Ma, L., & Wu, L. (2016). Compression behavior and energy absorption of carbon fiber reinforced composite sandwich panels made of three-dimensional honeycomb grid cores. *Extreme Mechanics Letters,* 7, 114-120.

[85.] Azaman, M. D., Sapuan, S. M., Sulaiman, S., Zainudin, E. S., & Khalina, A. (2013). Shrinkages and warpage in the processability of wood-filled polypropylene composite thin-walled parts formed by injection molding. *Materials & Design* (1980-2015), 52, 1018-1026.

[86.] Miller, W., Smith, C. W., & Evans, K. E. (2011). Honeycomb cores with enhanced buckling strength. *Composite Structures,* 93(3), 1072-1077.

[87.] Xu, G. D., Yang, F., Zeng, T., Cheng, S., & Wang, Z. H. (2016). Bending behavior of graded corrugated truss core composite sandwich beams. *Composite Structures*, 138, 342-351.

[88.] Kong, B., Cai, C. S., & Kong, X. (2013). Thermal behaviors of concrete and steel bridges after slab replacements with GFRP honeycomb sandwich panels. *Engineering structures*, 56, 2041-2051.

[89.] Zuhri, M. Y. M., Guan, Z. W., & Cantwell, W. J. (2014). The mechanical properties of natural fibre based honeycomb core materials. *Composites Part B: Engineering*, 58, 1-9.

[90.] Petrone, G., Rao, S., De Rosa, S., Mace, B. R., Franco, F., & Bhattacharyya, D. (2013). Behaviour of fibre-reinforced honeycomb core under low velocity impact loading. *Composite Structures*, 100, 356-362.

[91.] Lu, C., Zhao, M., Jie, L., Wang, J., Gao, Y., Cui, X., & Chen, P. (2015). Stress distribution on composite honeycomb sandwich structure suffered from bending load. *Procedia Engineering,* 99, 405-412.

[92.] Shi, S., Sun, Z., Hu, X., & Chen, H. (2014). Flexural strength and energy absorption of carbon-fiber–aluminum-honeycomb composite sandwich reinforced by aluminum grid. *Thin-Walled Structures,* 84, 416-422.

[93.] Stocchi, A., Colabella, L., Cisilino, A., & Álvarez, V. (2014). Manufacturing and testing of a sandwich panel honeycomb core reinforced with natural-fiber fabrics. *Materials & Design*, 55, 394-403.

[94.] Yang, F. and Fei, B.,(2012). The research on bamboo-wood corrugated sandwich panel. in *Proceedings of the 55th International Convention of Society of Wood Science and Technology, Beijing, China*.

[95.] Rao, S., Jayaraman, K., & Bhattacharyya, D. (2011). Short fibre reinforced cores and their sandwich panels: Processing and evaluation. *Composites Part A: Applied Science and Manufacturing,* 42(9), 1236-1246.

[96.] Nishino, T., Hirao, K., Kotera, M., Nakamae, K., & Inagaki, H. (2003). Kenaf reinforced biodegradable composite. *Composites science and technology,* 63(9), 1281-1286.

[97.] Jawaid, M. H. P. S., & Khalil, H. A. (2011). Cellulosic/synthetic fibre reinforced polymer hybrid composites: A review. *Carbohydrate polymer*s, 86(1), 1-18.

[98.] Aisyah, H. A., Paridah, M. T., Sapuan, S. M., Khalina, A., Berkalp, O. B., Lee, S. H., Ilyas, R. A. (2019). Thermal properties of woven kenaf/carbon fibre-reinforced epoxy hybrid composite panels. *International Journal of Polymer Science,* 2019, 1-8.

[99.] Saba, N., Jawaid, M., Alothman, O. Y., & Paridah, M. T. (2016). A review on dynamic mechanical properties of natural fibre reinforced polymer composites. *Construction and Building Materials,* 106, 149-159.

[100.] Nurazzi, N. M., Khalina, A., Sapuan, S. M., & Ilyas, R. A. (2019). Mechanical properties of sugar palm yarn/woven glass fiber reinforced unsaturated polyester composites: Effect of fiber loadings and alkaline treatment. *Polimery*, 64(10), 665-675.

[101.] Baihaqi, N. N., Khalina, A., Nurazzi, N. M., Aisyah, H. A., Sapuan, S. M., & Ilyas, R. A. (2021). Effect of fiber content and their hybridization on bending and torsional strength of hybrid epoxy composites reinforced with carbon and sugar palm fibers. *Polimery*, 66(1), 36-43.

[102.] Nurazzi, N. M., Khalina, A., Sapuan, S. M., Ilyas, R. A., Rafiqah, S. A., & Hanafee, Z. M. (2020). Thermal properties of treated sugar palm yarn/glass fiber reinforced unsaturated polyester hybrid composites. *Journal of Materials Research and Technology,* 9(2), 1606-1618.

[103.] Kumar, T. S. M., Chandrasekar, M., Senthilkumar, K., Ilyas, R. A., Sapuan, S. M., Hariram, N., & Siengchin, S. (2021). Characterization, thermal and antimicrobial properties of hybrid cellulose nanocomposite films with in-situ generated copper nanoparticles in Tamarindus indica Nut Powder. *Journal of Polymers and the Environment,* 29, 1134-1142..

[104.] Alavudeen, A., Rajini, N., Karthikeyan, S., Thiruchitrambalam, M., & Venkateshwaren, N. (2015). Mechanical properties of banana/kenaf fiber-reinforced hybrid polyester composites: Effect of woven fabric and random orientation. *Materials & Design* (1980-2015), 66, 246-257.

[105.] Venkatesh, R. P., Ramanathan, K., & Krishnan, S. R. (2015). Study on physical and mechanical properties of NFRP hybrid composites. *niscair online periodicals repository (nopr)*

[106.] Wu, C., Yang, K., Gu, Y., Xu, J., Ritchie, R. O., & Guan, J. (2019). Mechanical properties and impact performance of silk-epoxy resin composites modulated by flax fibres. *Composites Part A: Applied Science and Manufacturing*, 117, 357-368..

[107.] Gupta, M. K. (2017). Effect of frequencies on dynamic mechanical properties of hybrid jute/sisal fibre reinforced epoxy composite. *Advances in Materials and Processing Technologies,* 3(4), 651-664.

[108.] Fiore, V., Scalici, T., Calabrese, L., Valenza, A., & Proverbio, E. (2016). Effect of external basalt layers on durability behaviour of flax reinforced composites. *Composites Part B: Engineering,* 84, 258-265.

[109.] Živković, I., Fragassa, C., Pavlović, A., & Brugo, T. (2017). Influence of moisture absorption on the impact properties of flax, basalt and hybrid flax/basalt fiber reinforced green composites. *Composites Part B: Engineering,* 111, 148-164.

[110.] Kumar, K. S., Siva, I., Rajini, N., Jappes, J. W., & Amico, S. C. (2016). Layering pattern effects on vibrational behavior of coconut sheath/banana fiber hybrid composites. *Materials & Design*, *90*, 795-803.

[111.] Shen, Y., Guo, Y., & Li, Y. (2019, March). Investigation of Hybrid Natural Fibre Reinforced Composite for Impact Energy Absorption. In *IOP Conference Series: Materials Science and Engineering* (Vol. 484, No. 1, p. 012014). IOP Publishing..

[112.] Phillips, C., Kortschot, M., & Azhari, F. (2022). Towards standardizing the preparation of test specimens made with material extrusion: Review of current techniques for tensile testing. *Additive Manufacturing*, 103050..

[113.] Dizon, J. R. C., Espera Jr, A. H., Chen, Q., & Advincula, R. C. (2018). Mechanical characterization of 3D-printed polymers. *Additive manufacturing*, *20*, 44-67.

[114.] Saba, N., Jawaid, M., & Sultan, M. T. H. (2019). An overview of mechanical and physical testing of composite materials. *Mechanical and physical testing of biocomposites, fibre-reinforced composites and hybrid composites*, 1-12.

[115.] International Organization for Standardization. (2014). *Rigid Cellular Plastics-Determination of Compression Properties*. ISO..

[116.] Forster, A. M. (2015). *Materials Testing Standards for Additive Manufacturing of Polymer Materials:* (p. 8059). US Department of Commerce, National Institute of Standards and Technology.

[117.] Asyraf, M. R. M., Ishak, M. R., Sapuan, S. M., Yidris, N., Johari, A. N., Ashraf, W., & Mazlan, R. (2019, April). Creep test rig for full-scale composite crossarm:

Simulation modelling and analysis. In *Proceedings of the Seminar Enau Kebangsaan, Bahau, Malaysia* (pp. 34-38).

[118.] Du, Y., Yan, N., & Kortschot, M. T. (2012). Light-weight honeycomb core sandwich panels containing biofiber-reinforced thermoset polymer composite skins: Fabrication and evaluation. *Composites Part B: Engineering*, *43*(7), 2875-2882.

[119.] Du, Y., Yan, N., & Kortschot, M. T. (2014). Novel lightweight sandwich-structured bio-fiber-reinforced poly (lactic acid) composites. *Journal of Materials Science*, *49*, 2018-2026.

[120.] Sezgin, F. E., Tanoğlu, M., Eğilmez, O. Ö., & Dönmez, C. (2010). Mechanical behavior of polypropylene-based honeycomb-core composite sandwich structures. *Journal of reinforced plastics and composites*, *29*(10), 1569-1579.

[121.] Jusoh, A. F., Rejab, M. R. M., Siregar, J. P., & Bachtiar, D. (2016). Natural fiber reinforced composites: a review on potential for corrugated core of sandwich structures. In *MATEC Web of conferences* (Vol. 74, p. 00033). EDP Sciences.

[122.] Zuhri, M. Y. M., Liao, Y., Wang, Q. Y., & Guan, Z. W. (2019). The energy absorbing properties of bamboo-based structures. *Journal of Sandwich Structures & Materials*, *21*(3), 1032-1054.

[123.] Roslan, S. A. H., Hassan, M. Z., Rasid, Z. A., Zaki, S. A., Daud, Y., Aziz, S., & Ismail, Z. (2015). Mechanical properties of bamboo reinforced epoxy sandwich structure composites. *International Journal of Automotive and Mechanical Engineering*..

[124.] Kim, N. K., Dutta, S., & Bhattacharyya, D. (2018). A review of flammability of natural fibre reinforced polymeric composites. *Composites Science and Technology*, *162*, 64-78..

[125.] Zulkarnain, M., Tofrowaih, K. A., & Ariyanti, S. (2022). Effect of Natural Fibers Reinforcement of Honeycomb Sandwich Using Numerical Analysis. *International Journal of Technology*, *13*(4).

[126.] Labans, E., & Kalnins, K. (2014). Experimental validation of the stiffness optimisation for plywood sandwich panels with rib-stiffened core. *Wood Res*, *59*(4), 793-802.

[127.] Edgars, L., Kaspars, Z., & Kaspars, K. (2017). Structural performance of wood based sandwich panels in four point bending. *Procedia Engineering*, *172*, 628-633.

[128.] Najmi, H., Luche, J., & Rogaume, T. (2021). Thermal decomposition of multilayer honeycomb core laminate sandwich composite panels in cone calorimeter apparatus–Effect of the top decomposed layer. *Journal of Composite Materials*, *55*(17), 2349-2368.

[129.] Makovicka Osvaldova, L., Kadlicova, P., & Rychly, J. (2020). Fire characteristics of selected tropical woods without and with fire retardant. *Coatings*, *10*(6), 527.

[130.] Xu, Q., Chen, L., Harries, K. A., Zhang, F., Liu, Q., & Feng, J. (2015). Combustion and charring properties of five common constructional wood species from cone calorimeter tests. *Construction and Building Materials*, *96*, 416-427..

[131.] Lacasta Palacio, A. M., Haurie Ibarra, L., Montón Lecumberri, J., Navarro Ezquerra, A., Giraldo, P., Sotomayor, J., & Palumbo, M. (2016). Characterization of the fire behaviour of tropical wood species for use in the construction industry. In *WCTE 2016: World Conference on Timber Engineering: August 22-25, 2016, Vienna, Austria: e-book* (pp. 5387-5395). Technischen Universität Graz..

[132.] Pornwannachai, W., Ebdon, J. R., & Kandola, B. K. (2020). Fire-resistant flax-reinforced polypropylene/polylactic acid composites with optimized fire and mechanical performances. *Journal of Thermoplastic Composite Materials*, *33*(7), 898-914..

[133.] Pornwannachai, W., Ebdon, J. R., & Kandola, B. K. (2018). Fire-resistant natural fibre-reinforced composites from flame retarded textiles. *Polymer Degradation and Stability*, *154*, 115-123.

[134.] Kandare, E., Luangtriratana, P., & Kandola, B. K. (2014). Fire reaction properties of flax/epoxy laminates and their balsa-core sandwich composites with or without fire protection. *Composites Part B: Engineering*, *56*, 602-610.

[135.] Kandola, B. K., Pornwannachai, W., & Ebdon, J. R. (2020). Flax/pp and flax/pla thermoplastic composites: Influence of fire retardants on the individual components. *Polymers*, *12*(11), 2452.

[136.] Dutta, S., Kim, N. K., Das, R., & Bhattacharyya, D. (2021). Evaluating orientation effects on the fire reaction properties of flax-polypropylene composites. *Polymers*, *13*(16), 2586.

[137.] Dutta, S., Kim, N. K., Das, R., & Bhattacharyya, D. (2019). Effects of sample orientation on the fire reaction properties of natural fibre composites. *Composites Part B: Engineering*, *157*, 195-206.

[138.] Dutta, S., Kim, N. K., Das, R., & Bhattacharyya, D. (2021). Evaluating orientation effects on the fire reaction properties of flax-polypropylene composites. *Polymers*, *13*(16), 2586.

[139.] Chukwunwike, S. A., Ike-Eze, I. E., Aigbodion, V. S., & Okafor, K. J. (2019). Flammability properties of flame retarded natural fibre reinforced polymer composites: An overview. *J. Mater. Environ. Sci*, *10*(7), 647-656..

[140.] Bachtiar, E. V., Kurkowiak, K., Yan, L., Kasal, B., & Kolb, T. (2019). Thermal stability, fire performance, and mechanical properties of natural fibre fabric-reinforced polymer composites with different fire retardants. *Polymers*, *11*(4), 699.

[141.] Kim, N. K., Dutta, S., & Bhattacharyya, D. (2019). Heat and smoke production of flax fibre reinforced composites under horizontal and vertical orientations. *Composites Part B: Engineering*, *178*, 107467.

[142.] Helwig, M., & Paukszta, D. (2000). Flammability of composites based on polypropylene and flax fibers. *Molecular Crystals and Liquid Crystals Science and Technology. Section A. Molecular Crystals and Liquid Crystals*, *354*(1), 373-380.

[143.] Subasinghe, A., Das, R., & Bhattacharyya, D. (2016). Study of thermal, flammability and mechanical properties of intumescent flame retardant PP/kenaf nanocomposites. *International Journal of Smart and Nano Materials*, *7*(3), 202-220.

[144.] Zheng, D., Ding, R. Y., Lei, Z., Xingqun, Z., & Chong-Wen, Y. (2015). Thermal properties of flax fiber scoured by different methods. *Thermal Science*, *19*(3), 939-945.

[145.] Chanda, A., Kim, N. K., Wijaya, W., & Bhattacharyya, D. (2021). Fire reaction of sandwich panels with corrugated and honeycomb cores made from natural materials. *Journal of Sandwich Structures & Materials*, *23*(8), 4196-4217.

[146.] John, M. J., Anandjiwala, R. D., Wambua, P., Chapple, S. A., Klems, T., Doecker, M., ... & Erasmus, L. D. (2008). Bio-based structural composite materials for aerospace applications. South African International Aerospace Symposium.

[147.] Chen, W., Yu, H., Liu, Y., Chen, P., Zhang, M., & Hai, Y. (2011). Individualization of cellulose nanofibers from wood using high-intensity ultrasonication combined with chemical pretreatments. *Carbohydrate Polymers*, *83*(4), 1804-1811.

[148.] de Oliveira, L. Á., Vieira, M. M., dos Santos, J. C., Freire, R. T. S., Tonatto, M. L. P., Panzera, T. H., ... & Scarpa, F. (2022). An investigation on the mechanical behaviour of sandwich composite structures with circular honeycomb bamboo core. *Discover Mechanical Engineering*, *1*(1), 7.

[149.] Li, S., Feng, Y., Wang, M., & Hu, Y. (2018). Mechanical behavior of natural fiber-based bi-directional corrugated lattice sandwich structure. *Materials*, *11*(12), 2578.

[150.] Wang, Y., Cui, G., Shao, Z., Bao, Y., & Gao, H. (2019). Optimization of the hot pressing process for preparing flax fiber/PE thermoplastic composite. *Mechanical Engineering Science*, *1*(1).

[151.] Kiran, G. B., Suman, K. N. S., Rao, N. M., & Rao, R. U. M. (2011). A study on the influence of hot press forming process parameters on mechanical properties of green composites using Taguchi experimental design. *International Journal of Engineering, Science and Technology*, *3*(4).

[152.] Sanivada, U. K., Mármol, G., Brito, F. P., & Fangueiro, R. (2020). PLA composites reinforced with flax and jute fibers—A review of recent trends, processing parameters and mechanical properties. *Polymers*, *12*(10), 2373.

[153.] Standard, A., D3039, (2017),"Standard Test Method for Tensile Properties of Polymer Matrix Composite Materials*," ASTM International, West Conshohocken,* PA, 2017, DOI: 10.1520/D3039_D3039M-17.

[154.] Bin, H., Bo, Y., Yu, X., Chang-Qing, C., Qian-Cheng, Z., & Jian, L. T. (2015). Foam filling radically enhances transverse shear response of corrugated sandwich plates. *Materials & Design*, *77*, 132-141.

[155.] Wahid, A., Mouhib, N., Kartouni, A., Chakir, H., & ELghorba, M. (2019). Energy method for experimental life prediction of central core strand constituting a steel wire rope. *Engineering Failure Analysis*, *97*, 61-71.

[156.] Reaction-to-fire tests—Heat, I. S. O. (2015). release, smoke production and mass loss rate—Part 1: Heat release rate (cone calorimeter method) and smoke production rate (dynamic measurement): ISO 5660-1: 2015.

[157.] Chee, S. S., Jawaid, M., Alothman, O. Y., & Yahaya, R. (2020). Thermo-oxidative stability and flammability properties of bamboo/kenaf/nanoclay/epoxy hybrid nanocomposites. *RSC advances*, *10*(37), 21686-21697.

[158.] Ma, Q., Xiang, J. C., Wu, N. Z., & Xiao, H. L. (2020). Effect of microstructure change on permeability of flax-fiber reinforced silty clay soaked with zinc-ion solution. *Scientific Reports*, *10*(1), 11296.

[159.] Ejaz, M., Azad, M. M., Shah, A. U. R., Afaq, S. K., & Song, J. I. (2020). Mechanical and biodegradable properties of jute/flax reinforced PLA composites. *Fibers and Polymers*, *21*, 2635-2641.

[160.] Bourmaud, A., Le Duigou, A., Gourier, C., & Baley, C. (2016). Influence of processing temperature on mechanical performance of unidirectional polyamide 11–flax fibre composites. *Industrial Crops and Products*, *84*, 151-165.

[161.] Li, Q., Li, Y., Ma, H., Cai, S., & Huang, X. (2020). Effect of processing temperature on the static and dynamic mechanical properties and failure mechanisms of flax fiber reinforced composites. *Composites Communications*, *20*, 100343.

[162.] Gourier, C., Le Duigou, A., Bourmaud, A., & Baley, C. (2014). Mechanical analysis of elementary flax fibre tensile properties after different thermal cycles. *Composites Part A: Applied science and manufacturing*, *64*, 159-166.

[163.] Gourier, C., Le Duigou, A., Bourmaud, A., & Baley, C. (2014). Mechanical analysis of elementary flax fibre tensile properties after different thermal cycles. *Composites Part A: Applied science and manufacturing*, *64*, 159-166.

[164.] Zuhri, M. Y. M., Nasrudin, M. A., Nasrodin, M. A. M., Sapuan, S. M., & Hassan, M. Z. (2021). Mechanical properties under quasi-static loading of the core made of flax/poly (lactic acid) composite. *Polimery*, *66*(3), 193-197.

[165.] Mozafari, H., Khatami, S., & Molatefi, H. (2015). Out of plane crushing and local stiffness determination of proposed foam filled sandwich panel for Korean Tilting Train eXpress–Numerical study. *Materials & Design*, *66*, 400-411.

[166.] Yan, L., Su, P., Han, Y., & Han, B. (2020). Effects of Aluminum Foam Filling on Compressive Strength and Energy Absorption of Metallic Y-Shape Cored Sandwich Panel. *Metals*, *10*(12), 1670.

[167.] Zhang, J., Supernak, P., Mueller-Alander, S., & Wang, C. H. (2013). Improving the bending strength and energy absorption of corrugated sandwich composite structure. *Materials & Design (1980-2015)*, *52*, 767-773.

[168.] Li, Z., & Ma, J. (2020). Experimental study on mechanical properties of the sandwich composite structure reinforced by basalt fiber and nomex honeycomb. *Materials*, *13*(8), 1870.

[169.] Schartel, B., & Hull, T. R. (2007). Development of fire-retarded materials—interpretation of cone calorimeter data. *Fire and Materials: An International Journal*, *31*(5), 327-354.

APPENDICES

Appendix A: Flow chart

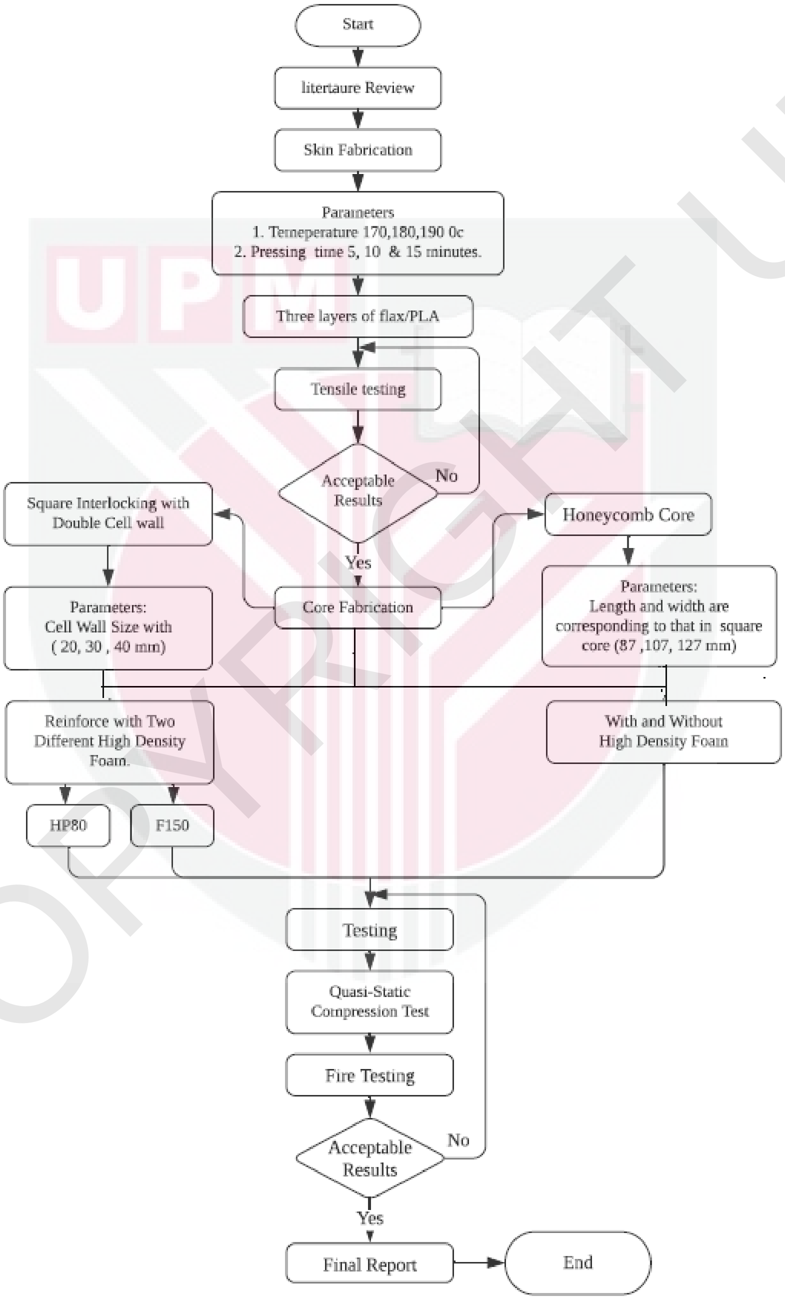

Appendix A: Detailed frame work of the research Methodology

Appendix B: DOE of Manufacturing Temperature

Appendix B: DOE of the experiment
Design scheme of processing parameters

Factor symbol	**Parameters**	**Level**		
		Low (-1)	**Center (0)**	**High (+1)**
MT	Manufacturing Temperature, (°C)	170	180	190
Pt	Pressing time, (min)	5	10	15

Full Factorial Design Table of Experimental Runs

StdOrder	RunOrder	CenterPt	Blocks	MT	Pt
1	1	1	1	170	5
2	2	1	1	190	5
3	3	1	1	170	15
4	4	1	1	190	15
5	5	1	1	180	5
6	6	1	1	180	15
7	7	1	1	170	10
8	8	0	1	180	10
9	9	1	1	190	10

StdOrder = Standard order
CenterPt = center point
MT = Manufacturing Temperature, (°C)
Pt = Pressing time, (min)

Results of tensile strength and tensile modulus with different combinations of processing condition

Sample No.	Input Factors		Output responses	
	MT	Pt	TS, σ (MPa)	TM, E (GPa)
1	170	5	21.97	1.29
2	190	5	22.64	2.22
3	170	15	19.22	1.87
4	190	15	19.20	4.07
5	180	5	26.81	2.04
6	180	15	20.99	2.70
7	170	10	20.68	1.98
8	180	10	23.61	2.64
9	190	10	20.77	3.23

Appendix C: SEA Calculation Sample

SEA values calculations using the trapezius method by calculating the area under the load-displacement curve. The area required to calculate the energy absorption in this example is 0 mm to 12 mm)

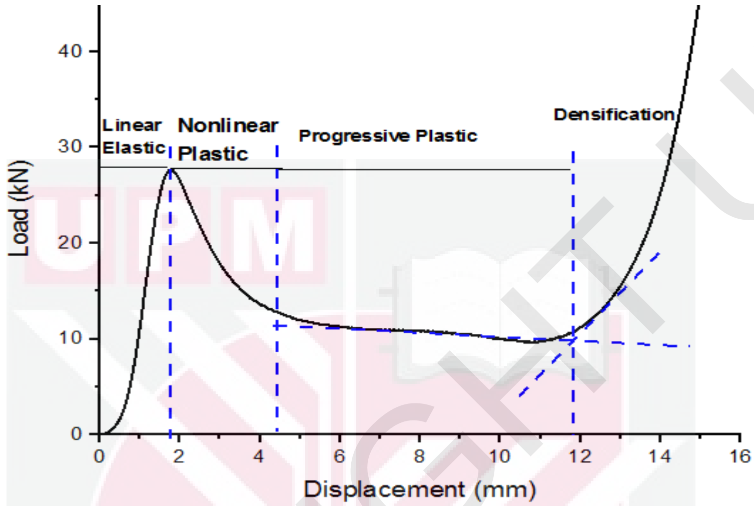

Sample of Raw data and SEA values calculation

SEA = Energy/ (Mass of the sample)

= 156.1868 kN-mm/ 28g

= **5.6 kJ/kg**

Appendix D: Part of Row data and SEA Calculation Sample

Compressive extension mm	Compressive load N	Displacement (mm)	Load (kN)	The area under the curve	Energy Absorption	SEA value
0.558195	462.8915	0	0	1.36151E-06	156.1868	**5.578099**
0.559032	466.1448	0.000837	0.003253	4.22689E-06		
0.559869	469.7371	0.001674	0.006846	8.27917E-06		
0.560766	474.5097	0.002571	0.011618	1.05152E-05		
0.561543	478.3289	0.003348	0.015437	1.5908E-05		
0.56244	482.9313	0.004245	0.02004	2.16775E-05		
0.563397	488.1689	0.005202	0.025277	2.71479E-05		
0.564353	494.3733	0.006158	0.031482	2.61194E-05		
0.56513	498.6152	0.006936	0.035724	2.85245E-05		
0.565908	500.5711	0.007713	0.03768	3.02681E-05		
0.566685	503.0919	0.00849	0.0402	3.24986E-05		
0.567462	506.3103	0.009267	0.043419	3.49026E-05		
0.568239	509.2889	0.010045	0.046397	3.76148E-05		
0.569017	513.2773	0.010822	0.050386	4.36151E-05		
0.569854	516.7234	0.011659	0.053832	5.39253E-05		
0.57081	521.7914	0.012616	0.0589	5.11797E-05		
0.571647	526.2849	0.013453	0.063393	5.48899E-05		
0.572485	530.6411	0.01429	0.06775	6.30144E-05		
0.573381	535.6736	0.015187	0.072782	7.27176E-05		
0.574338	542.1269	0.016143	0.079235	6.33048E-05		
0.575115	546.5818	0.01692	0.08369	6.64536E-05		
0.575893	550.1649	0.017698	0.087273	7.43965E-05		
0.57673	553.3876	0.018535	0.090496	7.20954E-05		
0.577507	557.8974	0.019312	0.095006	8.10153E-05		
0.578344	561.4474	0.020149	0.098556	7.7814E-05		
0.579121	564.5776	0.020926	0.101686	8.04149E-05		
0.579898	568.1403	0.021704	0.105249	8.33083E-05		
0.580676	571.9682	0.022481	0.109077	0.000100412		
0.581573	577.7484	0.023378	0.114857	9.8371E-05		
0.58241	583.0627	0.024215	0.120171	0.000102264		
0.583247	587.0776	0.025052	0.124186	0.000121878		

0.584203	593.5203	0.026008	0.130629	0.000128739		
0.58516	601.3931	0.026965	0.138502	0.000109571		
0.585937	606.3545	0.027742	0.143463	0.000112833		
0.586714	609.7867	0.02852	0.146895	0.00012467		
0.587552	613.8232	0.029357	0.150932	0.000118877		
0.588329	617.8708	0.030134	0.154979	0.000121968		
0.589106	621.7769	0.030911	0.158885	0.000124639		
0.589883	624.7039	0.031688	0.161812	0.000137272		
0.59072	629.0894	0.032525	0.166198	0.000151696		
0.591617	634.9608	0.033422	0.172069	0.000146173		
0.592454	640.1016	0.034259	0.17721	0.000150592		
0.593291	645.4771	0.035096	0.182586	0.000166292		
0.594188	651.1613	0.035993	0.18827	0.000195087		
0.595205	658.4618	0.03701	0.19557	0.000166633		
0.596042	665.4409	0.037847	0.202549	0.000158843		
0.596819	669.1528	0.038624	0.206261	0.000161491		
0.597596	672.1483	0.039401	0.209257	0.00017711		
0.598433	676.7862	0.040238	0.213895	0.000168274		
0.59921	681.9674	0.041016	0.219076	0.000158296		
0.599928	685.119	0.041733	0.222228	0.000173892		
0.600705	688.0908	0.04251	0.225199	0.000190359		
0.601542	692.4987	0.043347	0.229607	0.000194722		
0.602379	698.569	0.044184	0.235678	0.000199701		
0.603216	704.3408	0.045022	0.241449	0.000219034		
0.604113	709.866	0.045918	0.246975	0.000224433		
0.60501	716.4371	0.046815	0.253546	0.000246169		
0.605967	724.0217	0.047772	0.26113	0.000220689		
0.606804	729.0306	0.048609	0.266139	0.000208803		
0.607581	734.0743	0.049386	0.271183	0.000212268		
0.608358	737.8759	0.050163	0.274984	0.000232279		
0.609195	742.8678	0.051001	0.279976	0.000219304		
0.609973	747.2585	0.051778	0.284367	0.000204958		
0.61069	749.9168	0.052495	0.287025	0.000224888		
0.611467	754.5058	0.053272	0.291614	0.000264159		
0.612364	760.3251	0.054169	0.297434	0.000269625		
0.613261	766.7635	0.055066	0.303872	0.000257168		

0.614098	773.4458	0.055903	0.310554	0.000261928		
0.614935	778.2117	0.05674	0.31532	0.000324538		
0.615951	786.1744	0.057757	0.323283	0.000293335		
0.616848	793.7168	0.058654	0.330825	0.0002594		
0.617626	799.5901	0.059431	0.336699	0.000263531		
0.618403	804.2596	0.060208	0.341368	0.000287666		
0.61924	808.815	0.061045	0.345924	0.000270709		
0.620017	813.5931	0.061822	0.350702	0.000253021		
0.620735	817.4756	0.06254	0.354584	0.000277134		
0.621512	821.3769	0.063317	0.358485	0.00028058		
0.622289	826.3411	0.064094	0.36345	0.000351869		
0.623246	835.1068	0.065051	0.372215	0.00031436		
0.624083	841.834	0.065888	0.378943	0.00031961		
0.62492	847.4699	0.066725	0.384578	0.000372254		
0.625877	856.6799	0.067682	0.393788	0.000381174		
0.626833	866.0391	0.068638	0.403148	0.0003399		
0.62767	871.8326	0.069475	0.408941	0.000294816		
0.628388	875.8524	0.070193	0.412961	0.000322406		
0.629165	879.4846	0.07097	0.416593	0.000351166		
0.630002	885.3053	0.071807	0.422414	0.000330463		
0.630779	890.7628	0.072585	0.427871	0.00033413		
0.631557	894.8501	0.073362	0.431959	0.000337472		
0.632334	899.2513	0.074139	0.43636	0.000394541		
0.633231	906.4178	0.075036	0.443526	0.000401304		
0.634128	914.2345	0.075933	0.451343	0.000353409		
0.634905	920.9906	0.07671	0.458099	0.000413368		
0.635802	926.5627	0.077607	0.463671	0.000447611		
0.636758	935.0579	0.078563	0.472166	0.00045692		
0.637715	945.9247	0.07952	0.483033	0.000377304		
0.638492	950.7896	0.080297	0.487898	0.000351304		
0.63921	954.2368	0.081015	0.491345	0.000414163		
0.640047	961.065	0.081852	0.498174	0.000419835		
0.640884	967.9084	0.082689	0.505017	0.000363651		
0.641601	971.6774	0.083406	0.508786	0.000397541		
0.642378	976.9814	0.084184	0.51409	0.000432878		
0.643216	983.0333	0.085021	0.520142	0.000470219		

0.644112	991.4089	0.085918	0.528517	0.000445465		
0.644949	998.6792	0.086755	0.535788	0.000451321		
0.645786	1005.529	0.087592	0.542638	0.000523185		
0.646743	1013.982	0.088548	0.551091	0.000532449		
0.6477	1025.013	0.089505	0.562122	0.000439917		
0.648477	1032.825	0.090282	0.569934	0.000444367		
0.649254	1036.319	0.091059	0.573428	0.000448141		
0.650032	1042.536	0.091837	0.579645	0.000488093		
0.650869	1049.539	0.092674	0.586648	0.000458123		
0.651646	1054.999	0.093451	0.592108	0.000426407		
0.652363	1059.542	0.094168	0.596651	0.000501833		
0.6532	1065.22	0.095006	0.602329	0.00050747		
0.654037	1073.011	0.095843	0.61012	0.000551173		
0.654934	1081.971	0.096739	0.61908	0.000483872		
0.655712	1088.819	0.097517	0.625928	0.000564454		
0.656608	1095.782	0.098414	0.632891	0.000648202		
0.657625	1105.362	0.09943	0.642471	0.000580865		
0.658522	1115.837	0.100327	0.652946	0.000509922		
0.659299	1122.15	0.101104	0.659259	0.000514431		
0.660076	1127.269	0.101881	0.664378	0.000558614		
0.660913	1133.154	0.102718	0.670263	0.000523835		
0.66169	1140.635	0.103496	0.677744	0.00052914		
0.662468	1146.629	0.104273	0.683738	0.000532985		
0.663245	1150.53	0.10505	0.687639	0.000578183		
0.664082	1156.649	0.105887	0.693758	0.00058406		
0.664919	1164.738	0.106724	0.701847	0.000590865		
0.665756	1172.909	0.107561	0.710018	0.000597225		
0.666593	1179.934	0.108398	0.717043	0.000690268		
0.66755	1189.018	0.109355	0.726127	0.000700935		
0.668506	1202.083	0.110312	0.739192	0.000577514		
0.669284	1209.648	0.111089	0.746757	0.000582294		
0.670061	1214.575	0.111866	0.751684	0.00058657		
0.670838	1220.458	0.112643	0.757567	0.000637712		
0.671675	1229.13	0.11348	0.766239	0.000644731		
0.672512	1236.86	0.114318	0.773969	0.00060353		
0.67329	1242.01	0.115095	0.779119	0.000607787		

0.674067	1247.817	0.115872	0.784926	0.000660267		
0.674904	1255.477	0.116709	0.792586	0.000667748		
0.675741	1265.691	0.117546	0.8028	0.000627003		
0.676518	1273.584	0.118323	0.810693	0.000730623		
0.677415	1281.417	0.11922	0.818526	0.000837796		
0.678432	1292.921	0.120237	0.83003	0.000750026		
0.679328	1305.348	0.121134	0.842457	0.000657366		
0.680106	1312.061	0.121911	0.84917	0.00066204		
0.680883	1317.376	0.122688	0.854485	0.000718257		
0.68172	1324.467	0.123525	0.861576	0.000724497		
0.682557	1332.491	0.124362	0.8696	0.000626321		
0.683274	1339.135	0.12508	0.876244	0.000630091		
0.683992	1343	0.125797	0.880109	0.000739463		
0.684829	1349.509	0.126634	0.886618	0.000799271		
0.685726	1358.77	0.127531	0.895879	0.000754222		
0.686563	1369.215	0.128368	0.906324	0.000816432		
0.68746	1377.133	0.129265	0.914242	0.000879758		
0.688416	1387.994	0.130222	0.925103	0.000891694		
0.689373	1401.892	0.131178	0.939001	0.000790107		
0.69021	1411.841	0.132015	0.94895	0.000682396		
0.690928	1416.092	0.132733	0.953201	0.000800687		
0.691765	1422.922	0.13357	0.960031	0.000749712		
0.692542	1431.878	0.134347	0.968987	0.000755449		
0.693319	1437.682	0.135124	0.974791	0.000701293		
0.694037	1443.198	0.135842	0.980307	0.000764534		
0.694814	1449.738	0.136619	0.986847	0.000829877		
0.695651	1458.788	0.137456	0.995897	0.000898283		
0.696548	1470.526	0.138353	1.007635	0.000847534		
0.697385	1479.945	0.13919	1.017054	0.000915931		
0.698282	1488.503	0.140087	1.025612	0.000986807		
0.699238	1500.435	0.141043	1.037544	0.000936409		
0.700135	1513.45	0.14194	1.050559	0.000819354		
0.700912	1520.538	0.142718	1.057647	0.000888004		
0.701749	1527.118	0.143555	1.064227	0.000894162		
0.702586	1535.253	0.144392	1.072362	0.000836577		
0.703364	1543.05	0.145169	1.080159	0.000841907		

0.704141	1548.968	0.145946	1.086077	0.000846114		
0.704918	1554.153	0.146723	1.091262	0.000851451		
0.705696	1562.422	0.147501	1.099531	0.000924362		
0.706533	1571.848	0.148338	1.108957	0.000998991		
0.707429	1582.085	0.149235	1.119194	0.000940902		
0.708266	1591.703	0.150072	1.128812	0.001085063		
0.709223	1602.425	0.151028	1.139534	0.001097214		
0.71018	1617.344	0.151985	1.154453	0.000970473		
0.711017	1627.095	0.152822	1.164204	0.000837132		
0.711734	1632.481	0.153539	1.16959	0.000982055		
0.712571	1639.629	0.154377	1.176738	0.000988719		
0.713408	1648.402	0.155214	1.185511	0.000924362		
0.714186	1656.078	0.155991	1.193187	0.00085876		
0.714903	1663.462	0.156708	1.200571	0.00093544		
0.71568	1669.217	0.157486	1.206326	0.001013895		
0.716517	1679.255	0.158323	1.216364	0.001096468		
0.717414	1691.818	0.159219	1.228927	0.001033138		
0.718251	1702.633	0.160056	1.239742	0.001041312		
0.719088	1710.757	0.160894	1.247866	0.001199907		
0.720045	1723.979	0.16185	1.261088	0.001137159		
0.720942	1737.558	0.162747	1.274667	0.001071138		
0.721779	1747.388	0.163584	1.284497	0.001001455		
0.722556	1755.48	0.164361	1.292589	0.001085345		
0.723393	1763.72	0.165198	1.300829	0.001014376		
0.72417	1772.061	0.165976	1.30917	0.000941393		
0.724888	1777.449	0.166693	1.314558	0.001024051		
0.725665	1783.566	0.16747	1.320675	0.001109141		
0.726502	1792.494	0.168307	1.329603	0.001198113		
0.727399	1804.965	0.169204	1.342074	0.00120926		
0.728296	1817.651	0.170101	1.35476	0.001137882		
0.729133	1826.76	0.170938	1.363869	0.001228002		
0.73003	1837.349	0.171835	1.374458	0.001321953		
0.730987	1852.292	0.172792	1.389401	0.001084696		
0.731764	1864.784	0.173569	1.401893	0.001176763		
0.732601	1872.859	0.174406	1.409968	0.001099294		
0.733378	1881.054	0.175183	1.418163	0.001190725		

0.734215	1889.951	0.17602	1.42706	0.001198534		
0.735052	1899.371	0.176857	1.43648	0.001032968		
0.73577	1906.167	0.177575	1.443276	0.001124595		
0.736547	1913.209	0.178352	1.450318	0.001305755		
0.737444	1924.605	0.179249	1.461714	0.001228075		
0.738281	1935.647	0.180086	1.472756	0.001237159		
0.739118	1945.958	0.180923	1.483067	0.001245446		
0.739955	1955.802	0.18176	1.492911	0.001344751		
0.740852	1968.311	0.182657	1.50542	0.001356925		
0.741749	1983.957	0.183554	1.521066	0.001277555		
0.742586	1994.161	0.184391	1.53127	0.001193253		
0.743363	2002.267	0.185168	1.539376	0.001293078		
0.7442	2012.938	0.186005	1.550047	0.001208386		
0.744977	2022.033	0.186782	1.559142	0.001214576		
0.745754	2029.266	0.18756	1.566375	0.001220264		
0.746532	2036.267	0.188337	1.573376	0.00122637		
0.747309	2044.976	0.189114	1.582085	0.001424433		
0.748206	2057.509	0.190011	1.594618	0.001435927		
0.749103	2070.253	0.190908	1.607362	0.001253111		
0.74988	2080.211	0.191685	1.61732	0.001553424		
0.750837	2093.035	0.192642	1.630144	0.001567327		
0.751793	2109.619	0.193598	1.646728	0.001384668		
0.75263	2124.808	0.194435	1.661917	0.001295205		
0.753408	2133.549	0.195213	1.670658	0.001402174		
0.754245	2142.31	0.19605	1.679419	0.001410047		
0.755082	2152.761	0.196887	1.68987	0.001317559		
0.755859	2163.55	0.197664	1.700659	0.001325079		
0.756636	2171.673	0.198441	1.708782	0.001331204		
0.757413	2179.31	0.199219	1.716419	0.001441276		
0.758251	2189.97	0.200056	1.727079	0.001450741		
0.759088	2202.339	0.200893	1.739448	0.001460771		
0.759925	2213.52	0.20173	1.750629	0.001470129		
0.760762	2225.116	0.202567	1.762225	0.001586161		
0.761658	2238.046	0.203464	1.775155	0.001706441		
0.762615	2255.085	0.20442	1.792194	0.001505635		
0.763452	2268.393	0.205257	1.805502	0.001407203		

0.764229	2278.135	0.206035	1.815244	0.001523728		
0.765066	2288.575	0.206872	1.825684	0.001422654		
0.765844	2297.711	0.207649	1.83482	0.001319429		
0.766561	2305.922	0.208366	1.843031	0.001435448		
0.767338	2313.758	0.209144	1.850867	0.001553526		
0.768176	2323.71	0.209981	1.860819	0.001675227		
0.769072	2337.666	0.210878	1.874775	0.001575189		
0.769909	2352.009	0.211715	1.889118	0.001585705		
0.770746	2362.794	0.212552	1.899903	0.00170971		
0.771643	2375.476	0.213449	1.912585	0.001953116		
0.77266	2393.511	0.214465	1.93062	0.001622401		
0.773497	2408.514	0.215302	1.945623	0.001515216		
0.774274	2416.436	0.216079	1.953545	0.001521468		
0.775051	2424.099	0.216857	1.961208	0.0016461		
0.775888	2434.547	0.217694	1.971656	0.001536963		
0.776666	2446.364	0.218471	1.983473	0.00154536		
0.777443	2456.155	0.219248	1.993264	0.001552487		
0.77822	2464.192	0.220025	2.001301	0.001679678		
0.779057	2474.679	0.220862	2.011788	0.001689849		
0.779894	2488.975	0.221699	2.026084	0.001701542		
0.780731	2502.133	0.222537	2.039242	0.001834239		
0.781628	2514.282	0.223433	2.051391	0.001970006		
0.782585	2529.837	0.22439	2.066946	0.001986472		
0.783541	2549.138	0.225347	2.086247	0.001625879		
0.784319	2560.585	0.226124	2.097694	0.001633509		
0.785096	2567.692	0.226901	2.104801	0.001639641		
0.785873	2577.444	0.227678	2.114553	0.001774035		
0.78671	2587.372	0.228515	2.124481	0.001655485		
0.787488	2597.988	0.229293	2.135097	0.001535108		
0.788205	2606.842	0.23001	2.143951	0.001670052		
0.788982	2616.552	0.230787	2.153661	0.001937947		
0.789879	2630.664	0.231684	2.167773	0.001951009		
0.790776	2646.164	0.232581	2.183273	0.001701434		
0.791553	2656.862	0.233359	2.193971	0.001974072		
0.79245	2671.893	0.234255	2.209002	0.002253808		
0.793466	2688.773	0.235272	2.225882	0.001870498		

0.794304	2706.006	0.236109	2.243115	0.00174802		
0.795081	2717.448	0.236886	2.254557	0.001755556		
0.795858	2725.979	0.237663	2.263088	0.001899173		
0.796695	2737.309	0.2385	2.274418	0.001909183		
0.797532	2750.44	0.239337	2.287549	0.001782209		
0.798309	2760.983	0.240115	2.298092	0.00165222		
0.799027	2770.292	0.240832	2.307401	0.00193587		
0.799864	2781.226	0.241669	2.318335	0.002086366		
0.800761	2796.951	0.242566	2.33406	0.001959762		
0.801598	2811.657	0.243403	2.348766	0.002112173		
0.802495	2824.068	0.2443	2.361177	0.002124678		
0.803392	2840.069	0.245197	2.377178	0.002284101		
0.804348	2860.671	0.246153	2.39778	0.00201284		
0.805185	2874.766	0.24699	2.411875	0.001733583		
0.805903	2883.303	0.247708	2.420412	0.001884819		
0.80668	2892.136	0.248485	2.429245	0.002038205		

Appendix E: Calculation of relative density given in Equation 3.1 and Table 3.2

$$\overline{\mathrm{v}}_{\mathrm{s}} = \frac{v}{v_s} = \frac{n\left(\frac{L_{out}}{2} - \frac{t_1}{2}\right) th}{L^2 h} \qquad \text{Equation 3.1}$$

$$\overline{\mathrm{v}}_{\mathrm{s}} = \frac{4\mathrm{t}(L_{out} - \mathrm{t}_1)}{(L_{out})^2}$$

Table 3.2: Dimensions of the square interlocking flax/PLA core structures and their relative densities

Core ID	Height, *h* (mm)	Cell size (mm)		Thickness (mm)		Relative density ($\overline{\rho}$)		
		L_{in}	L_{out}	t_1	t	Empty	Filled-foam core	
							HP80	F150
SC20	20	20	24.5	3	1.4	0.20	0.44	0.55
SC30	20	30	34.5	3	1.4	0.15	0.45	0.58
SC40	20	40	44.5	3	1.4	0.12	0.47	0.62

Taking Sample SC20 as an example:

$$\overline{\mathrm{v}}_{\mathrm{s}} = \frac{4\mathrm{t}(L_{out} - \mathrm{t}_1)}{(L_{out})^2}$$

$$\overline{\mathrm{v}}_{\mathrm{s}} = \frac{4(1.4)(24.5 - 3)}{(24.5)^2}$$

$$\overline{\mathrm{v}}_{\mathrm{s}} = \frac{120.4}{(24.5)^2}$$

$$= 0.20$$

LIST OF PUBLICATIONS

Journal Papers

S. Alsubari, M. Y. M. Zuhri, S. M. Sapuana, & M. R. Ishak. (2020). Quasi-static compression behaviour of interlocking core structures made of flax fibre reinforced polylactic acid composite. Journal of Materials Research and Technology, 9(6), 12065-12070. (Impact factor: 5.03: Q1)

S. Alsubari, M. Y. M. Zuhri, S. M. Sapuan, M. R. Ishak, R. A. Ilyas, & M. R. M. Asyraf. (2021). Potential of natural fibre reinforced polymer composites in sandwich structures: A review on its mechanical properties. *Polymers*, *13*(3), 423. (Impact Factor 4.49: Q1)

S. Alsubari, M. Y. M. Zuhri, S. M. Sapuan, & M. R. Ishak. (2022). Effect of Foam Filling on the Energy Absorption Behaviour of Flax/Polylactic Acid Composite Interlocking Sandwich Structures. *Composite Structures*, 115685. (Impact factor: 5.407: Q1)

Conference Proceedings

S. Alsubari, M. Y. M. Zuhri, S. M. Sapuan, & M. R. Ishak. (2019). Sensitivity to Variations of Manufacturing Temperature And Pressing Time on The Tensile Properties Of Flax Reinforced Polylactide Composites, on 1-2 April 2019, Negeri Sembilan, Malaysia.

S. Alsubari, M. Y. M. Zuhri, S. M. Sapuan, M. R. Ishak, & M.I.J. Ibrahim. (2019). Quasi-static Compression Behaviour of Environmentally-Friendly Interlocking Core Structures Made of Flax/Polylactic Acid Composite ICAM2E2019, 21-23 October 2019, Langkawi, Malaysia.

S. Alsubari, M. Y. M. Zuhri, S. M. Sapuan, & M. R. Ishak. (2020). Potential Use of Hybrid Natural Fibre Composites in Sandwich Structure, 7th Postgraduate Seminar on Natural Fibre Reinforced Polymer Composites 2020, 27th June 2020, UPM, Selangor Malaysia.

S. Alsubari, M. Y. M. Zuhri, S. M. Sapuan, & M. R. Ishak. (2021). The energy-absorbing capability of foam-filled honeycomb structures made of flax/polylactide composite, 5th Wood and Biofibre International Conference 2021, 23 - 24 November 2021, Bangi, Selangor, Malaysia.

S. Alsubari, M. Y. M. Zuhri, S. M. Sapuan, & M. R. Ishak. (2021). The energy-absorbing characteristic of cellular core structures made of flax-based composites, International Conference On Sugar Palm And Allied Fibre Polymer Composites (Sapc20), 11th December 2021.